THE ORIGIN OF BUBBLES IN FLUIDIZED SYSTEMS

TECHNISCHE HOGESCHOOL
DELFT

1937 4049

J. VERLOOP

P1937
4049

VERVALLEN

C10063
89322

THE ORIGIN OF BUBBLES IN FLUIDIZED SYSTEMS

PROEFSCHRIFT

ter verkrijging van de graad van doctor in de technische wetenschappen aan de Technische Hogeschool Delft, op gezag van de rector magnificus ir. H. R. van Nauta Lemke, hoogleraar in de afdeling der elektrotechniek, voor een commissie uit de senaat te verdedigen op donderdag 28 oktober 1971 te 14.00 uur door

1937 4049

JAN VERLOOP

scheikundig ingenieur

geboren te Alblasserdam

Bibliotheek Technische Hogeschool
Doelenstr. 101
Delft
007406

BIBLIOTHEEK TU Delft
P 1937 4049
C 638932
17011

Dit proefschrift is goedgekeurd door
de promotor prof.dr.ir. P.M. Heertjes

STELLINGEN

1. In eerste benadering is het ontstaan van turbulentie bij stroming langs een vlakke plaat goed te vergelijken met het optreden van schieten in ondiep stromend water.

   L. Prandtl, Essentials of fluid dynamics, 1952, Blackie and Son Ltd., London, p. 113, 94.

2. Howard, Morris, Ward and Pyle vonden dat bij horizontale stroming uit gefluidiseerde bedden de deeltjesstraal instabiel wordt bij verhoogde druk. Waarschijnlijk zijn deze instabiliteiten schokgolven.

   A.J. Howard, P.J. Morris, K.A. Ward en D.L. Pyle, The flow of particles from pressurised fluidized beds, Chem.Eng., 47 (1969) CE 364.

3. In een pas getapt, goed glas pils is een stabiele continuiteitsschokgolf waar te nemen.

4. De methode ter bepaling van de minimum fluidisatiesnelheid, voorgesteld door Motamedi en Jameson, berust op een foutieve vooronderstelling.

   M. Motamedi en G.J. Jameson, A new method for the measurement of the incipient fluidizing velocity, Chem.Eng.Sci., 23 (1968) 791.

5. Bij de fabrikage van cementklinker is fluidisatie een minder geschikte techniek voor het sinterproces.

   o.a. R. Pyzel, Hydraulic cement process, Patent U.S.A. 3, 022,989, (1962).
   S. Hata en T. Sanari, Zementbrennen im Fliessbett, Zement-Kalk-Gips, 12 (1968) 509.
   P.M. Heertjes, L.H. de Nie en J. Verloop, The manufacture of portland cement clinker in a spouting bed, Powder Techn. 4 (1970/71) 269.

6. Bij alle gebruikte experimentele methoden voor de bepaling van de viscositeit van gefluidiseerde systemen is het stromingsprofiel onvoldoende bekend om op verantwoorde wijze de viscositeit te berekenen uit de gemeten stromingsweerstand.

   o.a. W. Siemes en L. Hellmer, Die Messung der Wirbelschichtviskosität mit der pneumatische Rinne, Chem.Eng.Sci., 17 (1962) 555.
   K. Schügerl, M. Merz en F. Fetting, Rheologische Eigenschaften von gasdurchströmten Fliessbettsystemen, Chem.Eng.Sci., 15 (1961) 1.

7. Uit de experimentele relatie van De Nie blijkt, dat de loslaatsnelheid van de druppel bij vorming aan een capillair niet wordt beïnvloed door de viscositeit van de continue fase. De achtergrond hiervan is, dat de loslaattijd van de druppel wordt bepaald door de insnoertijd van de nek.

   L.H. de Nie, Druppels, vorming en stofoverdracht, proefschrift T.H. Delft, 1970, p. 108.

8. Het dynamisch dispersiemodel, voorgesteld door Buffham heeft onvoldoende fysische achtergrond en is van weinig praktische betekenis.

   B.A. Buffham, The application of a time delay model to chemical engineering operations, Ph.D.Thesis, Loughborough University of Technology, 1969.

9. De 'technopolis' van Harvey Cox als 'Stad van de mens' is meer mogelijkheid dan werkelijkheid. Nog is nu de voorstad meer karakteristiek dan de grootstad.

   Harvey Cox, De stad van de mens, 1966.
   J. Verloop, 'Beeldenstorm zonder hagepreek' in Hagepreek en beeldenstorm, 1966.

10. De onderscheiding van Buber tussen het joods en christelijk geloof is wel karakteristiek, doch niet essentiëel.

    M. Buber, Twee wijzen van geloven, 1950.

Aan

Jane en Robert

Aan het ontstaan van dit proefschrift hebben velen direkt of indirekt meegewerkt. Ik wil hun heel hartelijk dank zeggen.
In het bijzonder wil ik noemen mijn afstudeerders R. Willems, M. Marskamp, H.M.W. Werker, H.A. Droog, F.R. Storm, A.W. Both, L.A. Lerk, A. Pot, J.H.O. Hazewinkel, B. Sikma, G.J.M.Kamperman, J.A.L. van Driel, die veel stof tot schrijven hebben geleverd en Th.E. van Bruggen, J.J.B. van Holst, J.H. Kamps die het manuscript hielpen persklaar maken.

CONTENTS

SUMMARY 7

SAMENVATTING 9

1 INTRODUCTION 11
1.1 General assumptions 12
1.2 Synopsis 14

2 THE ONSET OF FLUIDIZATION 16
2.1 The prediction of U_{mf} 16
2.2 The experimental determination of U_{mf} 17
2.2.1 The pressure drop method 17
2.2.2 The angle of repose method 19
2.2.3 Experimental results 23
2.3 Conductivity experiments 27
2.4 Conclusions 30

3 CONTINUITY WAVES 31
3.1 The velocity of continuity waves 31
3.2 The attenuation of continuity waves 35
3.3 The direction of the continuity wave 43
3.4 The dynamic wave velocity 43
3.5 Conclusions 46

4 VIBRATIONS 47
4.1 The dynamics of vibrating systems 47
4.2 Vibrations in a fluidized system 50
4.2.1 The frequency 50
4.2.2 The maximum height 55
4.2.3 The damping 56
4.2.4 Slugging 61
4.3 Experimental results 62
4.3.1 The experimental set-up 62
4.3.2 The relation between ν and L 63
4.3.3 The relation between ν and U 64
4.4 Conclusions 66

5 THE ONSET OF BUBBLING 67
5.1 The dynamic shock wave criterion 67
5.2 The vibration criterion 68
5.3 Other proposed criteria 72
5.4 Comparison of the criteria 76
5.5 Conclusions 78

6 CONCLUSION 79
6.1 Dimensional analysis 79
6.2 Critical deductions 79

NOTATION 81

REFERENCES 83

APPENDICES

A THE ANGLE OF REPOSE 86
A.1 Instability mechanisms 86
A.2 The effect of the gas velocity 87
A.2.1 Sliding 87
A.2.2 Rolling 88
A.3 The effect of interparticle forces 90
A.3.1 Sliding 91
A.3.2 Rolling 91
A.4 Conclusions 92

B NON LINEAR VIBRATIONS 93
B.1 Large amplitudes 93
B.2 Restricted large amplitudes 97

C THE CONTINUITY WAVE CRITERION 100
C.1 Experimental observations 100
C.2 Theoretical analyses 101
C.3 Experimental results 103

SUMMARY

In this thesis five subjects have been discussed :
1. The determination of the minimum fluidization velocity
2. The influence of interparticle forces (cohesion and friction) in homogeneous fluidized beds.
3. The propagation velocity of a porosity wave.
4. The frequency of the vibrations occurring in shallow fluidized beds.
5. The transition from homogeneous to heterogeneous fluidization.

The last subject - the origin of bubbles - is the central theme. It has a confining influence on the scope of the treatment of the other subjects and is the relating factor between the various topics. The approach has been based on the concept that bubbles are the results of some process occurring in the homogeneous fluidized state. Therefore, the analysis starts with the minimum fluidization velocity. The conditions at the onset of fluidization are characteristic of homogeneous fluidization. Special attention has been paid to the influence of interparticle forces.

The minimum fluidization velocity has been determined by two distinct experimental methods : the well-known pressure drop method and a new method based on the relationship between the tangent of the angle of repose and the fluid velocity. The combined results make it possible to determine and to define the value of the minimum fluidization velocity unequivocally. Furthermore, the important conclusion can be drawn that interparticle forces can be neglected when the effects are not visually observable. Additional support is presented by a renewed analysis of the mechanisms by which an electrical current in a fluidized system can be conducted.

Two processes leading to bubble formation have been analyzed: one is an instability phenomenon occurring in porosity waves, in the other voids are formed caused by the oscillation of the bottom layer of a fluidized bed.
The porosity wave has been treated as a continuity wave. In this approach equilibrium is assumed at both sides of the wave front and thereby the momentum balances reduce to the equilibrium relations between the fluid velocity and the voidage. The propagation velocity of the continuity wave has been derived for the general one-dimensional case. Further, the stability in time of the wave front has been investigated. The knowledge of the stability conditions is of importance in the interpretation of the results of the wave velocity experiments. The maximum value of the continuity wave velocity is given by the

velocity of the dynamic wave. When the propagation velocity of the continuity wave exceeds this velocity, dynamic shock waves arise. This phenomenon causes the onset of bubbling in liquid fluidized systems; the critical conditions are given by the dynamic shock wave criterion.

The vibration frequency of a shallow fluidized bed has been calculated from a balance of the drag forces and the gravitational forces across the whole bed. The maximum height which can oscillate harmonically is given by the wave velocity.

When the actual height of the bed is above this maximum height, bubbling or slugging occurs; the vibration criterion. The oscillation mechanism of bubble formation is limited by two factors :

1. No oscillations occur when the ratio of solids/fluid density is not sufficiently large.
2. At low fluid velocities the amplitude of the vibration is too small to promote bubbling.

Compared with the dynamic shock wave mechanism the vibration mechanism leads to instabilities at lower porosities. Therefore, the transition from homogeneous to heterogeneous fluidization is given by the vibration criterion for high ratios of the solids/fluid densities and by the dynamic shock wave criteria for low ratios of the densities. The influence of increased pressure on the stability of gas/solids sytems can be understood as a change in the governing mechanism. A comparison with other criteria presented in the literature shows that they do not impose any restriction upon the two proposed criteria.

Bubbles can also be formed artificially when a fast downcoming stream of fluidized solids hits a fixed object. The critical solids velocity at which this occurs can be calculated from the wave velocity.

SAMENVATTING

In dit proefschrift komen 5 onderwerpen aan de orde.

1. De bepaling en definiëring van de minimum fluïdisatiesnelheid.
2. De invloed van interaktiekrachten (cohesie en wrijving) tussen de deeltjes in homogeen gefluïdiseerde systemen.
3. De voortplantingssnelheid van een porositeitsgolf.
4. De vibratiefrekwentie van lage gefluïdiseerde bedden.
5. De overgang van homogene naar heterogene fluïdisatie.

Het laatste onderwerp - het ontstaan van bellen - vormt het centrale thema en fungeert tot op zekere hoogte als leidraad en verbindende faktor bij de behandeling van de andere onderwerpen. Uitgangspunt bij de benadering is, dat bellen ontstaan ten gevolge van een of ander proces in de homogeen gefluïdiseerde toestand. Daarom wordt begonnen met een analyse van de minimum fluidisatiesnelheid. De omstandigheden bij het begin van fluïdisatie zijn karakteristiek voor homogene fluidisatie. Speciaal is de aandacht hierbij gericht op de invloed van de interaktiekrachten tussen de deeltjes.

De minimum fluidisatiesnelheid is met twee verschillende experimentele methoden bepaald; de bekende drukval methode en een nieuwe methode die berust op de afhankelijkheid van de storthoek van de fluïdum snelheid. De gezamenlijke resultaten van deze methoden maken het mogelijk de minimum fluidisatiesnelheid eenduidig vast te leggen en te definiëren. Bovendien kan de belangrijke konklusie worden getrokken, dat de invloed van interaktiekrachten tussen de deeltjes kan worden verwaarloosd, wanneer die invloed niet visueel waarneembaar is. Deze konklusie wordt ondersteund met een hernieuwde analyse van de geleidingsmechanismen voor een elektrische stroom in gefluïdiseerde systemen.

Twee processen, die tot belvorming kunnen leiden, worden geanalyseerd. De een berust op een instabiliteitsmechanisme in porositeitsgolven, de ander op holtevorming ten gevolge van de oscillatie van de bodemlaag van een gefluïdiseerd bed. De porositeitsgolf is behandeld als een kontinuïteitsgolf. Hierbij wordt evenwicht aangenomen aan beide zijden van het golffront, zodat de evenwichtsrelaties tussen fluïdumsnelheid en porositeit kunnen worden toegepast in de impulsbalansen. De voortplantingssnelheid van de kontinuïteitsgolf is afgeleid voor het algemene, één-dimensionale geval. Voorts is de stabiliteit in de tijd van het golffront onderzocht. Deze is van belang bij de interpretatie van de resultaten bij de experimentele bepaling van de golfsnelheid. De grenswaarde van de snelheid van de kontinuïteitsgolf wordt gegeven door

de snelheid van de dynamische golf. Wanneer de eerstgenoemde snelheid groter wordt dan laatstgenoemde, ontstaan dynamische schokgolven. Dit verschijnsel veroorzaakt het ontstaan van bellen in vloeistof gefluïdiseerde systemen; de kritische kondities zijn vastgelegd in het dynamische schokgolf kriterium.
De vibratiefrekwentie van een laag fluïde bed is berekend met de balans van de weerstands- en gravitatie-krachten over het gehele bed. De maximale hoogte die harmonisch kan oscilleren, worden bepaald door de golfsnelheid. Is de werkelijke hoogte van het bed meer dan deze maximale hoogte, dan treed belvorming op; het vibratie kriterium. Het oscillatie mechanisme van belvorming wordt door twee faktoren beperkt :

1. In systemen met niet voldoend grote verhouding van de dichtheden van de vaste stof en het fluïdum treden geen oscillaties op.
2. Bij zeer lage fluïdumsnelheden is de amplitude van de vibraties te klein om holten te vormen die kunnen uitgroeien tot bellen.

Vergeleken met het dynamische schokgolf mechanisme leidt het vibratiemechanisme tot instabiliteiten bij lagere porositeiten. De overgang van homogene naar heterogene fluïdisatie wordt daarom gegeven door het vibratie kriterium bij hoge verhoudingen van de vaste stof/fluïdum dichtheden en door het dynamische schokgolf kriterium bij lage verhoudingen.
De invloed van verhoogde druk op de stabiliteit van vast/gas systemen kan worden verklaard met een verandering van mechanisme.
Een vergelijking met andere kriteria uit de literatuur levert o.m. als resultaat, dat deze geen beperkingen opleggen aan de twee voorgestelde kriteria.
Bellen kunnen ook op 'kunstmatige' wijze worden verkregen door een snelle stroom gefluïdiseerde deeltjes te laten botsen tegen een gefixeerd object. De kritieke deeltjessnelheid waarbij belvorming optreedt, wordt bepaald door de golfsnelheid.

1 INTRODUCTION

A paper titled 'Fluidization Nomenclature and Symbols (1) is included in the proceedings of the symposium on 'Dynamics of fluid-solids systems' held at Cambridge (Mass.), 1948. This paper tries to reduce the overlap in terminology by proposing definitions and symbols.
A proposed definition is :

> A 'fluidized mass' of solid particles is one which exhibits the mobility and hydrostatic pressure characteristic of a fluid. (This condition may be achieved through suspending the particles by means of a stream of fluid rising past the particles).

The proceedings of the symposium on fluidization at Eindhoven (1967) are accompanied by a definition given in the announcement (2).

> Fluidization is the phenomenon in which the gravitational force acting on a dense swarm of particles is counteracted by an upward fluid stream which causes these particles to be kept more or less in a floating state.

The similarity between the two definitions is striking. Both refer to a fluid like behaviour of a mass of particles which can be obtained by fluid flow. They are descriptive and qualitative. Neither explicitly defines state or flow conditions nor refers to an idealized model.

The foregoing may be sufficient to illustrate the limited, only slowly progressing, understanding of the fundamentals of fluidization.
To provide some background for the idealized conditions which will be adopted for the further analyses, fluidization will be described phenomenologically for a representative case.
When the velocity of a fluid, flowing through a packed bed of particles is increased, the pressure drop across the bed will also increase. When the pressure drop equals the weight of the bed per unit area, the bed will expand. When the loosest stable packing has been passed the bed is said to be fluidized. The velocity at which this occurs is called U_{mf}, the minimum fluidization velocity. On further increase of the fluid velocity the dynamic pressure drop remains constant and the porosity ε, the void fraction, will increase.
Depending on the system two modes of expansion can be followed.

a. The bed can remain homogeneous; ε will increase continuously and the particle motion will become more and more random till U becomes larger than V_T, the terminal fall velocity

of the single particle and the fluidized bed will very soon cease to exist.

b. Other systems will not expand homogeneously, or only over a limited range. At a critical porosity the system will start to fluidize heterogeneously and big voids can be seen rising up through the bed. The fluid velocity at the critical porosity is called U_{bp}, the fluid velocity at the bubble point. On passing ε_{bp} the porosity may temporarily decrease. For heterogeneous systems the fluid velocity can often pass V_T with only a limited carry-over of particles (3, 4). Although in the long run the fluidization equipment may be emptied, it is not useful to identify V_T with the maximum fluidization velocity for these systems.

1.1 General assumptions

The subject of this thesis is the onset of bubbling. It is clear from the preceding description that bubbling is thought to be the result of some process occurring in the homogeneous fluidized state. Therefore the set of idealizing conditions adopted to simplify the description only have to apply for the homogeneous state and the assumptions have to be tested under homogeneous conditions.
The following idealized conditions have been adopted :

1. The fluid is incompressible.
2. The particles are uniform spheres of constant shape and equal density.
3. The flow is vertical and evenly distributed.
4. The flow is laminar.
5. The fluidized system is radially isentropic.
6. Interparticle forces and friction are absent.

The comments given below on each of the assumptions have to be seen as preliminary justifications.

ad 1. It is known that the distinction between homogeneous and heterogeneous fluidization more or less coïncides with liquid and gas fluidization. This may indicate an influence of the compressibility of the fluid. However, Simpson and Rodger (73) found no fundamental difference between liquid and gas fluidized beds in their expansion experiments and observed small bubbles in certain liquid fluidized beds. Furthermore the effect of the compressibility is small in shallow beds fluidized at low velocities.

ad 2. Although this assumption does not affect the essence of fluidization, it might be of importance for the accuracy of prediction. It is shown in chapter 5 that not accounting for the particle shape and particle size distribution does not affect the results for the systems reported in the literature. There are no experimental data on the onset of bubbling for systems with an extreme or a changing particle shape, a very wide size distribution or a mixture of particulates having different densities.

ad 3. The condition of even flow distribution is a restriction on the scope of the subject. It is known that bubbles can be formed at the end of a fluid jet e.g. in a spouting bed operated above the maximal spoutable bed height. Although this mechanism may be important for poor distributors, it is not considered in this thesis. However, the usual aim is an even flow distribution.

ad 4. The flow is usually considered laminar for $Re = \rho_f U D_p/\mu < 10$. The adoption of this condition is not only a matter of convenience. The flow is always laminar in the theoretically most important cases of homogeneous gas/solids fluidized systems. The condition is required in experimental work on the onset of bubbling in liquid fluidized systems. In this case 'bubbles' are so small that they would be hard to distinguish from heterogeneities caused by turbulence.

ad 5. It is very likely that the properties of a homogeneous fluidized bed differ in horizontal and vertical direction. There are no manifest reasons why a homogeneous fluidized bed cannot be isentropic in the horizontal sense. A one-dimensional treatment of the problem would seem acceptable when the influence of the wall and circulation of the particles can be neglected. Besides changing the expansion behaviour, there are no indications that any of these effects have an influence on the onset of bubbling.

ad 6. It has often been observed that interparticle forces can cause channeling and void formation. This can lead to local spouts and in this way promote the occurrence of bubbles. As stated before, this mechanism is beyond the scope of this thesis. However, it is feasable that interparticle forces and friction can cause bubbling via other unknown mechanisms. Therefore, before analyzing the onset of bubbling, the influence of these forces will be investigated. It has to be shown that systems without interparticle forces are representative for homogeneously fluidized systems, exhibiting bubbling at higher porosities or fluid velocities.

1.2 Synopsis

The effects of interparticle forces are discussed in chapter 2. It is shown that in many common systems exhibiting bubbling, fluidization starts when interparticle forces and friction become unnoticeable. Further, the electrical conductivity of fluidized systems of conducting particles does not have to be caused by continuous interparticle contact. This has often been assumed and taken as proof of the existence of direct particle interaction.
Two mechanisms are proposed for the formation of bubbles :

1. The formation of shock waves caused by an instability phenomenon in porosity waves. This mechanism has been worked out in chapter 3.
   The analysis is not formally correct, it treats the phenomenon as the limit of a simplified description of the wave propagation.

2. The formation of voids caused by an oscillation of the bottom layer of the bed. This mechanism, described in chapter 4, is based on the vibrations occurring in a very shallow gas fluidized bed as reported by Hiby (55).

The critical conditions for the onset of bubbling are formulated in chapter 5 and the theoretical relations are compared with the experimental data. Mechanism 1 is a general mechanism and is valid for all fluidized systems.
Mechanism 2 only applies to systems with a high value of ρ_s/ρ_f; in systems with a low value the oscillations are subject to severe damping. The second mechanism provokes instabilities at lower values of U or ε and therefore bubbling is governed by mechanism 2 in the case of $\rho_s/\rho_f \gg 1$ (gas/solids systems) and otherwise by mechanism 1 (liquid/solids or high pressure gas/solids systems).

A method by which a bubble can be formed 'artificially' has been described in Appendix C. When a stream of fluidized solids hits a fixed object at such a solids velocity that the direction of the continuity wave changes from upwards to downwards, a stable void is formed below the object.

The theoretical analysis has not been extended beyond the point of defining a critical velocity or porosity, above which homogeneous fluidization becomes impossible. Although the predicted conditions appear to coïncide with the experimentally determined U_{bp} (ε_{bp}); the observed and predicted 'instabilities ' do not have to be identical.

In order to establish this identity a growth history of the instabilities into bubbles has to be described. This is not yet possible. However, for the proposed instabilities the conditions for growth into or the existence of stable bubbles are fulfilled. For convenience sake the transition from homogeneous to heterogeneous fluidization will be described as the onset of bubbling.

2 THE ONSET OF FLUIDIZATION

2.1 The prediction of U_{mf}

The usual method applied to calculate U_{mf} is to determine at which velocity the dynamic pressure drop across the bed becomes equal to the apparent weight of the solids per unit area. The equation proposed by Leva (3) gives good results for most systems (87) :

$$\Delta P = \frac{200\ \mu\ U\ (1-\varepsilon)^2\ L}{D_p^2\ \varepsilon^3} = (1-\varepsilon)(\rho_s-\rho_f)\ g\ L \qquad (2.1)$$

$$U = \frac{5.10^{-3}\ D_p^{\ 2}\ (\rho_s-\rho_f)\ g}{\mu}\ \frac{\varepsilon^3}{1-\varepsilon} \qquad (2.2)$$

Eq. (2.2) holds for laminar flow and low porosities ($\varepsilon < 0.8$). U_{mf} can be obtained from eq. (2.2) by introducing $\varepsilon = \varepsilon_{mf}$.

For most systems the value of ε_{mf} is not known. The use of the available estimates (3) relating ε_{mf} to D_p and a shape factor can lead to serious errors. The simplest and most accurate method is to determine ε_{mf} experimentally.
Another method to estimate U_{mf} is to calculate at which velocity a 'falling' dense swarm of particles would be held stationary by the fluid flow. Richardson and Zaki (5) propose the relation :

$$U = C_T\ \varepsilon^n \qquad (2.3)$$

C_T and n are constants. C_T has the dimension of a velocity and should have the same numerical value as the terminal free fall velocity V_T of a single particle. This is often not the case. Eq. (2.3) is less suited for the numerical estimation of U_{mf}, but it provides a very useful relation between U and ε. The value of n depends on the Re-number ($\rho_f V_T D_p/\mu$) and the ratio D_p/D_t.
Typical values given gy Richardson and Zaki of n are :
turbulent flow n = 2.39
laminar flow n = 4.65
although higher and lower values of n have been found (3, 7).
U_{mf} can also be estimated via a method given by Rowe (8). He measured the drag force F on a particle in an artificial swarm of cubical array, and correlated F to the drag force F_∞ on a single particle in an infinite medium for the same Re-number with the relation :

$$\frac{F}{F_\infty} = \frac{0.68}{d} + 1 \qquad (2.4)$$

herein is :

d = dimensionless distance $\frac{s}{D_p}$ between the particles

s = distance between the particles, $s + D_p$ = distance between the centers.

Rowe argues that at minimum fluidization conditions the value of d can be taken as 0.01. U_{mf} can the be calculated from eq. (2.4) and the F_∞ - U relation for a single particle. The method is of more theoretical than of practical importance. The value of d has not been firmly established. For regularly shaped particles the predictions of U_{mf} are usually not too far off. A large number of other equations and empirical correlations have been published (3, 9-13). Their validity is limited, since they always include an estimate of ε_{mf}.

2.2 The experimental determination of U_{mf}

2.2.1 The pressure drop method

The usual method to determine U_{mf} experimentally is by measuring the pressure drop ΔP across the bed. For laminar flow conditions the pressure drop across a packed bed increases linearly with the velocity and remains constant for a fluidized bed. The point of intersection of these two straight lines is often taken for U_{mf}. This is not correct because the packed bed has to expand before it can be fluidized.
The expansion usually starts at a pressure drop a little above the one needed for fluidization. This so-called 'sur'-pressure is often followed by a depression before the region of constant pressure is reached. The velocity where the pressure drop becomes constant coincides with the velocity where ΔP starts to decrease when the gas velocity in a fluidized bed is reduced. This velocity is proposed as the best value of U_{mf}; the bed has been fully expanded and lost all the characteristics of a packed bed. The decrease in ΔP is not linear with U because the porosity does not remain constant; the bed will compact from ε_{mf} till a stable porosity has been reached.These changes in porosity cause the hysteresis in the pressure drop (see figure 2.1 b) and obstruct the accurate determination of U_{mf}.
Many mechanisms have been proposed to explain the observed 'sur'-pressure. Reboux (14) ascribes this phenomenon to the acceleration energy of the particles needed for expansion. Leva (3) to an 'unlock' energy and Davidson and Harrison (15)

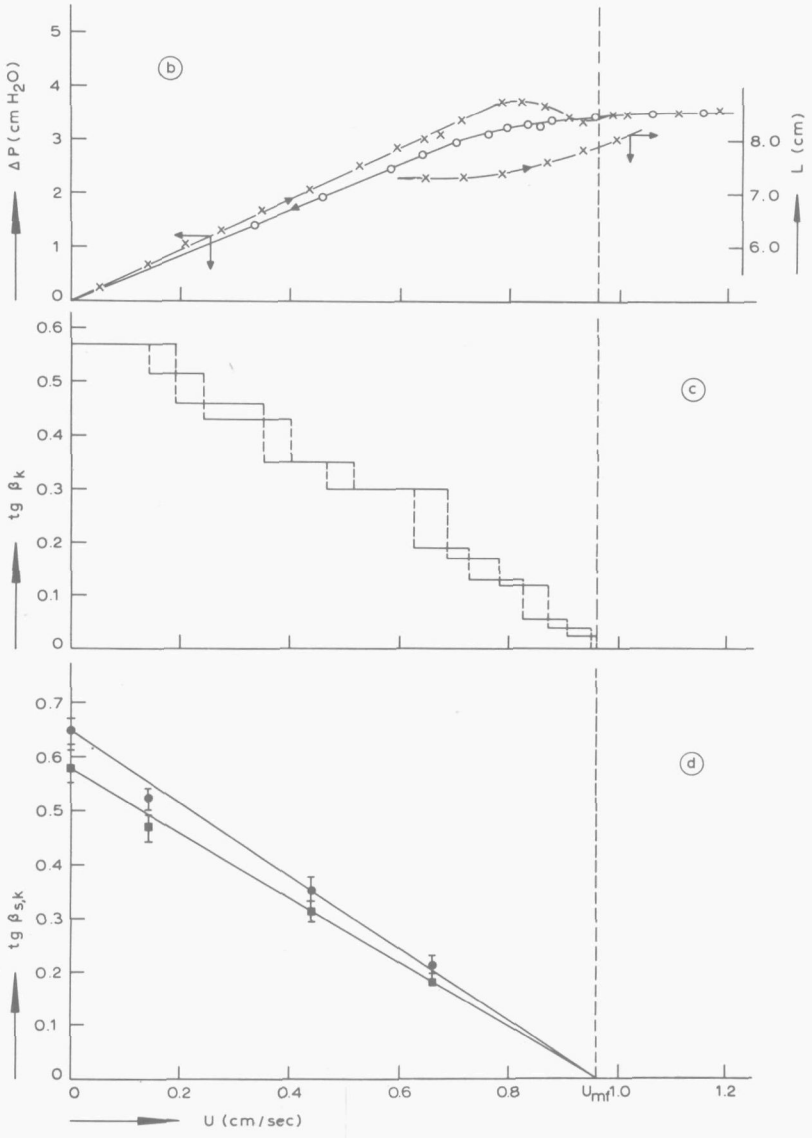

Figure 2.1 Experimental determination of U_{mf} (silicagel, D_p = 125-150 μ)
(a) pressure drop method (large bed)
(b) pressure drop method (small bed)
(c) angle of repose method I
(d) angle of repose method II

to the wedging action of the bed. Rietema (16) relates the 'sur'-pressure to interparticle forces and derives from soil-mechanical principles the relation for yielding :

$$\Delta P_s \sim \frac{2\tau_c}{D_t} \frac{\cos \iota}{1 + \sin \iota} \qquad (2.5)$$

ΔP_s = 'sur'-pressure

τ_c = cohesion constant in Coulomb criterion (cohesion stress)

ι = angle of internal friction.

Drinkenburg (17) and de Jong (18) calculate the 'sur'-pressure via the critical shear stress τ_w between the particles and the wall at which the packed structure will yield. ΔP_s can then be obtained from the equation :

$$\Delta P_s \tfrac{1}{4}\pi D_t^2 = L \pi D_t \tau_w$$

$$\Delta P_s = \frac{4 L}{D_t} \tau_w \qquad (2.6)$$

The minimum in the pressure drop curve has not received much attention. Channeling, as proposed by Leva (3), also leads to a lower pressure drop for $U > U_{mf}$. When this is not the case the simplest explanation for the slight depression is the orientation of the particles in such a way as to offer the least resistance to the fluid flow (38).
Before a further analysis is given, another method to determine U_{mf} will be introduced and the results compared with the ΔP-method.

2.2.2 The angle of repose method.

A characteristic feature of a fluidized bed is its horizontal surface, or better, its inability to sustain a tilted surface for any length of time, in contrast to a packed structure of solids. This characteristic difference can conveniently be used to indicate the transition from packed to fluidized conditions. In this way U_{mf} can be determined by the velocity at which the angle of repose β becomes zero. Depending on the method of determination various angles of repose can be defined (9, 19). Here, only two angles of repose will be distinguished :

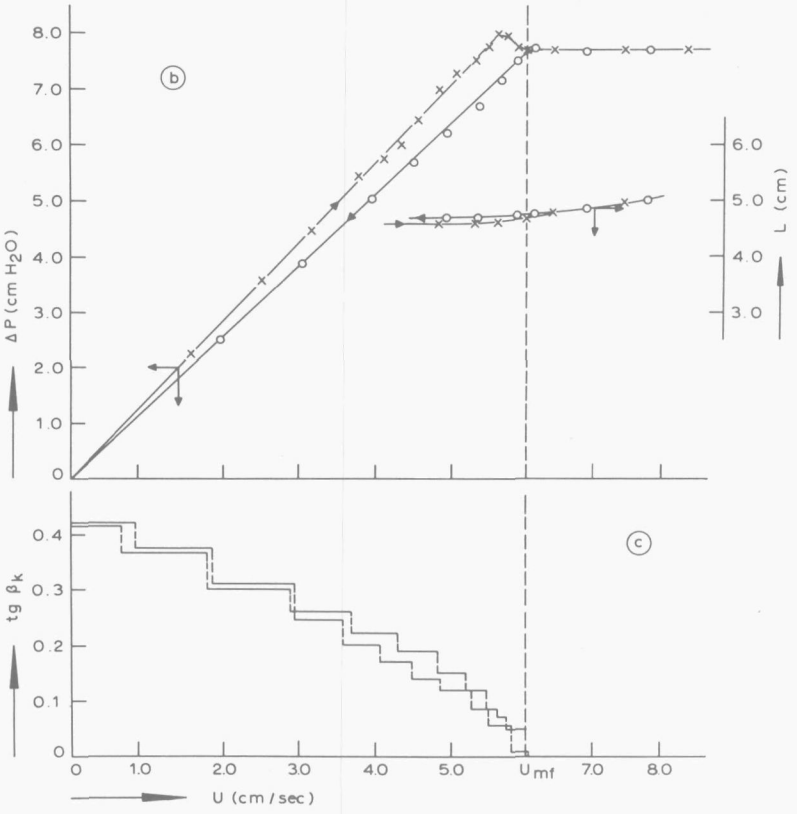

Figure 2.2 Experimental determination of U_{mf} (glass beads, D_p = 250-320 μ) Legend as in figure 2.1

β_s = the static angle of repose; the maximum stable angle of a pile of solids with the horizontal.

β_k = the kinetic angle of repose; the angle of the slope with the horizontal obtained when the pile of solids is allowed to drain.

By definition β_s should be independent of the experimental technique; this does not hold for β_k, due to the eroding effect of the rolling particles. β_s, always higher than β_k, represents the critical static equilibrium conditions between uncontained solids and the surrounding fluid medium.
The value of β depends on interparticle friction and forces. The smaller and more irregular the particles are, the larger β will be. When strong cohesional forces are present the slope can be very irregular (9, 20, 21).
The experimental value of β_k, given as tg β_k, has simply been obtained by allowing a heap of contained solids to drain via a slot in one of the sides of the container (9). From the height and length of the remaining heap tg β can be calculated. The value of tg β_s can subsequently be obtained by slowly tilting the container till the solids start to drain again. The maximum obtainable angle before instability occurs, gives β_s. The value of β_s can be calculated from the sum of the original kinetic angle of repose and the angle of the bottom of the container with the horizontal γ. In equation :

$$(\beta_s)_j = (\beta_k)_{j-1} + (\gamma)_j$$

The process can be repeated by continuously increasing γ. The given values of β_s and β_k are the arithmetic average value of a number of such series.

A fluid flow introduced via the bottom of the container will affect the value of β_s and β_k. The value of tg β reduces gradually with increasing fluid velocity from the initial value tg β_o to zero (22). This decrease occurs because the fluid leaves the solids perpendicular to the surface (see Appendix A). It can be deduced that in the absence of interparticle forces tg β decreases linearly with increasing U. The experimental relations between tg β and U have been obtained via two methods.

1. The container is filled and the solids are allowed to drain to obtain the value of tg β_{ko}. Then the gas velocity is very slowly increased until instability occurs, the new value of tg β_k at that gas velocity is measured, whereafter U is increased again. This method leads to a step curve as shown in the section c of the figures 2.1-2.4.

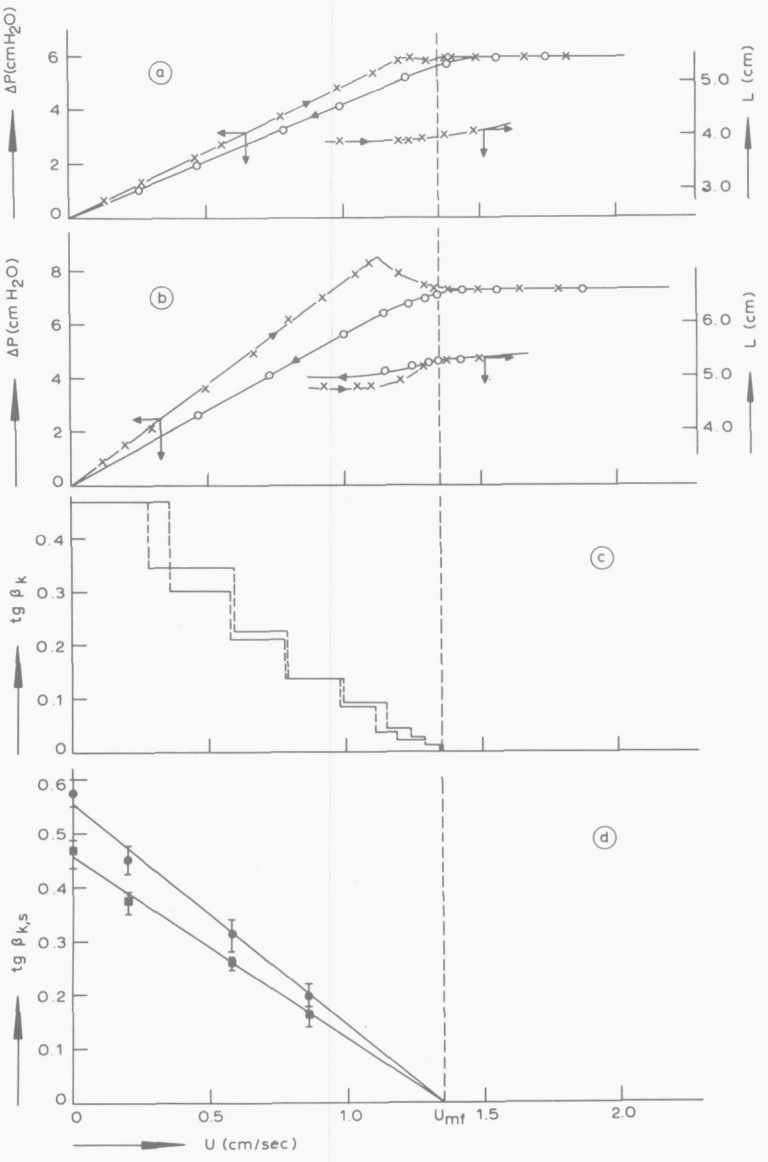

Figure 2.3 Experimental determination of U_{mf}
(glass beads, D_p = 65-90 μ)
Legend as in figure 2.1

The end of the horizontal part of the step can be seen as the value of tg β_s at that velocity. The steps are not very reproduceable except for the beginning and end points (U = 0 and U = U_{mf}). Through the average values of the extremes of the steps for a number of experiments, lines can be drawn representing the relation between tg $\beta_{s,k}$ and U.

2. Before the bed is filled and the solids are drained the gas velocity is set at a certain value. By tilting the container a number of values of tg β_s and tg β can be obtained in the same way as described before for tg β_{so} and tg β_{ko}. The variation of the average value of tg β has been indicated in the section d of the figures 2.1-2.4. By varying the gas velocity the relation between tg β and U can be found. This method gives very reproduceable results.

2.2.3 Experimental results

The angle of repose experiments have been performed in a rectangular bed (10 x 2 cm) with a slot in one of the short sides. The pressure drop experiments have been carried out in rectangular beds of 10 x 2 cm and 20 x 4 cm. A little ammonia has been added to the air to diminish electrostatic effects. The experiments have been carried out with shallow beds to reduce the effect of the compressibility of the air. The pressure drop across the distributor - a sintered steel plate of 3 mm - was at least 20 times the pressure drop across the bed. The experiments have been performed very carefully to avoid electrostatic charging of the particles as a result of particle collisions. Experiments with visible effects of interparticle forces - e.g. channeling, stable voids, low pressure drop, irregular slope - have been rejected. The influence of interparticle forces has been analyzed as follows : the first experiments were performed with large particles ($D_p \sim 300\ \mu$) and the experimental relations were established in the absence of interparticle forces. In the following experiments the particle size was gradually decreased till the influence of interparticle forces showed up in the experimental results. Typical experimental curves are given for the particle size ranges $D_p > 100\ \mu$; $50\ \mu < D_p < 100\ \mu$ and $D_p < 50\ \mu$ in the figures 2.1-2.5.

In the figures 2.1 and 2.2 experiments using large particles are shown. For large particles it is plausible to assume that interparticle forces are of negligible importance compared with the frictional forces. This is confirmed by the straight relation between tg β and U. The pressure drop method and the angle of repose method give the same value for U_{mf} when the

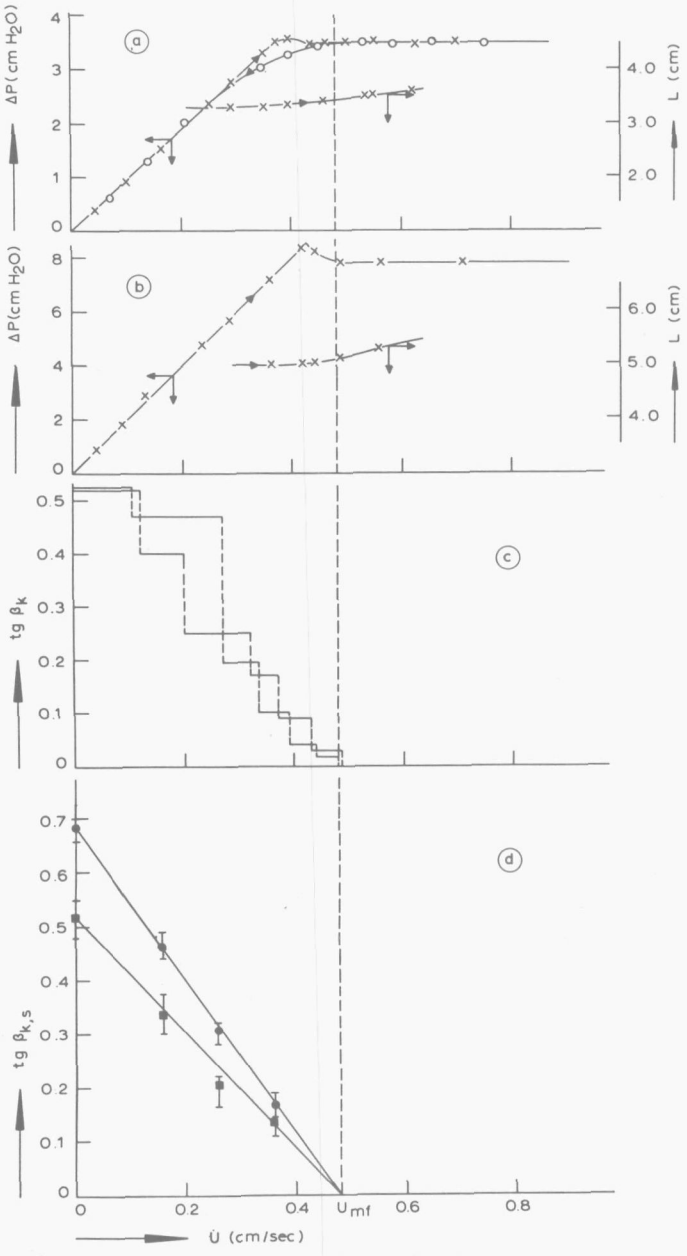

Figure 2.4 Experimental determination of U_{mf} (glass beads, D_p = 45-60 μ) Legend as in figure 2.1

minimum fluidization velocity is defined as the velocity above which interparticle friction does not add to the stability of the solids structure; $U_{mf} = U_{\beta=0}$. Experimental results for smaller particles where interparticle forces could be of importance, although no effects of interparticle forces could visually be observed, are shown in the figures 2.3 and 2.4. The curves in the figures 2.3-2.4 are of similar shape as in the figures 2.1-2.2 and also the values of U_{mf} coïncide, indicating that interparticle forces are not effective.
The presence of interparticle forces is easier recognized in the tg β - U curve than in the ΔP - U curve. This can be seen in the results of experiments using very small particles (figure 2.5). Glass beads smaller than 40 μ always showed visible effects of interparticle forces. The experimental curves of such small particles are not reproduceable and it is rather difficult to deduce a value of U_{mf}. The indicated value of U_{mf} has been obtained by extrapolating the U_{mf} - values of larger glass beads as a function of D_p, with a correction for the difference in porosity as given by eq. (2.2).
The effect of the interparticle forces on the tg β - U curve is the strongest at $U \sim U_{mf}$. The decrease of tg β with U is very gradual in that region and usually bubbling or channeling occurs before the point tg $\beta = 0$ has been reached.
As long as channeling does not occur, the ΔP - U curve is not too much affected by the presence of interparticle forces; the region of the 'sur'-pressure is extended, the pressure drop for $U > U_{mf}$ tends to increase and the hysteresis effect is usually larger. Channeling, the more probable to occur the stronger the interparticle forces are and the higher the velocity is, can simply be traced in a ΔP - U curve by steep pressure decreases and too low a value of ΔP for $U > U_{mf}$. The weight of the solids and the bed geometry is the same in the experiments shown in the sections b and b'. It has been concluded that interparticle forces can be neglected when the effects do not show up in the ΔP - U and tg β - U curves. This criterion coïncides with the criterion of visual observability.
The figures 2.3 and 2.4 also show the influence of the dimensions of the bed on the 'sur'-pressure. ΔP_s is much lower in the larger beds (section a) than in the smaller beds (section b). The figures 2.1-2.4 show that in the region of 'sur'-pressure interparticle friction is still present, for tg $\beta \neq 0$. These two facts indicate that eq. (2.6) is possibly correct. According to de Jong (18) eq. (2.6) predicts the correct order of magnitude of the 'sur'-pressure. It will be clear from the figures that the determination of U_{mf} from the pressure drop curve easily leads to errors. When ΔP_s is small the maximum is difficult to notice and too low a value for U_{mf} will be adopted. When the orientation effect of the particles

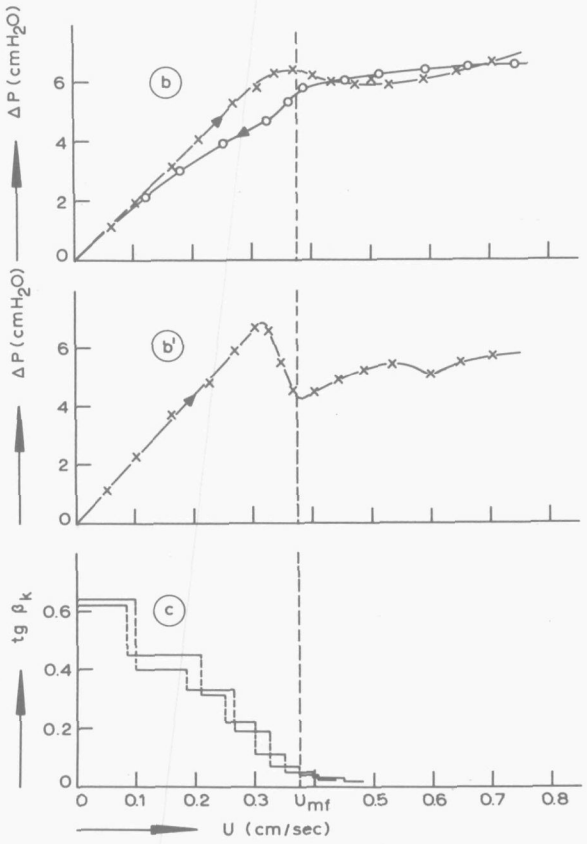

Figure 2.5 The influence of interparticle forces on the experimental determination of U_{mf}
(glass beads, $D_p < 40\ \mu$)
Legend as in figure 2.1

continues to exist above U_{mf} the pressure drop will not be constant at fluidization conditions but will gradually increase. The value of U_{mf} will be taken too high. These phenomena make it difficult to obtain from a ΔP - U curve the true value of U_{mf} and has lead to many different decisions (7, 23-25).
These problems are considerably reduced with the angle of repose method. In method I it is difficult to determine the point $\beta = 0$ with great accuracy as this point can vary a bit from experiment to experiment, because the final instability also depends on the foregoing one. In the expanded bed region the system is rather sensitive to irreproducible effects, like vibrations.
The value of U when $tg\ \beta = 0$ indicated via method II is a little arbitrary. However, the value of U_{mf} coïncides very closely with the values obtained via method I and the pressure drop method, is reproduceable and simple to determine. The angle is formed at the porosity corresponding to the applied gas velocity, so the smoothest relation between β and U is obtained. In the other methods the bed expands shockwise, therefore U and ε do not always correspond leading to irregular effects.

2.3 Conductivity experiments

The analysis given in the previous paragraph can also be of use in the interpretation of other experiments. Jones and Wheelock (26) measured the electrical resistivity of fluidized carbon particles. They observed that the maximum value of the resistivity r_M occurred at a gas velocity a little above U_{mf}. This observation is based on a mistaken estimate of U_{mf}. Figure 2.6 shows their results for the determination of U_{mf} and r_M for a broad sieve fraction of graphite (60 - 200 μ). Jones and Wheelock accepted the value U_1 for U_{mf}. However, the value U_2 seems more appropriate. The description of the influence of the gas velocity on the resistivity becomes then more logical. For $U < U_1$ the porosity does not change and the resistivity remains constant. At $U \sim U_1$ the bed starts to expand, the total area of interparticle contact decreases and the resistivity increases sharply. (Goldschmidt and Le Goff (27) found for spherical particles an increase by a factor of $10^3 - 10^4$). At U_{bp} the resistivity will decrease again due to the increased mobility of the particles. For these coarse particles U_{bp} and U_{mf} will coïncide ($N_{TR} \sim 600$, see chapter 5, figure 5.1)
The phenomenon that fluidized beds of conducting particles can sustain an electrical current has been used as an argument (16) for the existence of a continuous interparticle

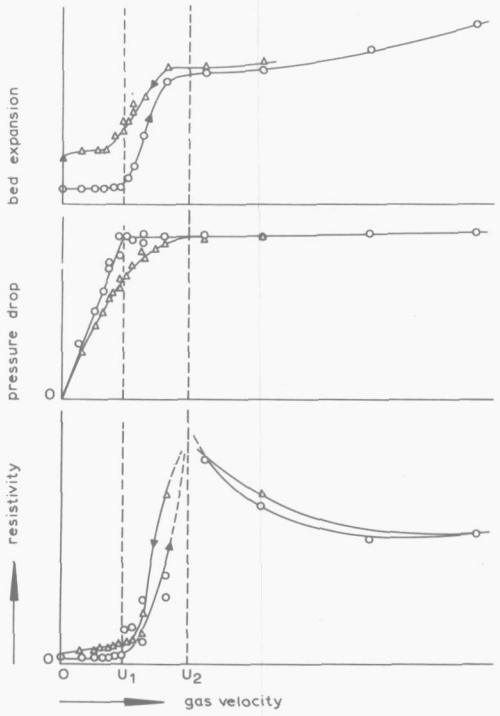

Figure 2.6 Effect on the gas velocity on the resistivity of fluidized graphite particles

contact and, therefore, frictional forces should be taken into account in the description of fluidized systems. However, a renewed analysis of the experimental results shows that there are insufficient grounds for such a conclusion. Three different mechanisms have been proposed via which the electrical current can be conducted.

1. Charge transfer due to particle collision and migration.
2. Particle to particle discharge through the fluid.
3. Intermittant chain formation of the particles or continuous interparticle contact.

Earlier investigators (16, 26, 77-80) thought the first two mechanisms to be of negligible importance and therefore proposed mechanism 3. However, recently Lee, Pyrcioch and Schora (81) measured the resistivity of homogeneous fluid-

ized beds at high pressures. They concluded from the influence of the pressure and the gas velocity on the resistivity that the current was only conducted via a discharge mechanism. The abandonment of mechanism 2 had been based on the calculations of Goldschmidt and Le Goff (77). In analogy with heat conduction, they derive for the resistivity r :

$$r = \frac{I}{(1-\varepsilon)\, C_s \rho_s \, \mathbb{D}} \qquad (2.7)$$

C_s = electric capacity of the solids ($\frac{\text{Coulomb}}{\text{gram}}$)
$\mathbb{D}$ = diffusion coefficient of the solids

$\mathbb{D}$ is taken as $\mathbb{D} = 5\ cm^2/sec$, the value found by Leva and Grummer (84). The product $C_s\rho_s$ is taken as $4.10^{-8}\ C/cm^3$ without further reference. From eq. (2.7) a value of $r = 10^7$ ohmcm is obtained; the experimental value is in the order of 10^2 ohmcm. They conclude that mechanism 1 can be neglected. However, they take very small values of $C_s\rho_s$ and $\mathbb{D}$. Stemerding (85) in his heat conduction experiments using the analogue equation of eq. (2.7) found for $\mathbb{D}$ a value of 360 cm^2/sec. Other investigations report even higher values of $\mathbb{D}$ in well fluidized beds (86). The value of $C_s\rho_s$ used is probably based on the maximal specific charge for contact charging (83). A better estimate is the maximal discharge value of $4.10^{-6}\ C/cm^3$. Adopting these values eq. (2.7) gives for r a value in the order of 10^3 and a factor 10 can easily be accounted for. Mechanism 1 can simply explain the large dependency of r on Dt and L as found by Jones and Wheelock (82); the dependency of r on D_t and L being of the same order of magnitude as the dependency of $\mathbb{D}$ (86).
The conclusion can be drawn that as long as the bed is fluidized homogeneously the current is conducted via mechanism 2. It has been found experimentally that the resistivity increases with increasing gas velocity (16, 26, 82). This can be explained by the interparticle distance. The resistivity will have its maximum value at U_{bp} (82). In heterogenous fluidized beds all three mechanisms can play a role. The bubbles will promote the migration of the particles and can cause chain formation. Mechanism 1 must play an important role. The conductivity experiments give no grounds to conclude that a continuous interparticle contact exists in homogeneous fluidized beds. Taking into consideration the angle of repose experiments there is even less reason to assume that the particles can transmit forces. Furthermore the relation between tg β and r_M, as found experimentally by Jones and Wheelock (26),

indicates that r_M becomes higher the stronger the interparticle friction and forces are.

2.4 Conclusions

1. In the absence of interparticle forces the onset of fluidization can be defined by the disappearance of interparticle friction.
   An equivalent definition is : U_{mf} is the velocity above which mechanical interparticle forces do not add to the stabilization of the solids structure.
2. Experimentally U_{mf} is easily determined with the angle of repose method. The pressure drop method presents some difficulties due to expansion of the bed, the wall friction and the orientation of the particles in the fluid flow. Both methods lead to the same values for U_{mf} if experiment and interpretation are carried out with care.
3. The 'sur'-pressure is very probably caused by solids-wall friction, resulting from interparticle friction. ΔP_s can be enlarged by cohesive interparticle forces.
4. The conductivity experiments do not support the assumption that in homogeneous fluidized beds a continuous interparticle contact exists.
5. For homogeneous fluidized systems the influence of interparticle forces can be neglected if no visible effects are present.

3 CONTINUITY WAVES

3.1 The velocity of continuity waves

Traditionally the idealized concept of a homogeneous fluidized bed has been a regular crystal like structure of particles individually supported by the fluid flow, hovering around an equilibrium position. This view is primarily based on visual observations of liquid fluidized systems of small, light particles. Support for this view can be drawn from the experiments of Rowe and Henwood (33), showing that adjacent particles repel each other. Based on this concept are the well-known potential flow analyses of Davidson and Harrison (15) and several of the investigations on the stability of a fluidized system (34, 35, 44, 45). The latter investigations show this crystal like structure to be unstable. Further there is an increasing amount of experimental indications that this concept should be amended. The porosity appears not to be strictly constant in a homogeneous fluidized bed. Instead there exist regions of lower and higher porosity, probably originating randomly at the distributor (41), which rise up through the bed. Although the evidence obtained so far (32, 37 - 42) is not conclusive, as none of the experiments are performed under the conditions assumed in the crystal concept - laminar flow, low porosity, large ratio D_t/D_p -, it seems likely that porosity waves are an inherent feature of fluidized systems. According to Wallis (43) continuity waves occur whenever the steady equilibrium flow rate of a substance depends on the amount of that substance which is present. In a fluidized bed the fluid flow and the voidage are related factors. Continuity waves, also called density or porosity waves, are small fluctuations of the average porosity where an equilibrium of forces is maintained on both sides of the waves and the inertia effects can be neglected. In the calculations the momentum balances are reduced to those presenting the steady states of uniform fluidization. When these approximations are not made the solution of the wave equations offers considerable difficulties (34-36, 44-46). Furthermore there is at present no general agreement on the form of the complete momentum equations (47) and the importance of many mechanisms is unknown (31).

Various authors (6, 43, 48) have derived expressions for the velocity of continuity waves with an infinitely small amplitude ($\Delta\varepsilon$ approaches 0) c_ε for fluidized beds with a solids velocity of zero.

In this chapter the equations for the propagation velocity of a porosity wave will be derived for the one-dimensional case. The velocity of continuity waves with large amplitudes ($\Delta\varepsilon$) will be denoted with c_{sh}, the continuity shock wave velocity.
Figure 3.1 shows a wave propagating with velocity c_{sh}. In front of the wave is a region with porosity ε_0, behind the wave is a region with porosity ε_1.

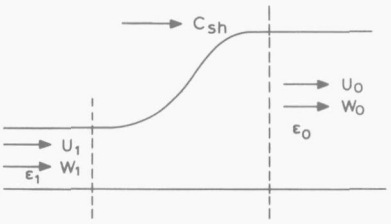

Figure 3.1 Propagation of a continuity wave

Relative to the wave front as much matter is approaching as departing and the mass balances for the two phases are for the fluid phase :

$$(U_{i1} - c_{sh})\ \varepsilon_1 = (U_{i0} - c_{sh})\ \varepsilon_0 \qquad (3.1)$$

and for the solids phase :

$$(W_1 - c_{sh})\ (1 - \varepsilon_1) = (W_0 - c_{sh})\ (1 - \varepsilon_0) \qquad (3.2)$$

U_i is the interstitial fluid velocity; W is the solids velocity.
From the eqs. (3.1) and (3.2) follows :

$$c_{sh} = \frac{U_{i1}\varepsilon_1 - U_{i0}\varepsilon_0}{\varepsilon_1 - \varepsilon_0} = \frac{W_1(1 - \varepsilon_1) - W_0(1 - \varepsilon_0)}{\varepsilon_0 - \varepsilon_1} \qquad (3.3)$$

As equilibrium conditions are assumed in front of and behind the wave the correlations between U and ε for steady, uniform fluidization (eqs. 2.2 and 2.3) can be used. Upon introduction of the slip velocity $U_s = U_i - W = U/\varepsilon - W$ the two

relations between U and ε become respectively :

$$\frac{U_{s1}\ (1 - \varepsilon_1)}{\varepsilon_1^{\,2}} = \frac{U_{s0}\ (1 - \varepsilon_0)}{\varepsilon_0^{\,2}} \qquad (3.4a)$$

$$\frac{U_{s1}}{\varepsilon_1^{\,n-1}} = \frac{U_{s0}}{\varepsilon_0^{\,n-1}} \qquad (3.4b)$$

Combining the eqs. (3.3) and (3.4) gives for the wave velocity :

$$c_{sh} = U_{s1}\left[\frac{\varepsilon_1^{\,2}(1-\varepsilon_0) + \varepsilon_0^{\,2}\ (1-\varepsilon_1) + \varepsilon_0\varepsilon_1}{\varepsilon_1^{\,2}}\right] + W_1 \qquad (3.5a)$$

$$c_{sh} = U_{s1}\left[\frac{(1 - \varepsilon_0)\ (\varepsilon_1^{\,n} - \varepsilon_0^{\,n})}{(\varepsilon_1 - \varepsilon_0)\ \varepsilon_1^{\,n-1}}\right] + W_1 \qquad (3.5b)$$

(The value of c_{sh} expressed in U_0 en W_0 can be obtained from the eqs. (3.5a) and (3.5b) by reversing the indices 0 and 1). For small amplitude waves (ε_1 approaches ε_0) eq. (3.5) reduces to :

$$c_\varepsilon = (3 - 2\varepsilon)\ U_s + W \qquad (3.6a)$$

$$c_\varepsilon = n(1 - \varepsilon)\ U_s + W \qquad (3.6b)$$

When the solids velocity is zero eq. (3.6) reduces to the simple equations :

$$c_\varepsilon = \frac{(3 - 2\varepsilon)}{\varepsilon}\ U \qquad (3.7a)$$

$$c_\varepsilon = \frac{n\ (1 - \varepsilon)}{\varepsilon}\ U \qquad (3.7b)$$

The continuity wave concept has successfully been used by Slis, Willemse and Kramers (6) to predict the response of the level of a fluidized bed to a sudden change in the fluid velocity. In reverse it has been used for a determination of the porosity of the dense phase of a bubbling fluidized bed (49).

Given the present state of knowledge a more formal approach does not have much advantage above the continuity wave concept for obtaining the wave velocity. This may be illustrated by table 3.1 where the experimental and theoretical values of Anderson and Jackson (41) are listed together with the values obtained from eq. 3.7b. n has been calculated from the experimental values of U and ε. (The values of n calculated from the relations given by Richardson and Zaki (5) are higher).

TABLE 3.1

tube diameter D_t particle diameter D_p expansion constant n	U cm/sec	ε	c_ε cm/sec observed ref. 41	c_ε cm/sec calc. ref. 41	c_ε cm/sec calc. eq.(3.7b)
D_t = 3.81 cm	3.72	0.418	6.62	8.33	8.29
D_p = 0.20	3.93	0.433	8.01	7.88	8.24
n = 1.6	4.28	0.451	8.95	7.90	8.34
D_t = 2.54 cm	2.46	0.463	5.25	5.77	5.71
D_p = 0.127 cm	2.55	0.470	5.36	5.66	5.76
n = 2.0	2.72	0.483	5.87	5.68	5.81
	2.89	0.496	6.10	5.76	5.86
	2.96	0.500	6.48	5.85	5.94
D_t = 1.27 cm	2.53	0.503	3.92	4.63	6.25
D_p = 0.127 cm	2.70	0.515	4.42	4.74	6.36
n = 2.5	2.87	0.528	4.75	4.76	6.42
D_t = 1.27 cm	1.42	0.504	3.46	3.47	3.71
D_p = 0.086 cm	1.64	0.529	3.91	3.53	3.88
n = 2.6[5]	1.77	0.541	4.23	3.49	4.00
D_t = 1.27 cm	0.86	0.495	2.54	2.45	2.63
D_p = 0.064 cm	0.98	0.507	2.76	2.56	2.86
n = 3.0	1.02	0.511	2.95	2.60	2.93
	1.10	0.519	3.05	2.67	3.06
	1.20	0.530	3.26	2.77	3.19

Except for the experiments with the very small ratio $D_t/D_p = 10$ the values of c_ε obtained with eq. (3.7b) are close to the experimental values, usually closer than the values of Anderson and Jackson. Their values of c_ε were obtained by a

best fit procedure on the grow velocity of the wave by varying four unknown parameters, which describe the combined effect of shear and bulk viscosity; the effective pressure of the particulate phase; the fluid-particle drag and the restricting effect of the walls on the vertical motion of the particles respectively.

3.2 The attenuation of continuity shock waves

In order for a shock wave to remain steep its propagation velocity should be both larger than the wave velocity in front of and smaller than the wave velocity behind the shock wave. Otherwise the smaller waves will run ahead or stay behind the shock wave and the front will gradually flatten. Thus the attenuation of a continuity shock wave is governed by the relation :

$$c_{\varepsilon 1} \gtrless c_{sh} \gtrless c_{\varepsilon 0} \qquad (3.8)$$

when the absolute values of the velocities are taken.
If eq. (3.8) is satisfied the front will remain steep. If one or both conditions are not satisfied the shock wave will be attenuated at one or two sides respectively.
In order to compare the three velocities c_{ε_0} has to be expressed in U_1 and W_1.
Substitution of the eqs. (3.3 - 3.5) into eq. (3.6) gives :

$$c_{\varepsilon_0} = U_{s1}\left[\frac{\varepsilon_1^{\,3} + 3\varepsilon_0^{\,2}(1-\varepsilon_1)}{\varepsilon_1^{\,2}}\right] + W_1 \qquad (3.9a)$$

$$c_{\varepsilon_0} = U_{s1}\left[\frac{n(1-\varepsilon_0)\,\varepsilon_0^{\,n-1} - \varepsilon_0^{\,n} + \varepsilon_1^{\,n}}{\varepsilon_1^{\,n-1}}\right] + W_1 \qquad (3.9b)$$

Using the eqs. (3.5) (3.6) and (3.9) it is possible to write eq. (3.8) as :

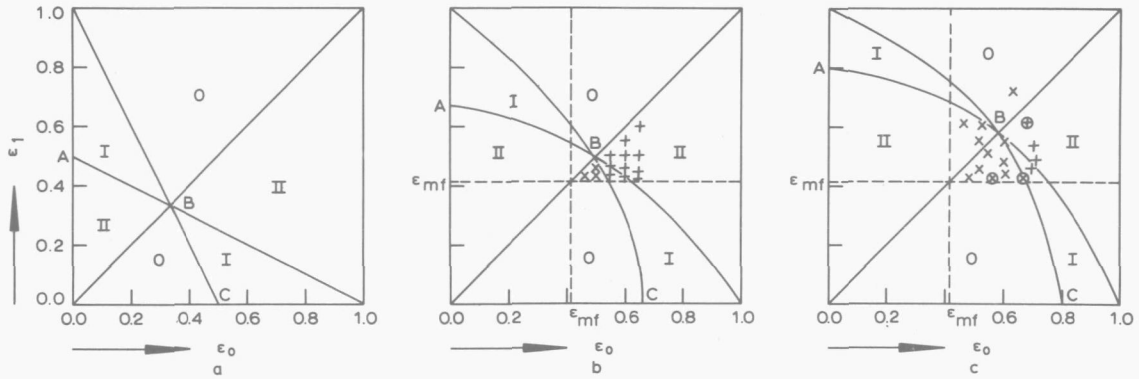

Figure 3.2 Stability regions of continuity shock waves
a : n = 2; b : n = 3; c : n = 3.85

0 $c_{\varepsilon 1} < c_{sh} < c_{\varepsilon 0}$; I $c_{\varepsilon 1} < c_{sh} > c_{\varepsilon 0}$; II $c_{\varepsilon 1} > c_{sh} > c_{\varepsilon 0}$

$$U_{s1}(3-2\varepsilon_1) + W_1 \gtrless U_{s1}\left[\frac{\varepsilon_1^{\,2}(1-\varepsilon_0) + \varepsilon_0^{\,2}(1-\varepsilon_1) + \varepsilon_1\varepsilon_0}{\varepsilon_1^{\,2}}\right] + W_1 \gtrless$$

$$\gtrless U_{s1}\left[\frac{\varepsilon_1^{\,3} + 3\varepsilon_0^{\,2}(1-\varepsilon_1)}{\varepsilon_1^{\,2}}\right] + W_1 \qquad (3.10a)$$

$$U_{s1}\, n(1-\varepsilon_1) + W_1 \gtrless U_{s1}\left[\frac{(1-\varepsilon_0)}{(\varepsilon_1-\varepsilon_0)}\,\frac{\varepsilon_1^{\,n} - \varepsilon_0^{\,n}}{\varepsilon_1^{\,n-1}}\right] + W_1 \gtrless$$

$$\gtrless U_{s1}\left[\frac{n(1-\varepsilon_0)\,\varepsilon_0^{\,n-1} + \varepsilon_1^{\,n} - \varepsilon_0^{\,n}}{\varepsilon_1^{\,n-1}}\right] + W_1 \qquad (3.10b)$$

Since only the absolute values of the velocities are compared eq. (3.10) can be written as :

$$3-2\varepsilon_1 \gtrless \frac{\varepsilon_1^2(1-\varepsilon_0) + \varepsilon_0^2(1-\varepsilon_1) + \varepsilon_1\varepsilon_0}{\varepsilon_1^{\,2}} \gtrless \frac{\varepsilon_1^3 + 3\varepsilon_0^2(1-\varepsilon_1)}{\varepsilon_1^{\,2}} \qquad (3.11a)$$

$$n(1-\varepsilon_1) \gtrless \frac{(1-\varepsilon_0)\left[\varepsilon_1^{\,n} - \varepsilon_0^{\,n}\right]}{(\varepsilon_1-\varepsilon_0)\,\varepsilon_1^{\,n-1}} \gtrless \frac{n(1-\varepsilon_0)\,\varepsilon_0^{\,n-1} + \varepsilon_1^{\,n} - \varepsilon_0^{\,n}}{\varepsilon_1^{\,n-1}} \qquad (3.11b)$$

The stability conditions given by eq. (3.11) can be represented in a $\varepsilon_0 - \varepsilon_1$ plot. Figure 3.2 shows three such plots, based on eq. (3.11b) for n = 2, n = 3 and n = 3.85. Figure 3.2 illustrates that the stability of a shock wave depends very strongly on the value of n. Depending upon the change in porosity, both expansion and contraction waves can be stable or unstable. Attenuation can only occur at both sides or behind the wave front. For low values of n the theoretically stable expansion waves and unstable contraction waves occur at lower porosities than physically possible. The indicated points in figure 3.2 have the characteristic

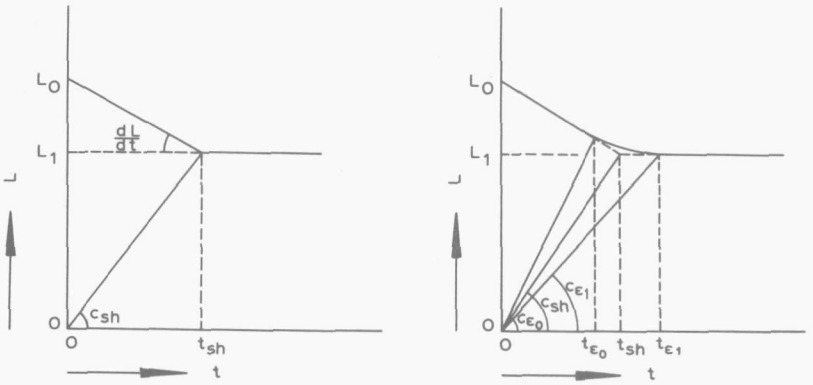

Figure 3.3 Response curves to a step decrease of the fluid velocity at time t = 0
a. stable shock wave ($c_{\varepsilon 1} > c_{sh} > c_{\varepsilon 0}$)
b. attenuating shock wave ($c_{\varepsilon 1} < c_{sh} < c_{\varepsilon 0}$)

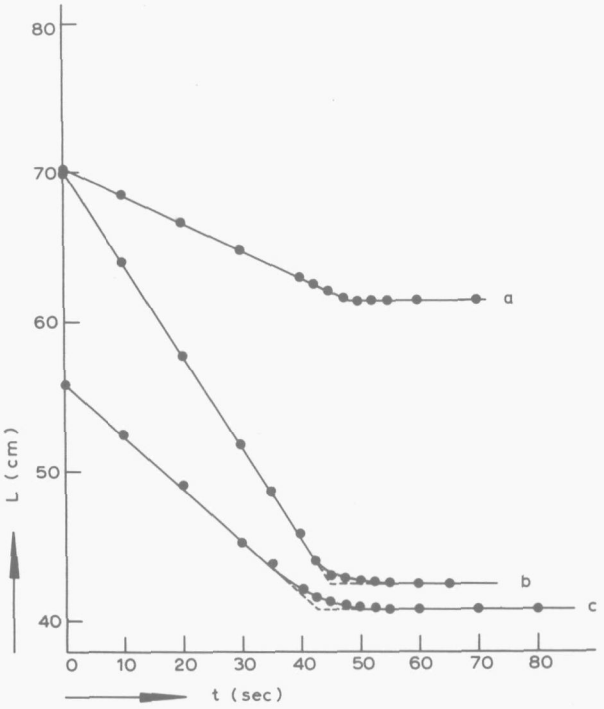

Figure 3.4 Experimental bed level response curves
a: region II; b: region I; c: region 0

values; A : $\varepsilon_0 = 0$, $\varepsilon_1 = (n-1)/n$; B : $\varepsilon_0 = \varepsilon_1 = (n-1)/(n+1)$ and C : $\varepsilon_0 = (n-1)/n$, $\varepsilon_1 = 0$.
Eq. (3.11a) only distinguishes between expansion and contraction waves; the former being stable and the latter being unstable. Since eq. (3.11a) is not valid above $\varepsilon = 0.8$ the result could be compared with the result of eq. (3.11b) for high values of n ($n/(n-1) > 0.8 \longrightarrow n > 5$). Although not incorrect, the results from (3.11a) are not very useful.

The predictions resulting from eq. (3.11b) have been checked experimentally by measuring the response of the bed level to a step change in the fluid velocity; similar to the experiments of Slis et al. (6) and Oltrogge (49). As a result of the sudden change in velocity a shock wave will rise up through the bed and reach the surface at $t = t_{sh}$. When the front of the shock wave is steep the time t_{sh} will coincide with the time at which the bed level comes to a rest and all particles will have found the new equilibrium position. For attenuating waves the bed level will gradually reach the final position. The boundaries of the transition region are given by $t_{\varepsilon 0}$ and $t_{\varepsilon 1}$; the times at which the fastest and the slowest porosity wave reach the surface of the bed. Two possibilities have been sketched in figure 3.3 for a decrease in fluid velocity at $t = 0$.

Two more phenomena are of importance in the experimental verification of the shock wave stability via bed level response measurements.

1. Level response curves to shock waves with attenuation at one side are sometimes hard to distinguish from those of stable shock waves, particularly when the difference between c_{sh} and $c_{\varepsilon 1}$ is small. Figure 3.4 gives characteristic experimental response curves for the three possible stability regions. The experimental conditions are indicated in figure 3.2c by open dots.
2. Only contraction waves can be used in the experiments. The stability of expansion waves can be distorted by other mechanisms. Rice and Wilhelm (50) and Volpicelli (51) have shown that a dense layer above a less dense layer in a fluidized system is unstable and phase inversion will occur.

The wave velocities given by the eqs. (3.5b) (3.6b) and (3.9b) can be written as ($W_1 = 0$) :

$$c_{\varepsilon 0} = \frac{n\,(1-\varepsilon_0)\,U_0}{\varepsilon_0} + (U_1 - U_0) \qquad (3.12)$$

$$c_{sh} = \frac{1-\varepsilon_0}{\varepsilon_1-\varepsilon_0}\,(U_1 - U_0) \qquad (3.13)$$

$$c_{\varepsilon 1} = \frac{n\,(1-\varepsilon_1)\,U_1}{\varepsilon_1} \qquad (3.14)$$

The response of the bed level can be calculated from the propagation velocity of the shock wave. A mass balance for the solids phase at time t reads :

$$t_0(1-\varepsilon_0) = c_{sh}(1-\varepsilon_1)t + (L-c_{sh}t)(1-\varepsilon_0) \qquad (3.15)$$

or $$\frac{dL}{dt} = c_{sh}\,\frac{\varepsilon_1-\varepsilon_0}{1-\varepsilon_0} \qquad (3.16)$$

Introducing eq. (3.13) into eq. (3.16) gives :

$$\frac{dL}{dt} = U_1 - U_0 \qquad (3.17)$$

It may be noted that eq. (3.17) results for any wave velocity. As long as the outflow is not affected by the change in velocity at the inlet of the system the mass balances for the two phases are :

$$\frac{d\,L(1-\varepsilon)}{dt} = (1-\varepsilon)\,\frac{dL}{dt} - L\,\frac{d\varepsilon}{dt} = 0$$

$$\frac{d\,L\varepsilon}{dt} = \varepsilon\,\frac{dL}{dt} + L\,\frac{d\varepsilon}{dt} = U_1 - U_0$$

Summation of the two equations above gives eq. (3.17). Only when in the experiments with a sharp transition in the bed level response curve the theoretical and experimental values of $\frac{dL}{dt}$ and t_{sh} agree, can be decided that the average values of c_{sh} is correctly given by eq. (3.13). The degree of

attenuation will be represented by the ratio $(t_{\varepsilon 1}-t_{\varepsilon 0})/t_{sh}$. The values of $t_{\varepsilon 1}$, t_{sh} and $t_{\varepsilon 0}$ can be obtained with the eqs. (3.12) - (3.14):

$$t_{\varepsilon 1} = \frac{\varepsilon_1 L_1}{n\,(1-\varepsilon_1)\,U_1} \tag{3.18}$$

$$t_{sh} = \frac{(\varepsilon_1-\varepsilon_0)\,L_1}{(1-\varepsilon_0)(U_1-U_0)} \tag{3.19}$$

$$t_{\varepsilon 0} = \frac{\varepsilon_0 L_0}{n(1-\varepsilon_0)\,U_0} = \frac{\varepsilon_0\,(1-\varepsilon_1)\,L_1}{n\,(1-\varepsilon_0)^2\,U_0} \tag{3.20}$$

$$\frac{t_{\varepsilon 1}-t_{\varepsilon 0}}{t_{sh}} = \frac{U_1-U_0}{n\,(\varepsilon_1-\varepsilon_0)}\left[\frac{\varepsilon_1(1-\varepsilon_0)}{U_1(1-\varepsilon_1)} - \frac{\varepsilon_0(1-\varepsilon_1)}{U_0(1-\varepsilon_0)}\right] \tag{3.21}$$

Two systems have been used in the experimental analysis. Glass beads / water; D_p = 300 μ; ρ_s = 2.96 g/cm^3; L_{pb} = 62 cm and polystyrene particles / alcohol; D_p = 900 μ; ρ_s = 1.02 g/cm^3; ρ_f = 0.79 g/cm^3; L_{pb} = 40 cm. The fluidization column used was a glass tube (D_t = 4.87 cm) with a sintered glass distributor. The values of n, obtained from a log U - log ε graph were resp. n = 3.01 and n = 3.85. The position of the level of the bed was indicated by a millimeter scale attached to the wall of the column and simultaneously the time was read on a chronometer. In table 3.2 the experimental and theoretical values of dL/dt, t_{sh} and $(t_{\varepsilon 1}-t_{\varepsilon 0})/t_{sh}$ have been compared. The experimental conditions (given by n, ε_0 and ε_1) are also indicated in figure 3.2. The experimentally sharp transitions are indicated with +, the gradual transitions with x. The values of ε_{mf} are also indicated.

The agreement between theory and experiment is evident. Eq. (3.11b) discriminates accurately between stable and attenuating waves. The velocity of c_{sh} given by eq. (3.13) is correct as well as the degree of attenuation given by (3.21). Eq. (3.11b) also explains the observation of Slis et al. (6) that expansion waves broadened and contraction waves remained

a steep front. The value of n in these experiments was about 2.5 and the porosities ranged from 0.5-0.9. When the change in velocity was negative the value of ε_0 was always larger than n-1/n and when the velocity change was positive ε_1 was larger than n-1/n (see figure 3.2). It can be concluded that the simple continuity wave concept describes the response of be bed level with sufficient accuracy and that eq. (3.8) accurately discriminates between stable and attenuating continuity shock waves.

TABLE 3.2

n	stability condition	ε_0	ε_1	$-\frac{dL}{dt}$ cm/sec		t_{sh} sec		$\frac{t_{\varepsilon 1}-t_{\varepsilon 0}}{t_{sh}}$	
				exp.	theor.	exp.	theor.	exp.	theor.
3.01	$C_{\varepsilon 1}>C_{sh}>C_{\varepsilon 0}$	0.65	0.60	0.57	0.60	21.2	22.6	-	-
			0.50	1.64	1.72	19.2	18.7	-	-
			0.44[5]	2.02	2.22	19.2	18.0	-	-
			0.42[5]	2.30	2.38	18.1	17.9	-	-
		0.60	0.55	0.59	0.60	18.6	17.5	-	-
			0.50	1.05	1.10	18.3	17.2	-	-
			0.46	1.40	1.43	17.9	17.1	-	-
			0.43	1.60	1.70	17.5	16.8	-	-
		0.55	0.50	0.48	0.50	17.0	17.0	-	-
		0.54	0.46	0.87	0.87	16.1	16.5	-	-
	$C_{\varepsilon 1}<C_{sh}>C_{\varepsilon 0}$		0.42	1.03	1.10	17.1	16.1	0.0	0.06
	$C_{\varepsilon 1}<C_{sh}<C_{\varepsilon 0}$	0.50	0.45[5]	0.36	0.43	15.8	16.2	0.12	0.12
			0.43	0.56	0.57	15.8	16.3	0.11	0.10
		0.46	0.43	0.18	0.18	16.7	17.3	0.04	0.03
3.85	$C_{\varepsilon 1}>C_{sh}>C_{\varepsilon 0}$	0.67	0.61	0.19	0.20	48	46	-	-
		0.70	0.53	0.59	0.65	49	45	-	-
		0.71	0.49	0.77	0.77	49	47	-	-
	$C_{\varepsilon 1}<C_{sh}>C_{\varepsilon 0}$	0.70	0.46	0.77	0.80	49	45	0.0	0.05
		0.67	0.43	0.69	0.71	45	45	0.22	0.22
	$C_{\varepsilon 1}<C_{sh}<C_{\varepsilon 0}$	0.62	0.44	0.46	0.47	44	43	0.23	0.24
		0.60	0.48	0.34	0.33	42[5]	42	0.13	0.13
		0.60[5]	0.55	0.19	0.18	46[5]	41[5]	0.10	0.02
		0.57	0.41	0.35	0.33	42[5]	45[5]	0.35	0.35
		0.55	0.51	0.10	0.10	42	43	0.05	0.04
		0.51[5]	0.45[5]	0.12	0.12	42[5]	45	0.18	0.18
		0.48	0.42	0.10	0.10	50[5]	49	0.24	0.21
		0.63	0.72	-0.35	-0.40	59	51[5]	(0.78)	
	$C_{\varepsilon 1}>C_{sh}>C_{\varepsilon 0}$	0.52[5]	0.61	-0.25	-0.26	44[5]	42[5]	(0.52)	
		0.51[5]	0.55	-0.11	-0.11	43	43	(0.21)	
		0.46	0.61	-0.35	-0.40	46[5]	42[5]	(0.65)	

3.3 The direction of the continuity wave

Only the usual systems with $\rho_s > \rho_f$ will be considered here, thus the slip velocity is directed upwards and is taken as positive.
Eq. (3.5) shows that in regular fluidized beds for which W is zero, the direction of the continuity wave is always positive. The same holds in flowing fluidized beds for which $W > 0$. In flowing fluidized beds with $W < 0$ the wave velocity can become negative. The solids velocity at which this occurs will be called W_c.
The knowledge of the direction of c_{sh} is important because the motion of the waves enables the 'end conditions' to be propagated throughout the system (43) and at W_c the side governing the behaviour of a fluidized bed changes.
The value of W_c can be evaluated from eq. (3.5) for $c_{sh} = 0$.

$$-W_c = \left[\frac{\varepsilon_1^{\,2}(1-\varepsilon_0) - \varepsilon_0^{\,2}(1-\varepsilon_1) + \varepsilon_0\varepsilon_1}{\varepsilon_1^{\,2}} \right] U_{s_1} \qquad (3.12a)$$

$$-W_c = \left[\frac{(1-\varepsilon_0)\quad (\varepsilon_1^{\,n}-\varepsilon_0^{\,n})}{(\varepsilon_1-\varepsilon_0)\quad \varepsilon_1^{\,n-1}} \right] U_{s_1} \qquad (3.12b)$$

For small amplitudes ($\varepsilon_1 \longrightarrow \varepsilon_0$) eq. (3.12) can be written as :

$$-W_c = (3-2\varepsilon)\, U_s \qquad (3.13a)$$

$$-W_c = n\,(1-\varepsilon)\, U_s \qquad (3.13b)$$

Eq. (3.13) also follows from eq. (3.6).

3.4 The dynamic wave velocity

In the concept of the continuity wave inertia effects are neglected and the waves are treated as quasi steady state phenomena. This approach is unable to account for the acceleration which must take place across the wave front.
The mechanism producing this acceleration is the force caused by the concentration gradients. Waves based on this mechanism will be called dynamic or elastic waves.

Familiar examples of dynamic waves are sound waves and waves in elastic solids. When the solid obeys Hooke's law the velocity of the elastic wave is given by

$$c_e = \sqrt{\frac{e}{\rho_s}} \qquad (3.14)$$

e = modulus of elasticity.

Dynamic waves always occur within the structure of continuity waves and are the mechanism whereby the signal is transmitted to particles ahead so that adjustments in velocity can be made. Therefore, when the continuity wave velocity exceeds the dynamic wave velocity instability will occur; the response of the particles being insufficiently rapid. The result is the formation of dynamic shock waves.
The dynamic wave velocity in fluidized systems is difficult to calculate. The main problem is that the drag in unsteady flow is not known. Verloop and Heertjes (56) suggest a solution for the case of small amplitudes. They assume that the main fluid flow is unaffected by a small local porosity gradient. They apply the experimental relation of Rowe (8) to describe the relation between drag and the change in porosity, given as the dimensionless interparticle distance d in eq. (2.4).The wavelength has been taken as one particle diameter. A fluidized system can then be regarded as an elastic solid obeying Hooke's law. For low porosities the value of e can simply be derived from eq. (2.4) :

$$e = \frac{2\, D_p\, g\, (\rho_s - \rho_f)}{3\, d} \qquad (3.15)$$

This value substituted in eq. (3.14) gives for the velocity of the elastic waves :

$$c_e = \sqrt{\frac{4\, D_p\, g}{\pi\, d}} \qquad (3.16)$$

Introducing the value of $d = 10^{-2}$ as given by Rowe for minimum fluidization conditions and the linear relations between drag and velocity for laminar flow eq. (3.16) can also be written as :

$$c_e = \sqrt{\frac{400\, U_{mf}}{\pi\, U}\, D_p\, g} \qquad (3.17)$$

Wallis (59) used a similar approach. He assumed that the drag forces in accelerating flow obey similar relations as in the steady state flow. The dynamic wave velocity can then be expressed as :

$$c_e = f(\varepsilon, Re)\sqrt{D_p g \frac{\rho_s - \rho_f}{\rho_s}} \qquad (3.18)$$

D_p has been introduced in eq. (3.18) to make the concentration-gradient dimensionless. The factor $(\rho_s-\rho_f)/\rho_s$ has been included because only the frictional drag and not the buoyancy is perturbed. Wallis obtains a very approximate value of $f(\varepsilon,Re)$ from the experimental results of Rowe and Henwood (33).

The drag on a particle in the downstream layer is 1.35 times the drag on a particle within the assembly and the drag on a particle in the upstream layer about 0.5. From these values Wallis assumes $f(\varepsilon, Re)$ to be approximately 1. For minimum fluidization conditions eq. (3.18) becomes then :

$$c_{ds} = \sqrt{gD_p(\rho_s-\rho_f)/\rho_s} \qquad (3.19)$$

The derivation of eq. (3.19) has been based by Wallis on $\Delta\varepsilon\sim\frac{1}{2}$; eq. (3.19) therefore represents a dynamic shock wave velocity. It can be seen from the eqs. (3.17) and (3.19) that the dynamic shock velocity and the 'small wave' velocity differ by a factor of about 10. This is quite reasonable. The dimensionless groups, however, should be the same. The factor $(\rho_s-\rho_f)/\rho_s$ would appear in eq. (3.16/17) when the mass of the particles had not been represented by $1/6\ \pi\ D_p^3\ (\rho_s-\rho_f)$ but by $1/6\ \pi\ D_p^3\ \rho_s$. Wallis uses a formal argument to introduce the group $(\rho_s-\rho_f)/\rho_s$.
Since eq. (3.19) has been derived for minimum fluidization conditions it does not contain a dimensionless group to account for the influence of the fluid velocity or the interparticle distance.
It is very hard to check the eqs. (3.17) or (3.19) experimentally. It is virtually impossible to measure the velocity of dynamic waves directly. They either attenuate and disappear or grow into shocks depending on the continuity wave velocity (59). This latter phenomenon indicates that eq. (3.17) predicts the correct order of magnitude (56, chapter 5). Wallis has attempted to test eq. (3.19). A mass of particles in a vertical tube was packed against a porous roof by a high fluid flow. When the fluid flow is reduced below $U \sim 2U_{mf}$ the particles start to rain down. During the raining-off a sharp transition is maintained between the packed and the falling

particles. The front velocity V_F depends on the fluid velocity. Wallis considers the front as a plane dynamic shock wave; its velocity given by eq. (3.19).
When this concept is correct, a plot of V_F/c_{ds} against U/U_{mf} should pass through the point (1.1) as observed experimentally for a number of systems. It may be noted that eq. (3.16) probably also could be used to estimate c_{ds} or V_F. The porosities occurring behind the front are high. Eq. (3.16) with $d \sim 1$ gives approximately the same value as eq. (3.19) for the dynamic shock wave velocity.

3.5 Conclusions

1. Usually it is acceptable to treat a porosity wave as a steady state phenomenon. The limit of this approach is given by the dynamic wave velocity.
2. The attenuation of a continuity shock wave is governed by the relation $c_{\varepsilon 1} \geq c_{sh} \geq c_{\varepsilon 0}$.

4 VIBRATIONS

4.1 The dynamics of vibrating systems

In this section the general equations describing a vibrating system will be discussed and the equations for the frequency will be derived. The simplest mechanical system is a mass m with one degree of freedom, which means that its location at any time is specified by the one coordinate x.
The equation of motion can be written as (52) :

$$m \frac{d^2x}{dt^2} = F_r + F_d + F_{(t)} \qquad (4.1)$$

F_r is the restoring force; it is always directed toward the equilibrium position of the system.
F_d is the damping force; its direction is always such that it opposes the motion of the system.
$F_{(t)}$ is the exciting force; it is the externally applied force that causes the motion of the system. As only free vibrating systems will be considered $F_{(t)}$ can be taken as zero. For small displacements F_r is usually assumed to be linear in x.

$$F_r = -K_r x \qquad (4.2)$$

For non-linear vibrations no general solution of a simple form have been obtained. Damping can be caused by many different mechanisms. It is usually sufficient to consider two cases (53).

1) The damping force is constant (Coulomb damping)

2) The damping is linearly proportional to the velocity of the mass (viscous damping).

The first damping mechanism is not important for the case at hand. In fluidized systems Coulomb damping can be caused by interpartical forces and solids-wall friction. These forces will not be taken into account, (see chapter 2) and furthermore, this damping mechanism does not alter the frequency (54), the parameter of interest.
The viscous damping force is related to the velocity via :

$$F_d = -K_d \frac{dx}{dt} \qquad (4.3)$$

With the relations (4.2) and (4.3) eq.(4.1) can be written as:

$$m \frac{d^2x}{dt^2} = - K_r x - K_d \frac{dx}{dt} \qquad (4.4)$$

And upon introducing $p^2 = \frac{K_r}{m}$ and $2q = \frac{K_d}{m}$ as :

$$\frac{d^2x}{dt^2} + 2q \frac{dx}{dt} + p^2 x = 0 \qquad (4.5)$$

For a system without damping (q = 0) a solution of eq.(4.5) is :

$$x = A \sin \omega t \qquad (4.6)$$

Herein is : ω = the cyclic frequency
A = the amplitude

Eq.(4.6) is the description of a simple harmonic vibration. The frequency, the number of cycles per second, is

$$\nu = \frac{\omega}{2\pi} = \frac{p}{2\pi} = \frac{1}{2\pi} \sqrt{\frac{K_r}{m}} \qquad (4.7)$$

The potential energy of the system at any position is $E_{pot} = \frac{1}{2} K_r x^2$ and the kinetic energy is $E_{kin} = \frac{1}{2} m(dx/dt)^2$. In the case without damping there is no energy dissipation and the sum of E_{pot} and E_{kin} must be constant. The following can be deduced :

$$x = 0;\ E_{pot} = 0, \qquad E_{kin} = \tfrac{1}{2} m \omega^2 A^2$$
$$x = A;\ E_{pot} = \tfrac{1}{2} K_r A^2, \quad E_{kin} = 0$$

and therefore

$$\tfrac{1}{2} K_r A^2 = \tfrac{1}{2} m \omega^2 A^2 \longrightarrow \omega^2 = \frac{K_r}{m} \qquad (4.8)$$

For damped vibrations a solution of eq. (4.5) is :

$$x = A\, e^{-qt} \cos \sqrt{p^2 - q^2}\, t \qquad (4.9)$$

and

$$\nu = \frac{1}{2\pi} \sqrt{p^2 - q^2} \quad \text{if } p^2 > q^2 \qquad (4.10)$$

If $p^2 \leqslant q^2$ no vibration occurs, the system is overdamped and the initial displacement decays exponentially.
The effect of damping is (compare eq. (4.6) and eq. (4.9)) to increase the period of vibration and to decrease the amplitude exponentially with the time. A measure of damp-

ing is the ratio of the amplitudes of successive cycles, usually given as the logarithmic decrement δ :

$$\delta = \ln \frac{A_j}{A_{j+1}} = \ln \exp. \sqrt{\frac{2\pi q}{p^2 - q^2}} = \sqrt{\frac{2\pi q}{p^2 - q^2}} \qquad (4.11)$$

When the damping is small δ can be written as :

$$\delta = \ln \frac{A + \Delta A}{A} \sim \frac{\Delta A}{A} \qquad (4.12)$$

The energy lost per cycle ΔE can be expressed in δ. The total energy of the system is equal to the potential energy for x = A.

$$E_j = \tfrac{1}{2} K_r A^2$$

One cycle later : $E_{j+1} = \tfrac{1}{2} K_r (A - \Delta A)^2$

$$\Delta E = E_{j+1} - E_j = K_r A . \Delta A$$

$$\frac{\Delta E}{E} = \frac{K_r A \ \Delta A}{\tfrac{1}{2} K_r A^2} = \frac{2 \Delta A}{A} \sim 2 \delta \qquad (4.13)$$

For complicated problems it is often more convenient to obtain approximate frequencies via the energy method, as used for eq. (4.8). The motion has to be approximately harmonic and the damping negligeable.
As an example, the vibration frequency of an elastic bar of unit cross section, and length L (54) will be derived, see figure 4.1. This system has not one but infinite degrees of freedom as each element has a different displacement.

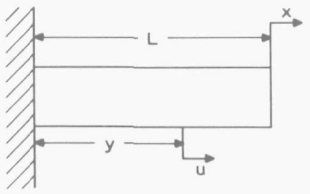

Figure 4.1 The displacements of an elastic bar

The displacement at y is $u = yx/L$, when x is the total displacement of the bar. The energies of the bar at a given displacement are :

$$E_{pot} = \int_0^L \tfrac{1}{2} K_r L\left(\frac{du}{dy}\right)^2 dy = \tfrac{1}{2} K_r x^2 \qquad (4.14)$$

$$E_{kin} = \frac{1}{L} \int_0^L \tfrac{1}{2} m \left(\frac{y}{L} \frac{dx}{dt}\right)^2 dy = \frac{1}{6} m \left(\frac{dx}{dt}\right)^2 \qquad (4.15)$$

From the eqs. (4.6) (4.14) and (4.15) follows :

$$1/6\ m A^2\omega^2 = \tfrac{1}{2} K_r A^2$$

$$\omega = \sqrt{\frac{K_r}{3m}}$$

The frequency of an elastic bar is $1/3\sqrt{3}$ of the frequency of mass with one degree of freedom.
In the case of a pure elastic bar holds that the restoring force is proportional to the relative displacement (x/L or u/y). If, however, F_r is proportional to the absolute displacement, a quasi -elastic system, then the potential energy becomes :

$$E_{pot} = \frac{1}{L} \int_0^L \tfrac{1}{2} K_r u^2 dy = 1/6\ K_r x^2 \qquad (4.16)$$

The kinetic energy remains the same, thus the frequency of a quasi-elastic system is :

$$\nu = \frac{\omega}{2\pi} = \frac{1}{2\pi} \sqrt{\frac{K_r}{m}} \qquad (4.17)$$

This frequency is identical to the frequency of a solid mass with one degree of freedom.

4.2 Vibrations in a fluidized system

4.2.1 The frequency

Hiby (55) observed spontaneous vertical oscillations in very shallow gas fluidized beds. The frequency was calculated from the quasi-elastic forces exerted by the fluid flow on a particle displaced from its equilibrium position. Hiby calculates

the total lifting forces of the gas flow from the Ergun equation and divides this total force by the number of particles present to obtain a force balance per particle.
Assuming that during the oscillation the voidage is only a function of time and not of the height coordinate y in the bed, the frequency ω_j of a particle j at height y_j can be calculated :

$$\omega_j^2 = \frac{3}{\rho_s y_j}\left[150\,\frac{U\,\mu}{D_p^2}\,\frac{(1-\varepsilon)(3-2\varepsilon)}{3\varepsilon^4} + 1.75\,\frac{\rho_f U^2}{D_p}\,\frac{(1-\varepsilon)}{\varepsilon^4}\right] \qquad (4.18)$$

However, eq. (4.18) shows the frequency to be dependent on the height coordinate. This result invalidates the assumption that all particles oscillate in tune ($\varepsilon \neq f(y)$). However, Hiby assumes that this discrepancy has only little effect on the frequency. To obtain a value for the average frequency each natural frequency ν_y was given a weight proportional to its amplitude A_y.

$$\bar{\nu} = \frac{\int_0^L \nu_y A_y dy}{\int_0^L A_y dy} = 4/3\ \nu_L \qquad (4.19)$$

This method gives the average frequency as 4/3 times the frequency of the top layer. From eq. (4.18) Hiby concluded that the frequency is independent of ρ_s and varies with U and D_p as $\nu \equiv U^{-0.3}$; $\nu \equiv D_p^{-1}$ in the laminar flow region and as $\nu \equiv U^{-1}$; $\nu \equiv D_p^{-0.5}$ under turbulent flow conditions.
The experiments of Hiby show that the frequency varies approximately with $L^{-0.5}$ and $D_p^{-0.3}$ (erroneously given as $D_p^{-0.8}$) and is independent of ρ_s and U.
There are a few deficiences in Hiby's theory.

1. The predicted relationship between U and ν deviates considerably from the experimental results.
2. There is a discrepancy between the assumption and the results. The particles motion is assumed to be coherent and the theory predicts an incoherent motion. Furthermore the 'valve-action' of the particles is assumed to be the driving mechanism for the oscillation, the necessary energy taken from the fluid flow. This means a higher energy-loss of the fluid flow in an oscillating system as compared to a non-oscillating system. This makes it less likely that spontane-

ous oscillations will occur.
3. The average frequency has been obtained in an arbitrary way.
4. The damping has been neglected.

For these reasons Hiby's model will be amended. The following assumptions have been made :

1. All particles move in phase. The system will be treated as a quasi-elastic continuum. The boundary condition for this assumption will be discussed in section 4.2.2.
2. Not the superficial but the slip velocity is assumed to be constant. Thus the gas moves in phase with the solids. This assumption is based on the damping characteristics as discussed in section 4.2.3.
3. The flow is assumed to be laminar.

At equilibrium conditions the pressure drop caused by friction across a fluidized bed is (eq. (2.2)) :

$$\Delta P_0 = \frac{200\ \mu\ U_s}{D_p^2} \left(\frac{1-\varepsilon}{\varepsilon}\right)^2 L = (1-\varepsilon)(\rho_s-\rho_f)\ g\ L \qquad (4.20)$$

When the height of the bed is altered by -x and thereby the porosity with $-\Delta\varepsilon$, the pressure drop will be :

$$\Delta P_x = \frac{200\ \mu\ U_s}{D_p^2} \left(\frac{1-\varepsilon+\Delta\varepsilon}{\varepsilon-\Delta\varepsilon}\right)^2 (L-x) \qquad (4.21)$$

The relation between $\Delta\varepsilon$ and x is given by the mass balance for the solid phase :

$$L(1-\varepsilon) = (L-x)(1-\varepsilon+\Delta\varepsilon) \qquad (4.22)$$

For small values of x :

$$\Delta\varepsilon = \frac{x}{L}(1-\varepsilon) \qquad (4.23)$$

Using eq. (4.23) $\Delta\varepsilon$ can be eliminated from eq. (4.21)

$$\Delta P_x = \frac{200\ \mu\ U_s}{D_p^2} \left(\frac{1-\varepsilon}{\varepsilon}\right)^2 L \left[1 + \frac{(2-\varepsilon)}{\varepsilon}\frac{x}{L}\right] \qquad (4.24)$$

The reduction in height and porosity causes an increase in

in pressure drop. The difference in pressure drop is :

$$\Delta P_x - \Delta P_0 = \Delta P_r = \frac{200\ \mu\ U_s}{D_p^2} \left(\frac{1-\varepsilon}{\varepsilon}\right)^2 \left(\frac{2-\varepsilon}{\varepsilon}\right) x \qquad (4.25)$$

or via eq. (4.20) :

$$\Delta P_r = (1-\varepsilon)\ (\rho_s-\rho_f)\ g\ \frac{2-\varepsilon}{\varepsilon}\ x \qquad (4.26)$$

Eq. (4.26) shows that the restoring force is linearly proportional to the absolute displacement and therefore the vibration will be harmonic.
The constant K_r for a fluidized system is :

$$K_r = (1-\varepsilon)(\rho_s-\rho_f)\ g\ \left(\frac{2-\varepsilon}{\varepsilon}\right) \qquad (4.27)$$

The system can now be treated as a quasi-elastic system with $F_r = -K_r x$ and the frequency can be calculated with eq. (4.17);

$$\nu = \frac{1}{2\pi}\sqrt{\frac{K_r}{m}} = \frac{1}{2\pi}\sqrt{\frac{(1-\varepsilon)\ (\rho_s-\rho_f)\ g\ \left(\frac{2-\varepsilon}{\varepsilon}\right)}{\left[(1-\varepsilon)\ \rho_s + \varepsilon\ \rho_f\right] L}} \qquad (4.28)$$

For $\rho_s >> \rho_f$, as in fact has been assumed for the damping has been neglected (see section 4.2.3), eq. (4.28) reduces to :

$$\nu = \frac{1}{2\pi}\sqrt{\frac{g\ (2-\varepsilon)}{L\ \varepsilon}} \qquad (4.29)$$

The frequency is not very sensitive to the condition of laminar flow. For the fully turbulent region Leva (3) proposes :

$$\Delta P \equiv \left(\frac{1-\varepsilon}{\varepsilon^2}\right).$$

In this case the frequency becomes :

$$\nu = \frac{1}{2\pi}\sqrt{\frac{2g\ (1-\varepsilon)}{L\ \ \varepsilon}} \qquad (4.29a)$$

Eq. (4.29a) predicts a slightly lower frequency than eq. (4.29).

When the expansion characteristics of the system are known

and can be represented by the Richardson-Zaki equation, the frequency can more precisely be described by the equation :

$$\nu = \frac{1}{2\pi}\sqrt{\frac{g}{L}\,\frac{(n-1)\,(1-\varepsilon)}{\varepsilon}} \qquad (4.29b)$$

However, for gas fluidized beds of coarse particles n cannot be determined from a U-ε plot, as bubbling will occur. Although phenomenologically quite different the eqs. (4.29) and (4.19) are very similar. If the Leva correlation instead of the Ergun equation had been used Hiby's prediction had been:

$$\bar{\nu} = \frac{1}{2\pi}\,\frac{4}{3}\sqrt{\frac{g\,(3-2\varepsilon)}{L\,\varepsilon}} \qquad (4.30)$$

Eq. (4.19) is difficult to interpret and has lead Hiby to erroneous conclusions. Eq. (4.29) shows that the frequency is independent of ρ_s and D_p. The influence of the gas velocity is small. A doubling of the velocity changes the porosity about 0.1 and reduces the frequency with about 20 %. In figure 4.2 the frequencies measured by Hiby are given as a function of L.

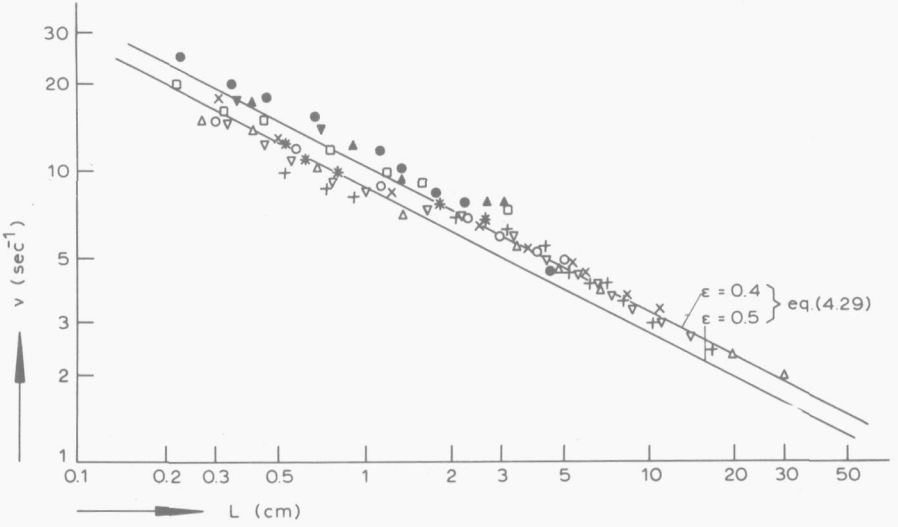

Figure 4.2 ν as a function of L for the experiments of Hiby (55)

●bronze spheres : 0.2-0.25 mm; + glass beads : 0.9-1.2 mm; ★ glass beads : 0.75-1.0 mm; x glass beads : 0.5-0.75 mm; ▲ glass beads : 0.4-0.5 mm; ▼glass beads : 0.3-0.4 mm; ▽ quartz sand : 1.0-1.2 mm; △ quartz sand : 0.6-0.75 mm; o quartz sand : 0.5-0.6 mm; □ quartz sand : 0.3-0.5 mm.

The lines in figure 4.2 are those predicted by eq.(4.29). The experimental porosities are not known but will probably be between 0.4 and 0.5. The solids density varies from 2 to 8 g/cm^3, the particle diameter from 0.2 to 1.2 mm and the relative gas velocity U/U_{mf} from 1.1 to 2.6. Figure 4.2 clearly shows that eq. (4.29) predicts the frequencies very well. The influence of U and ε on the frequency will be discussed in more detail in section 4.3.3.

4.2.2 The maximum height

For the calculation of the frequency it has been assumed that all the particles move in phase. This assumption is only valid when the fluidized bed is not too high. The particles can only move in phase when the porosity wave can reach the end of the system in a half period. The critical height L_c is given by

$$L_c = c_\varepsilon \cdot \tfrac{1}{2}T = \frac{c_\varepsilon}{2\nu} \qquad (4.31)$$

T is the period of a cycle. If eq. (3.7a) is adopted as a good approximation of the wave velocity, L_c can be written as :

$$L_c = \frac{U^2}{g}\,\frac{\pi^2(3-2\varepsilon)^2}{\varepsilon(2-\varepsilon)} \rightarrow \frac{U^2}{gL_c} = \frac{\varepsilon(2-\varepsilon)}{\pi^2(3-2\varepsilon)^2} \qquad (4.32)$$

As the wave velocity cannot increase unlimitedly, the critical bed height also has a maximum. L_{cM} can be calculated from eq. (4.31) and eq. (3.16/17) :

$$L_{cM} = \frac{c_e}{2\nu} = \frac{4\,\pi\,\varepsilon\,D_p}{(2-\varepsilon)\,d} = \frac{400\,\pi\,\varepsilon}{(2-\varepsilon)}\,\frac{U_{mf}}{U}\,D_p \qquad (4.33)$$

Eq. (4.33) shows that L_{cM} is in the order of a few hundred particle diameters ($\sim 300\ D_p$).

When the height of the bed surpasses L_c the system cannot be considered as an apparent one degree of freedom system, but should be treated as a system of a higher order. A number of frequencies are then possible.
Experimentally the effect of passing L_c is quite clear. Gradually the vibrations become more irregular, less sinusoidal, and the frequency no longer decreases with $L^{-0.5}$. Visually the bed starts to separate at $L \sim L_c$, voids are formed which grow in size with increasing gas velocity and bed height, and bubbles or slugs are formed. This void formation is much

stronger in systems where the critical bed height is given by eq. (4.33). In these systems the waves themselves form voids, because they are dynamic shock waves. Sometimes these voids form slugs for $L < L_{cM}$ which results in a decrease in frequency.
It is not easy to confirm eq. (4.32) experimentally, due to the strong dependency of L_c on U. An increase in particle diameter of $\sqrt{2}$ increases L_c with a factor 4. Therefore most systems with $L_c < L_{cM}$ have a critical height smaller than 1 cm, allowing only qualitative observations.
The particles available for a proper determination of L_c were glass beads with D_p = 320 - 420 μ. At a gas velocity of 12 cm/sec and a porosity of 0.55 harmonic vibrations were obtained till a height of 6 cm. Above that height the pressure fluctuations became irregular. Eq. (4.32) predicts a value of 6.5 cm. The phenomena described above strongly suggest that a gas fluidized bed can only fluidize homogeneously for $L \lesssim L_c$. Most fluidized beds are operated with $L >> L_c$. These fluidized beds will be heterogeneous; the voids being formed by the oscillation of the bottom layer. This mechanism has also been proposed by Hiby (55) who showed that the bottom layer of a deep bed oscillated with a frequency given by eq. (4.29) while the pressure fluctuations of the total bed had a much lower frequency, due to the bubbles. Hiby supports his opinion with a photo showing that bubbles are formed periodically and not at random. Furthermore all experimental evidence indicates that bubbles originate at the bottom of the bed in gas fluidized systems.

4.2.3 The damping

In section 4.2.1 the frequency has been derived assuming U_s = constant, instead of U = constant. Neglecting damping effects the theoretical frequencies are :

$$\text{for } U_s = \text{constant} : \nu = \frac{1}{2\pi}\sqrt{\frac{g\ (2-\varepsilon)}{L\quad \varepsilon}}$$

$$\text{for } U = \text{constant} : \nu = \frac{1}{2\pi}\sqrt{\frac{g\ (3-2\varepsilon)}{L\quad \varepsilon}}$$

On the basis of the experimental frequencies it is not possible to decide which assumption is the best since neither the experimental porosities, nor the expansion characteristics can be determined with sufficient accuracy.
However, the theoretical damping effects differ considerably for the two assumptions. When the superficial velocity is assumed to be constant the damping is such that no oscillat-

ion could occur in any fluidized bed. The assumption of constant slip velocity correctly discriminates between vibrating and non-vibrating systems. Furthermore, it is very probable that the gas phase oscillates; during the experiments the rotameters moved in phase with the fluidized bed. The damping will be analyzed below.

4.2.3a The damping for constant slip velocity

In order to keep U_s constant in an oscillating fluidized bed the fluid has to be accelerated and decelerated each half cycle. The change in velocity of the fluid is equal to the solids velocity; $U_s = U_i - W$ = constant. The 'kinetic energy of vibration' stored in the fluid cannot be recovered, but will leave the system. The damping can be calculated according to eq. (4.13) from the relative loss of energy.

$$\frac{\Delta A}{A} = \frac{\Delta E}{2E} \approx \frac{\text{loss of fluid mass}}{\text{total mass of the system}} =$$

$$= \frac{\rho_f U T}{2\left[(1-\varepsilon)\rho_s + \varepsilon\rho_f\right]L} = \frac{\rho_f U}{2\left[(1-\varepsilon)\rho_s + \varepsilon\rho_f\right]\nu L} \qquad (4.34)$$

Substituting eq. (4.29) into eq. (4.34) gives :

$$\frac{\Delta A}{A} = \frac{\pi \rho_f}{(1-\varepsilon)\rho_s + \varepsilon\rho_f}\sqrt{\frac{\varepsilon}{2-\varepsilon}\frac{U^2}{gL}} \qquad (4.35)$$

To obtain an impression of the importance of the damping, it is convenient to eliminate the factor U^2/gL. This can be done by considering the damping at critical conditions. Substitution of eq. (4.32) gives :

$$\left(\frac{\Delta A}{A}\right)_c = \frac{\rho_f}{(1-\varepsilon)\rho_s + \varepsilon\rho_f}\left(\frac{\varepsilon}{3-2\varepsilon}\right) \qquad (4.36)$$

With $\varepsilon = 0.5$ the value of $\left(\frac{\Delta A}{A}\right)_c = \frac{\rho_f}{2(\rho_s + \rho_f)}$

Thus in gas fluidized beds the damping can be neglected, but for liquid fluidized beds the damping is considerable. This can explain our experimental observation that in water fluidized beds no oscillations occurred with a frequency in the same order as predicted by eq. (4.29). The densest solids tested were copper particles.
This result combined with the proposed mechanism for bubble formation in section (4.2.2) explains why liquid fluidized beds are more stable than gas fluidized beds. The severe damping prevents the oscillation of the bottom layer of the bed. This concept can also illustrate the influence of the pressure on the stability of gas fluidized beds. The damping is governed by the ratio ρ_f/ρ_s. Increasing the pressure can decrease this ratio so much that the damping becomes too severe. Some quantitative data can be obtained from the experiments of Leung (15). Hollow phenolic micro balloons (ρ_s = 0.24 g/cm^3) were fluidized with carbon dioxide. At atmospheric pressure bubbling occurred; at 48 at. the system fluidized smoothly. The fluid density ρ_f increased from 0.0016 to 0.107 g/cm^3. It can be derived from eq. (4.36) and ε = 0.5 that the damping increased from $(\Delta A/A)_c$ = 0.0033 to $(\Delta A/A)_c$ = 0.16. At atmospheric pressure the damping is negligible; at 48 at. the damping is very large.

4.2.3b The damping for constant superficial velocity

To calculate the effect of the damping for U = constant the fluidized bed will be treated as a system with one degree of freedom instead of a quasi-elastic system with a multiple number degrees of freedom. This seems acceptable because both methods give the same frequency, due to the fact that the restoring force is proportional to the absolute displacement. In that case E_{pot} is averaged over absolute displacements and E_{kin} over absolute velocities. The damping force is also proportional to the absolute solids velocity. As the following calculations are only approximative the effect of the variation in ε has not been taken into account. Therefore the results derived also hold for the assumption of constant interstitial velocity.

From eq. (2.2) can easily be derived that for U = constant K_r becomes :

$$K_r = (1-\varepsilon)(\rho_s-\rho_f)\, g\, \frac{3-2\varepsilon}{\varepsilon} \qquad m = (1-\varepsilon)(\rho_s-\rho_f)\, L$$

and $$p^2 = \frac{3-2\varepsilon}{\varepsilon}\, \frac{g}{L}$$

The restoring force F_r is larger for U = constant than for U_s = constant. However, the fluid will now exert a damping force F_d opposing the motion of the solids. The drag force on a swarm of accelerating particles is not known, therefore an approximate value of F_d will be calculated from the steady state relations. This is a similar approach to that applied in chapter 3 for the wave velocity.

For the damping force per unit area can be obtained from eq. (4.20) :

$$F_d = \frac{200\ \mu\ W}{D_p^2}\ \frac{(1-\varepsilon)^2}{\varepsilon^2}\ L = (1-\varepsilon)(\rho_s-\rho_f)\ g\ L\ \frac{W}{U/\varepsilon}$$

Thus $K_d = (1-\varepsilon)\ (\rho_s - \rho_f)\ g\ L\ \frac{\varepsilon}{U} = \frac{m\ g\ \varepsilon}{U}$ $\qquad 2q = \frac{K_d}{m}$

and $2q = \frac{g\varepsilon}{U}$ or $q^2 = \frac{g^2\ \varepsilon^2}{4\ U^2}$

The frequency according to eq. (4.10) is :

$$\nu = \frac{1}{2\pi}\ \sqrt{\frac{g(3-2\varepsilon)}{\varepsilon L} - \frac{g^2\varepsilon^2}{4\ U^2}} \qquad (4.37)$$

According to eq. (4.11) the damping can be written as :

$$\frac{A_j}{A_{j+1}} = \exp.\ \frac{2\pi q}{\sqrt{p^2-q^2}} = \exp.\ \frac{2\ \pi}{\sqrt{p^2/q^2-1}} =$$

$$= \exp.\ \frac{2\ \pi}{\sqrt{\frac{U^2}{gL}\ \frac{4\ (3-2\varepsilon)}{\varepsilon^3} - 1}} \qquad (4.38)$$

To eliminate U^2/gL the damping will be considered under critical conditions, as given by eq. (4.32).

$$\left(\frac{A_j}{A_{j+1}}\right)_c = \exp.\ \frac{2\ \pi}{\sqrt{\frac{4\ (2-\varepsilon)}{\pi^2\ \varepsilon^2(3-2\varepsilon)} - 1}} \qquad (4.39)$$

For $\varepsilon = 0.5$ the damping is $\left(\frac{A_j}{A_{j+1}}\right)_c = e^{14}$. This damping is so high that any oscillation will immediately become unmeasurably small. The system will be overdamped for :

$$\frac{4\ (2-\varepsilon)}{\pi^2\varepsilon^2\ (3-2\varepsilon)} \lesssim 1 \quad \text{or} \quad \varepsilon \gtrsim 0.55.$$

These calculations may suffice to conclude that the assumption of a constant U_s is better than a constant U. The results also show that if the assumption of a constant U_s is not strictly valid, the damping will increase rapidly. It may be noted that the assumption of constant slip velocity does not violate the continuity condition. This can be shown by integrating the product of interstitial velocity and porosity over a full cycle. During the oscillation the gas velocity and the porosity are out of phase by $\pi/2$. The average superficial velocity over a cycle is :

$$\overline{U} = \frac{1}{2\pi} \int_0^{2\pi} (U_i \varepsilon)\ d\ \varphi$$

$$= \frac{1}{2\pi} \int_0^{2\pi} (U_{io} + A_{u_i} \sin (\phi - \pi/2)\ (\varepsilon_o + A_\varepsilon \sin \phi)\ d\phi$$

$$= U_{io}\ \varepsilon_o$$

$$= U.$$

The index o denotes the value for a non-oscillating system.

Furthermore, it can be shown that the average pressure drop across an oscillating fluidized bed is equal to the pressure drop under steady conditions. Integrating eq. (4.26)over a full cycle gives :

$$\overline{\Delta P}_r = \frac{1}{2\pi} \int_0^{2\pi} (1-\varepsilon)\ (\rho_s - \rho_f)\ \left(\frac{2-\varepsilon}{\varepsilon}\right) A \sin \phi\ d\phi = 0$$

The average deviation of the steady state pressure drop is zero.

4.2.4 Slugging

The frequency of the oscillations under slugging conditions can easily be obtained from simple principles. An oscillation cycle of a slugging bed consists of two distinct periods. The first period is given by the rising of a slug through the bed. The second period is the collapse of the bed; the slug bursts through the surface, throws up the particles which then rain down. This period is usually very short as compared with the first period. Thus in first approximation the frequency of a bed with one slug periodically rising up is given by :

$$\nu = \frac{U_{sl}}{L_M} \tag{4.40}$$

U_{sl} is the velocity of the slug

L_M is the maximum height of the bed.

L_M and U_{sl} are related. The increase in height is caused by the net inflow of the gas during the rise of the slug. The flow of the gas per unit area out of the slug is generally taken as U_{mf}.

$$L_M - L_{mf} = \left(\frac{L_M}{U_{sl}}\right) (U-U_{mf})$$

$$\frac{L_M}{L_{mf}} = \frac{U_{sl}}{U_{sl} - (U-U_{mf})} \tag{4.41}$$

Eqs. (4.40) and (4.41) combined gives :

$$\nu = \frac{U_{sl} - (U-U_{mf})}{L_{mf}} \tag{4.42}$$

Davidson and Harrison (15) give for the slug velocity :

$$U_{sl} = 0.35 \sqrt{gD_t} + 1.2 (U-U_{mf}) \tag{4.43}$$

This equation is based on the experimental results of Nicklin (57) for an air/water system. Matsen (58) argues that the uncorrected theoretical value for U_{sl} should be used in fluidized systems :

$$U_{sl} = 0.35 \sqrt{gD_t} + 1.0 \, (U-U_{mf}) \qquad (4.44)$$

The experimental data as given by Matsen (58) are not accurate enough to distinguish between eq. (4.43) and eq. (4.44). When eq. (4.44) is used, the frequency becomes independent of the gas velocity

$$\nu = \frac{0.35 \sqrt{gD_t}}{L_{mf}} \qquad (4.45)$$

When eq. (4.43) is used a slightly higher value for the frequency is predicted and ν increases with increasing gas velocity. A number of experiments under slugging conditions have been carried out to check eq. (4.45). The results with copper shot (D_p = 460 μ; U_{mf} = 40 cm/sec; D_t = 6.5 cm) are given in table 4.1. The agreement between the predicted and the observed frequencies is fair. The influence of the gas velocity is complex.

TABLE 4.1

L_{mf} = 30 cm			L_{mf} = 14 cm		
U cm/sec	ν (exp.) sec^{-1}	ν (eq. 4.45) sec^{-1}	U cm/sec	ν (exp.) sec^{-1}	ν (eq. 4.45) sec^{-1}
44	1.03	0.94	43	2.03	2.01
46	1.15	0.94	46	2.02	2.01
49	1.23	0.94	48	1.99	2.01
53	1.17	0.94			
57	1.04	0.94			

4.3 Experimental results

4.3.1 The experimental set up

The experiments have been carried out in a cylindrical perspex tube with D_t = 6.5 cm. The fluid used was air of ambient conditions. The frequency has been obtained from the pressure fluctuations, gauged via a hole of 0.2 mm, 3 mm above the distributor. As long as no bubbling occurs, the frequency measured at the wall is representative for the whole system

as shown by the experiments of Hiby (55) and visually confirmed for low frequencies.
The pressure has been measured with a Kistler quartz differential pressure transducer (type 7251; resonant frequency with air 350 Hz; resolution 0.15 mm H_2O). The transducer gives a charge proportional to the pressure difference. The signal of the transducer was amplified and transformed to a proportional output voltage in a Kistler charge amplifier (type 5001) and recorded on a fast recorder (Kelvin Hughes, paper velocity 5 or 10 cm/sec).

The properties of the particle systems used are listed in table 4.2.

TABLE 4.2

code	material	D_p μ	ρ_s g/cm^3	ε_{mf}	U_{mf} cm/sec
A	copper	300 - 420	8.56	0.40	29.5
B	copper	420 - 500	8.36	0.40	39.5
C	glass	320 - 420	2.96	0.40	9.8
D	glass	800 - 900	2.96	0.40	29.5

4.3.2 The relation between ν and L

The effect of the height of the bed is shown in figure 4.3. Figure 4.3a combines the results for the systems where the critical bed height is given by eq. (4.33). For these systems the frequency will gradually change at $L \sim L_{cM}$; the 'homogeneous' oscillations will transform into slugging. The theoretical frequencies given by the eqs. (4.29) and (4.45) resp. are represented in figure 4.3a by the solid lines. The critical heights for the three systems are resp. for material A : 9.5 cm; B : 11.5 cm and D : 25 cm. The porosity for all systems is 0.45.
Figure 4.3a shows that these systems follow the theoretical prediction very well with a gradual transition around L_{cM}. This indicates that eq. (3.17) gives a reasonable value for the dynamic wave velocity.
Figure 4.3b shows the experimental frequency of the glass beads C for which the critical height is given by eq. (4.32). This system will at $L = L_c$ transform into a more than one degree of freedom system. The theoretically critical height is 6.5 cm. As can be seen from figure 4.3b the dependency of ν upon L conforms to the theoretical expectations, however, the absolute value of the frequency is higher than predicted

by eq. (4.29). When eq. (4.29b) is used a value of n = 7 has to be adopted to obtain a good fit.

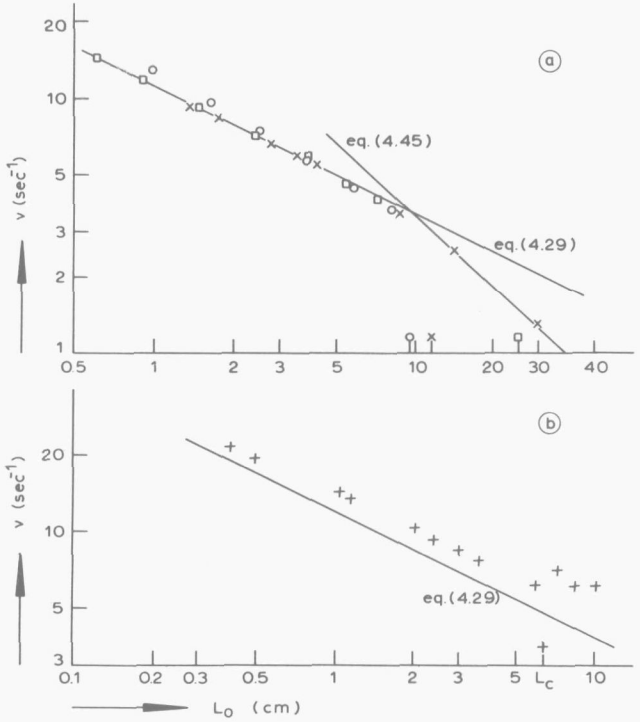

Figure 4.3 ν as a function of L_o

(a) $c_\varepsilon > c_e$
o copper particles : D_p = 270 μ; L_{cM} = 9.5 cm
x copper particles : D_p = 460 μ; L_{cM} = 11.5 cm
□ glass beads : D_p = 850 μ; L_{cM} = 25.0 cm

(b) $c_\varepsilon < c_e$
+ glass beads : D_p = 370 μ; L_c = 6.5 cm

4.3.3 The relation between ν and U

The influence of the gas velocity on the frequency is indirect via the porosity. The effect of U is small as can be seen from 4.4. The frequency decreases slightly with increasing gas velocity. The glass beads show a sudden increase in frequency at about U = 1.5 U_{mf}. Except for this irregularity the relation between U and ν is fairly well described by eq. (4.29); the solid lines in figure 4.4.

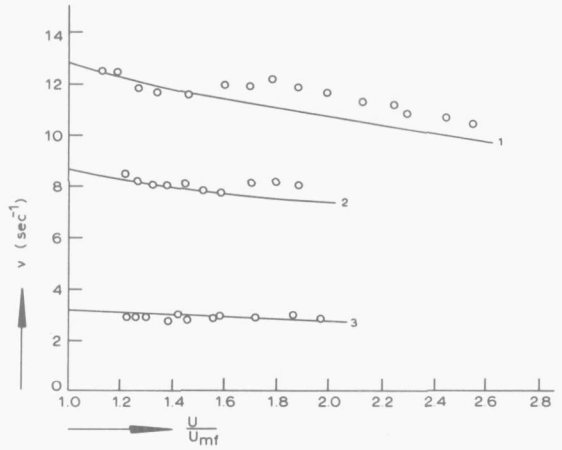

Figure 4.4 ν as a function of $\frac{U}{U_{mf}}$

1 : glass beads : D_p = 850 μ; L_0 = 0.6 cm
2 : glass beads : D_p = 370 μ; L_0 = 1.3 cm
3 : copper particles : D_p = 460 μ; L_0 = 8.8 cm

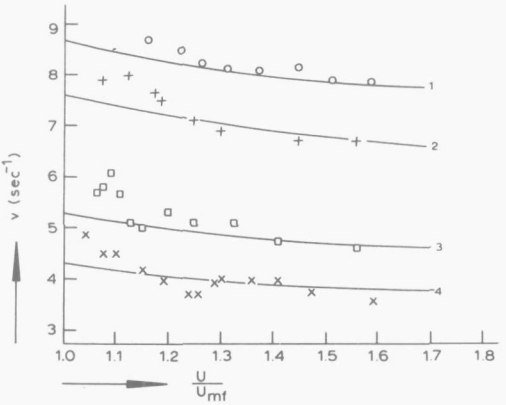

Figure 4.5 ν as a function of the gas velocity for low values of U/U_{mf}

copper particles : D_p = 460 μ
1. L_0 = 1.30 cm; 2. L_0 = 1.75 cm;
3. L_0 = 3.55 cm; 4. L_0 = 5.30 cm.

The value of the porosity used in eq. (4.29) is not experimentally obtained, but calculated with eq. (3.4a) from the values of U_{mf}, U and ε_{mf}. The experimental values of ε are rather inaccurate for a shallow oscillating fluidized bed. For low values of the gas velocity ($U/U_{mf} < 1.2$) the frequency increases rather sharply with decreasing gas velocity (figure 4.5). This can be expected. When ε is only slightly above ε_{mf} the force-displacement relation will not be linear in the compression stage. When a packed bed is formed F_r will increase very steeply with an increase in displacement resulting in a higher frequency. This is qualitatively shown in Appendix B. Also shown in Appendix B is the effect of the non-linear relation between F_r and x for larger amplitudes. This effect has no influence on the frequency.

4.4 Conclusions

1. For $L \leq L_c$ and $\rho_s/\rho_f >> 1$ fluidized systems oscillate with a frequency given by

$$\nu = \frac{1}{2\pi} \sqrt{\frac{g\ (2-\varepsilon)}{\varepsilon L}}$$

2. The oscillations are damped out in systems with low ratios of ρ_s/ρ_f.
3. Bubbling or slugging will occur when $L > L_c$.
4. The frequency of slugging systems is given by

$$\nu = \frac{0.35 \sqrt{g\ D_t}}{L_{mf}}$$

5. L_c can be calculated from the wave velocity.

5 THE ONSET OF BUBBLING

5.1 The dynamic shock wave criterion

In chapter 3 it has been shown that dynamic shock waves arise when the continuity wave velocity exceeds the dynamic wave velocity. Verloop and Heertjes (56) have adopted this condition as a criterion for the transition from homogeneous to heterogeneous fluidization.
Their results are summarized below. The critical condition can be written as :

$$c_\varepsilon = c_e \tag{5.1}$$

This equation can be developed into a number of relations between a dimensionless group and the porosity. Utilizing the eqs.(2.2), (3.7a) (3.17) and (5.1) the criterion can be written as :

$$N_{TR}^2 = \frac{D_p^3 g(\rho_s-\rho_f)^2}{\mu^2} = 5.10^6 \; \frac{\varepsilon_{mf}^3 (1-\varepsilon)^3}{\varepsilon^7 (1-\varepsilon_{mf})(3-2\varepsilon)^2} \tag{5.2}$$

$$Fr_{mf} = \frac{U_{mf}^2}{g D_p} = 128 \; \frac{\varepsilon_{mf}^9 (1-\varepsilon)^3}{\varepsilon^7 (1-\varepsilon_{mf})^3 (3-2\varepsilon)^2} \tag{5.3}$$

Another relation based on the eqs. (2.3),(3.7b) (3.17) and (5.1) is e.g. :

$$Fr = \frac{U^2}{g D_p} = \frac{128}{n^2} \left(\frac{\varepsilon}{1-\varepsilon}\right)^2 \left(\frac{\varepsilon_{mf}}{\varepsilon}\right)^n \tag{5.4}$$

Verloop and Heertjes showed that eq. (5.2) is in agreement with the experimental results for liquid fluidized beds of Harrison, Davidson and de Kock (60).
The condition $c_\varepsilon \geq c_e$ is a formal instability criterion for continuity waves. The resulting stable conditions have not been analysed theoretically. As the dynamic shock wave results from an insufficiently rapid response of the particles in the wave a likely concept of a dynamic shock wave is a few layers of collided particles. When the velocity of the dynamic shock

wave exceeds the elastic wave velocity the shock wave will be stable. Particles will collide at the front of the wave and rain off from the back of the wave. When the velocity of the dynamic shock wave drops below c_e the shock wave will disappear.
This concept of a dynamic shock wave may find some support from photo I, which shows a water fluidized bed of steel particles (D_p = 1 mm) at porosity $\varepsilon \sim 0.5$. According to the criterion given in eq. (5.2) this system fluidizes heterogeneously. In photo I a number of horizontal voids can be seen, together with a number of more bubble shaped voids. The photo suggests a rain off mechanism. Dynamic shock waves can also be observed in gas fluidized beds; most conveniently in oscillating systems with $L < L_{cM}$ and $c_\varepsilon > c_e$. A stable horizontal void can be observed rising up through the bed. Therefore it seems very likely that bubbles are the result of dynamic shock waves and that the condition $c_\varepsilon = c_e$ can be used as a criterion for the transition from homogeneous to heterogeneous fluidization.

5.2 The vibration criterion

In chapter 4 it has been shown that a gas fluidized bed can only oscillate 'homogeneously' when the bed height is below a certain critical height. Otherwise bubbling or slugging occurs. From the values calculated for L_c it appears that virtually all fluidized beds are operated far above L_c, thus all gas fluidized systems will be heterogeneous. This criterion can be written as :

$$L \gtrsim L_c \qquad (5.5)$$

However, it has often been observed that small, light particles can show homogeneous fluidization over a limited range of gas velocities. This phenomenon can be explained by considering the amplitude of the vibration. For small particles the vibrating layer (L_c) is very shallow, thus the amplitude is very small and the voids formed between the oscillating layer and the rest of the bed may be too small to initiate bubbling.
A fair assumption seems to be that the minimum amplitude needed for bubble formation is one particle diameter. To assume a much smaller minimum amplitude seems unrealistic and a much larger value overdone; furthermore, there is some supporting experimental evidence. Hiby observed that the oscillating height in a bubbling bed was about 10 D_p. The rela-

tive pressure amplitude had a constant asymptotic value $\Delta P_r/\Delta P \sim 0.3$. Combining the eqs. (4.20) and (4.26) gives for $\varepsilon = 0.5$:

$$\frac{A}{L} = \left(\frac{\varepsilon}{2-\varepsilon}\right) \frac{\Delta P_r}{\Delta P} = 0.1 \text{ or } A = 0.1\ L = 1\ D_p$$

From eq. (4.23) it follows : $A = \frac{\Delta\varepsilon}{1-\varepsilon} L$ (5.6)

The value of $\Delta\varepsilon$ will be assumed as $\varepsilon-\varepsilon_{mf}$. This is a reasonable estimate since in most cases ε_{bp} is only a little larger than ε_{mf}. The minimum bed height L_b needed to cause bubbling can now be determined from eq. (5.6) by introducing $A = D_p$ and $\Delta\varepsilon = \varepsilon-\varepsilon_{mf}$.

$$L_b = \frac{1-\varepsilon}{\varepsilon-\varepsilon_{mf}} D_p \tag{5.7}$$

The actual vibration height L_c is given by eq. (4.32). Bubbling can occur when L_c is larger than L_b :

$$L_c \geq L_b \tag{5.8}$$

Using the eqs. (2.2), (4.32) and (5.7) a number of relations between a dimensionless group and the porosity can be obtained :

$$Fr = \frac{U^2}{gD_p} = \frac{10^{-1}\ (1-\varepsilon)(2-\varepsilon)}{(3-2\varepsilon)^2\ (\varepsilon-\varepsilon_{mf})} \tag{5.9}$$

$$N_{TR}^2 = \frac{gD_p^3\ (\rho_s-\rho_f)^2}{\mu^2} = \frac{4.10^3\ (1-\varepsilon)^3(2-\varepsilon)}{\varepsilon^5\ (3-2\varepsilon)^2\ (\varepsilon-\varepsilon_{mf})} \tag{5.10}$$

The vibration criterion can be expressed in the same dimensionless numbers as the dynamic shock wave criterion.
The vibration criterion predicts bubbling at lower values of ε than the dynamic shock wave criterion. This can be seen from the ratio of N_{TR} for the two criteria, given by the eqs. (5.2) and (5.10).

$$\frac{N_{TR}^2 \text{ shock wave}}{N_{TR}^2 \text{ vibration}} = \frac{1.25 \times 10^3 \, \varepsilon_{mf}^3 \, (\varepsilon - \varepsilon_{mf})}{\varepsilon^2 \, (2-\varepsilon) \, (1-\varepsilon_{mf})} \qquad (5.11)$$

If $\varepsilon_{mf} = 0.4$ and $\varepsilon - \varepsilon_{mf} = 0.01$ are accepted as minimum values the ratio given by eq. (5.11) is always larger than one. This can also be seen in figure 5.1 where $(N_{TR})_c$ is plotted as a function of ε_c for both criteria.

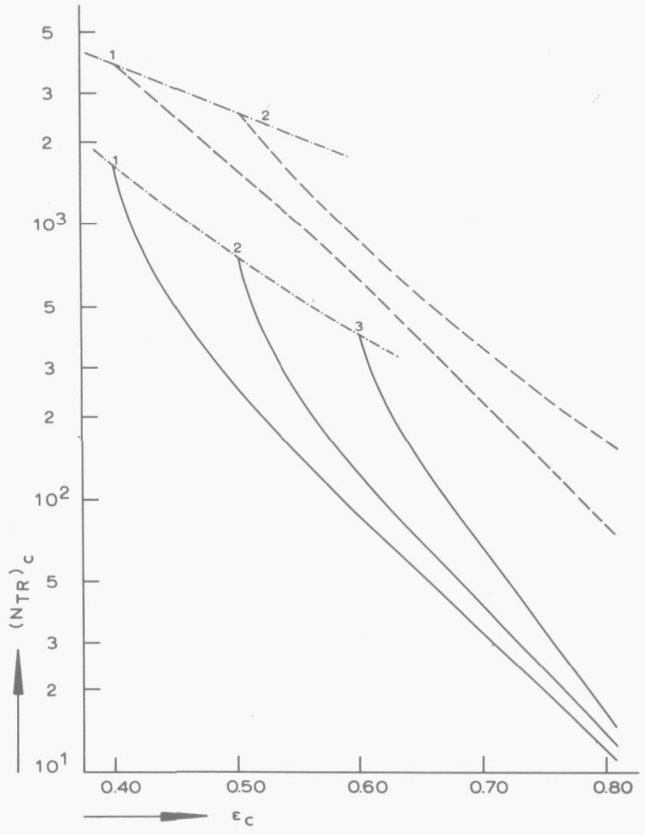

Figure 5.1 $(N_{TR})_c$ as a function of ε_c
– – – – eq.(5.2) ——— eq.(5.10)
1. $\varepsilon_{mf} = 0.4$; 2. $\varepsilon_{mf} = 0.5$; 3. $\varepsilon_{mf} = 0.6$

This confirms the use of L_c instead of L_{cM} in eq. (5.8), and shows that the stability of a gas fluidized system is governed by eq. (5.8) - the vibration criterion - and liquid or high pressure gas fluidized beds are governed by eq. (5.1) - the dynamic shock wave criterion.

TABLE 5.1

ref.	ρ_s g/cm^3	D_p μ	ε_{mf}	U_{bp} cm/sec	$(Fr)_{bp}$	N_{TR}	ε_{bp} exp.	ε_c eq. (5.9)	ε_c eq.(5.10)
(61)	0.94[5]	55	0.52[5]	0.40	0.029	77	0.62	-	0.66
	1.20	80	0.52[5]	0.75[5]	0.070	172	0.59[5] *	0.68	0.59
	1.27	116	0.56[5]	1.64	0.230	318	0.65[5] *	0.61[5]	0.58[5]
	1.17	128	0.41[5]	1.48	0.172	326	0.48[5] *	0.47[5]	0.48[5]
	1.23	142	0.57[5]	1.64	0.188	414	0.62 *	0.62[5]	0.58
(16)	1.57	40	0.46	0.35[5]	0.031	80	0.62	0.75	0.62[5]
	1.32	55	0.40	0.54[5]	0.055	108	0.54	0.58[5]	0.58
	1.56	140	0.39	2.10	0.314	516	0.47	0.42	0.45
	0.50	190	0.39	1.25	0.082	262	0.49	0.50[5]	0.48[5]
	2.60	110	0.42	1.43	0.186	600	0.46	0.47	0.46
(62)	1.18	115	0.45	1.17	0.119	382	0.50	0.53	0.50
	1.18	137	0.45	1.34	0.131	496	0.48[5]	0.52[5]	0.48
	1.18	165	0.45	1.60	0.155	616	0.47	0.51	0.47
	1.18	195	0.45	1.76	0.159	844	0.45[5]	0.51	0.45[5]
	1.18	230	0.45	2.51	0.275	1081	0.45	0.48	0.45
(63)	1.18[5]	125	0.44	1.80	0.258	332	0.51	0.48	0.50
	1.18[5]	125	0.44 *	1.68	0.216	332	0.50	0.49	0.50
	1.18[5]	186	0.43 *	2.50	0.336	600	0.47[5]	0.46	0.46
	0.24	121	0.65 *	1.00	0.083	64	0.73	0.75	0.73
(18)	0.82	30	0.50[5]		0.044	27	0.70	0.74	0.74
	0.84[5]	42	0.50		0.047	46	0.65	0.72	0.69
	0.85	59	0.49		0.058	78	0.60[5]	0.67	0.63[5]
	0.85	76	0.48		0.078	111	0.58	0.62	0.60
	0.84	88	0.46		0.080	140	0.56	0.58[5]	0.57
	0.88	94	0.47[5]		0.066	160	0.53	0.63	0.56
	0.89	117	0.46		0.077	224	0.49	0.59[5]	0.53
	0.91[5]	139	0.45[5]		0.092	298	0.49	0.56	0.51
	0.87	32	0.49			34	0.68		0.71
	0.87	40	0.43			60	0.63		0.65
	0.87	62	0.41			88	0.60		0.60
	0.87	87	0.43			147	0.55		0.56

* Calculated from the values of U_{mf}, U_{bp}, n and ε_{mf} or ε_{bp}.

Table 5.1 presents the experimental data of five investigations (16, 18, 61-63) and the theoretical predictions for ε_{bp}, the porosities at which bubbling starts. The difference between the values obtained from eq. (5.9) and eq. (5.10) is due to the expansion equation used (eq. 2.2) and gives an indication of the accuracy of prediction. In general eq.(5.10) predicts ε_{bp} more accurately than eq. (5.9). There is a high level of agreement between ε_c from eq. (5.10) and ε_{bp}. The average difference is less than 0.01 and the maximum difference is only 0.05. At high porosities the differences are the greatest.
It can be concluded that eq. (5.10) accurately accounts for the influence of ρ_s, D_p and ε_{mf}.

5.3 Other proposed criteria.

During the years the difference between homogeneous and heterogeneous fluidization has received much attention and many transition criteria have been proposed. The various criteria can be arranged into two, essentially complementary, categories. Criteria included in category I are concerned with the occurrence or growth of instabilities in homogeneous fluidized systems. Criteria of category II are based on the possibility of the existence of voids rising with a velocity $0.71\sqrt{gD_b}$, the rising velocity of a single bubble.
Each category can be subdivided into three groups.

I.1 The stability or growing velocity of a perturbation in a stable arrangement of fluidized particles (34-36, 44-46).

From these mathematical exercises only Molerus' approach (36) has lead to a qualitatively successful result. As perturbation Molerus introduces a sinusoidal fluctuation in the superficial fluid velocity. This leads to zones of growing solutions, indicated by the stability factor S (64).

$$S = \left[\frac{D_p^3 \, g \, \rho_s(\rho_s-\rho_f)}{\mu^2}\right]^{-0.5} \left[\varepsilon^3(1-\varepsilon)\right]^{-0.5} \exp.\left[\frac{4.1\ (1-\varepsilon)}{0.64 + \varepsilon}\right] \qquad (5.12)$$

The larger S the more stable the system will be. The critical S depends upon the amplitude of the velocity variation. Molerus estimates as a good value $S_c = 1.4\times10^{-2}$. However, if $S_c = 1.4\times10^{-1}$ is taken the agreement with the experimental data as given in table 5.1 is much closer.

Molerus assumed $\rho_s >> \rho_f$ and his criterion can then be written as :

$$N_{TR} = \frac{7 \exp.\left[\frac{4.1\ (1-\varepsilon)}{0.64 + \varepsilon}\right]}{\left[\varepsilon^3(1-\varepsilon)\right]^{0.5}} \qquad (5.13)$$

This criterion is numerically almost equivalent to the result obtained from the vibration criterion for the constant value of $L_b = 10\ D_p$. In the vibration criteria L_b is proportional to the amplitude. When the relation between S_c and the amplitude of the velocity fluctuation is known Molerus' criterion and the vibration criterion should probably coincide. Therefore it can be concluded that the voids formed by the oscillation of the bottom layer with $L_c > L_b$ are not growth restricted.
It is known (65, 66) that a forced vibration of a high frequency can have a favourable effect on the stability of a fluidized bed. Molerus (67) has developed his theory in terms of a critical frequency.

$$\nu_c = \frac{1}{2\pi}\sqrt{\frac{g}{D_p}\,\frac{\rho_s-\rho_f}{\rho_s}\,\frac{(1-\varepsilon)}{2\ N\ \varepsilon}} \sim \frac{1}{2\pi}\sqrt{\frac{g}{D_p}\,\frac{(1-\varepsilon)}{40\ \varepsilon}} \qquad (5.14)$$

N is a constant and taken as 20; ND_p represents a wave length. For higher frequencies than ν_c the disturbances will vanish, for lower frequencies the disturbances will grow.
The influence of a forced vibration is also easily understood from the vibration concept as given in section 5.2 and the critical frequency can easily be calculated. The higher the external frequency forced upon the system, the lower the height of the oscillating layer. For a sufficiently high frequency the height of the oscillating layer will be below L_b and no bubbling will occur. The critical frequency is :

$$\nu_c = \frac{1}{2\pi}\sqrt{\frac{g}{L_b}\,\frac{2-\varepsilon}{\varepsilon}} = \frac{1}{2\pi}\sqrt{\frac{g}{D_p}\,\frac{(2-\varepsilon)(\varepsilon-\varepsilon_{mf})}{\varepsilon\ (1-\varepsilon)}} \qquad (5.15)$$

This result is similar to that obtained by Molerus but is easier to derive, simpler to understand and has no arbitrary constants.

I.2 Interparticle forces (16, 22, 68)

Although it has been shown experimentally that interparticle forces can have a marked influence on the occurrence of

bubbles, the same experiments also show that bubbling occurs when interparticle forces have been overcome (69). The main effect of interparticle forces on bubbling seems to be the formation of channels. Maldistribution of the fluid promotes bubbling as can be observed in spouting beds.

I.3 Bubbling will occur when a certain critical condition has been passed (18, 56, 70-72)

The dynamic shock wave criterion (56, 71) and the vibration criterion belong to this group. Rowe (70) mentions a limited elasticity of the dense phase. De Jong (18) obtains, on the basis of his experiments, a phase diagram ($(\varepsilon^3/1-\varepsilon)$- U) distinguishing between a non-fluidized bed, a homogeneous fluidized bed and a heterogeneous fluidized bed. The triple point gives the maximum D_p allowing for homogeneous fluidization. This method gives reasonable results for particles of the density as used in the experiments of De Jong.

II.1 The minimum observable bubble (15, 60, 73)

The distinction homogeneous-heterogeneous is based on visual observation. Thus heterogeneity will only be recognized when a bubble has a certain size. Simpson and Rodger (73) conclude from pressure drop experiments that there is no fundamental difference between liquid and gas fluidized beds. Deviation from the theoretical pressure drop is caused by numerous small bubbles in liquid fluidized beds and by few large ones in gas fluidized beds. Davidson and Harrison (15) calculate a maximum stable bubble size. When the bubble velocity exceeds the fall velocity of the particles the bubble will gradually be filled up and disappear. They prefer to evaluate their results numerically. A simple relation can be derived for the case of laminar flow and $\rho_s/\rho_f \gg 1$. The critical condition is :

$$V_T \geq U_b \tag{5.16}$$

$$\frac{D_p^2(\rho_s-\rho_f)\,g}{18\,\mu} \geq 0.71\,\sqrt{gD_b} = 0.71\,\sqrt{g\,ND_p}$$

$$N_{TR} \geq 12.7\,\sqrt{N} \tag{5.17}$$

II.2 The minimum fluid flow for bubbling (28, 62, 70)

The amount of fluid transported through a bubbling bed is higher than for a non-bubbling bed of the same porosity. At least when the bubble velocity is greater than the interstitial fluid velocity, as is almost always the case. Therefore, in order to retain a fluidized dense phase at a lower porosity, the bed has first to expand before bubbling can start. The condition $U_b > U_i$ implies a minimum bubble size :

$$U_b = 0.71 \sqrt{gD_b} = 0.71 \sqrt{gND_p} > U_i = \frac{U}{\varepsilon} \qquad (5.18)$$

$$N > \frac{2}{\varepsilon^2} \frac{U^2}{gD_p} = \frac{2}{\varepsilon^2} Fr \qquad (5.19)$$

According to Geldart (62) experimental evidence indicates that at the bubbling point the fraction of the bed occupied by bubbles is about 0.01. This value has been used by Rietema (28) and for $\rho_s >> \rho_f$ his relation can be written as :

$$N_{TR} \geq \frac{1-\varepsilon}{\varepsilon^3} \sqrt{N} \qquad (5.20)$$

The relation given by Rowe (70) cannot be compared directly as this relation includes the diameter of the tube.

II.3 The potential energy of the solid phase (74, 75)

The idea is that a homogeneous fluidized system will become heterogeneous when this will decrease its potential energy. Assuming no difference in either pressure drop and kinetic energy of the solids, a bubbling bed has a lower energy level than a homogeneous bed when its expansion is less.
Molerus (75) takes the average velocity of a swarm of bubbles equal to the velocity of a single bubble. His condition for a bubbling system can be written as :

$$N_{TR} \leq 50\sqrt{N} \qquad (5.21)$$

The criterion given by eq. (5.21) differs from all the other criteria in this respect that it requires $(N_{TR})_c$ to be lower than a certain value instead of higher. The larger the value of N_{TR} of a system, the larger the rising velocity of the bubbles has to be. The requirement imposed by eq. (5.21) can always be realized as the following simple thought experiment

may show.
Assume the bubble has a porosity of $\varepsilon = 1$. For constant U the expansion of a homogeneous bed will decrease upon introduction of a bubble of limited dimensions if the bubble velocity is larger than the superficial fluid velocity. Thus the condition for a lower potential energy is :

$$U_b > U \tag{5.22}$$

This relation can always be fulfilled as can be seen by introducing the maximum velocity of a bubble given by eq. (5.16) into eq. (5.22).
This gives :

$$V_T > U \tag{5.23}$$

and this condition is always fulfilled in a fluidized system.
The condition given by eq. (5.22) is equivalent to the criterion of Molerus, eq. (5.21), for eq. (5.22) can be written as :

$$Fr = \frac{U^2}{gD_p} < 0.5\sqrt{N} \tag{5.24}$$

5.4 Comparison of the criteria

The equations derived for the critical conditions based on the respective criteria have been collected in table 5.2, together with the numerical values of N_{TR} for two porosities, assuming $\varepsilon_{mf} = 0.4$
The value of N used in table 5.2 to calculate N_{TR} is arbitrary; with very small particles ($D_p < 100$ μ) N has to be larger and and with very large particles ($D_p > 0.1$ cm) N can be smaller. Taking N = 10, the value of N_{TR} predicted by criterion f is very low and not in agreement with the experimental results given in table 5.1. The simplest solution to obtain a closer agreement with the experimental data is to assume that larger particles have a value of N higher than 10. Of course, one or more assumptions used in the derivation of eq. (5.21) can be wrong, e.g. the swarm velocity of the bubbles might be higher than $0.71\sqrt{gD_b}$. From the above it can be concluded that the criteria d, e and f do not impose a restriction on the criteria a, b and c in this sense that the instabilities predicted by the first three mechanisms could not grow into bubbles.

TABLE 5.2

criterion	equation	(number)	N_{TR}	
			$\varepsilon = 0.5$	$\varepsilon = 0.7$
a. shock wave $C_\varepsilon \geq C_e$	$N_{TR}^2 \geq \frac{5.10^6\ \varepsilon_{mf}^3\ (1-\varepsilon)^3}{\varepsilon^7 (1-\varepsilon_{mf})(3-2\varepsilon)^2}$	(5.2)	1500	220
b. vibration $L_c \geq L_b$	$N_{TR}^2 \geq \frac{4.10^3\ (1-\varepsilon)^3\ (2-\varepsilon)}{\varepsilon^5\ (3-2\varepsilon)^2\ (\varepsilon-\varepsilon_{mf})}$	(5.10)	230	35
c. perturbation $S_c = 0.14$	$N_{TR} \geq \frac{7\ \exp\left(\frac{4.1\ (1-\varepsilon)}{0.64+\ \varepsilon}\right)}{\varepsilon^3\ (1-\varepsilon)^{0.5}}$	(5.13)	200	60
d. bubble size $V_T \geq U_b$	$N_{TR} \geq 12.7\ \sqrt{N}$ (N = 10)	(5.17)	40	
e. fluid flow	$N_{TR} \geq \frac{1-\varepsilon}{\varepsilon^3}\ \sqrt{N}$ (N = 10)	(5.20)	13	3
f. potential energy $\varepsilon_{het} \leq \varepsilon_{hom}$	$N_{TR} \leq 50\sqrt{N}$ (N = 10)	(5.21)	160	

Criterion a applies for all fluidized systems, but can only be checked experimentally in liquid-solids systems since in gas fluidized beds bubble arise at lower values of N_{TR} than dynamic shock waves. The influence of increasing pressure on the onset of bubbling can be explained by the change in mechanism, which occurs when the ratio ρ_s/ρ_f decreases sufficiently. The transition number is rather insensitive to the pressure.

The criteria b and c are based on similar mechanisms. They predict the critical conditions at about the same value of N_{TR}. S_c has been treated as a constant, but it is likely that the value of S_c decreases with increasing porosity and as a result $(N_{TR})_c$ will be smaller at higher voidages. It is very reasonable to conclude that the voids originated by the oscillation of the bottom layer will grow.
It may be noted that in both mechanisms (a and b) proposed in this thesis the propagation velocity of the porosity waves plays an important role. The wave velocity has been derived using simplifying assumptions. The agreement between theory and experiment support the validity of the continuity wave concept. Another example of the influence of the continuity wave has been treated in Appendix C. The occurrence of artificially formed bubbles can be described by the effect of the direction of the wave.

5.5 Conclusions

1. When the ratio ρ_s/ρ_f is very large, the onset of bubbling is related to the oscillation of the bottom layer of the fluidized bed.
2. For smaller values of ρ_s/ρ_f the transition from homogeneous to heterogeneous fluidization can be described by the occurrence of dynamic shock waves.
3. The critical conditions related to the two proposed mechanisms are such that no restrictions are imposed by other criteria for the growth of the instabilities into bubbles.

6 CONCLUSION

6.1 Dimensional analysis

In chapter 5 it has been shown that most of the proposed criteria for the occurrence of bubbles could be represented by the transition number (or Froude number) as a function of the porosity and/or N, a constant relating a length to the particle diameter. It is evident that ε appears in the criteria. N_{TR} or Fr cannot unequivocally be established from a dimensional analysis based on the apparent mechanisms or parameters. The transition number appears to be the product of two dimensionless groups representing resp. a ratio of forces and of velocities.
Under the assumed laminar conditions only two forces are present caused by viscous drag and gravitation. The velocities involved differ for each criterion, but the numerator is always proportional to U and the denominator to $\sqrt{gD_p}$.

$$N_{TR} = \frac{D_p^2 \, g \, (\rho_s - \rho_f)}{\mu \, U} \qquad \frac{U}{\sqrt{gD_p}} = \frac{\sqrt{gD_p^3} \, (\rho_s - \rho_f)}{\mu}$$

The velocity ratios have been $\frac{c_\varepsilon}{c_e}$, $\frac{c_\varepsilon}{\nu L}$, $\frac{V_T}{U_b}$, $\frac{U}{U_b}$, $\frac{U_i}{U_b}$

When the buoyancy is considered as an independent force the transition number will include an additional density ratio $\rho_s/(\rho_s - \rho_f)$.
Since the ratio of velocities can always be expressed in the same dimensionless group, having the form of a Froude number, the success of the use of the Froude number as an indicator of the state of fluidization can be understood. However, the use of the Fr-number might be misleading as it does not represent in this case the ratio of gravitational and inertia forces.

6.2 Critical deductions

For convenience and clarity the most important deductions are listed here, followed by the evidence as presented. The validity of the statements is limited by the scope of this thesis.

A. In an idealized concept of a homogeneous fluidized bed it is allowed to neglect interparticle forces.
   1. The agreement between the two experimental methods to determine U_{mf}. (section 2.2.3).

2. The shape of the experimental tgβ-U curves (section 2.2.3; Appendix A)

3. The analysis of the resistivity experiments (section 2.3).

B. The propagation velocity of a porosity wave is accurately given by the velocity of the continuity wave.
1. The agreement with the experimental wave velocities measured by Anderson and Jackson (section 3.1).

2. The accurate prediction of the response of the bed level to a sudden change in the fluid velocity (section 3.2).

3. The correct estimate of L_c (section 4.2.2).

4. The description of the formation of artificial bubbles (Appendix C).

C. Eq. (3.15) gives a fair estimate of the dynamic wave velocity.
1. The experimental results of the rain-off experiments (section 3.4).
2. The good estimate of L_{cM} (section 4.2.2).

3. The reasonable prediction of the critical conditions in liquid fluidized beds (section 5.1).

D. The onset of bubbling is governed by two different criteria.
1. A closer agreement between theoretical predictions and experimental results (sections 5.1; 5.2).

2. The influence of the pressure on the stability of gas-fluidized beds can be accounted for (section 4.2.1).

3. Visual observations on gas fluidized beds with $c_\varepsilon > c_e$ and $L < L_{cM}$ (section 4.2.3)

4. The different appearence of the bubbles in gas and liquid fluidized beds (section 5.1).

NOTATION

A	amplitude
C	constant
c	wave velocity, LT^{-1}
D	diameter, L
d	dimensionless distance between two particles s/D_p
E	energy, ML^2T^{-2}
e	modulus of elasticity, $ML^{-1}T^{-2}$
F	force, MLT^{-2}
f	friction factor
g	acceleration of gravity, LT^{-2}
K	constant
L	length, L
m	mass, M
N	dimensionless length D/D_p
n	constant defined by eq. (2.3)
ΔP	pressure drop, $ML^{-1}T^{-2}$
p	parameter $(\sqrt{K_r/m})$, T^{-1}
q	parameter $(K_d/2m)$, T^{-1}
r	resistivity, LTC^{-1}
S	stability factor
s	distance between two particles, L
T	period of a cycle, T
t	time, T
U	superficial fluid velocity, LT^{-1}
U_i	interstitial fluid velocity, LT^{-1}
U_s	slip velocity, LT^{-1}
u	displacement at y, L
V_F	velocity of the rain-off front, LT^{-1}
V_T	terminal falling velocity of a single particle, LT^{-1}
W	solids velocity, LT^{-1}
x	displacement, L
y	coordinate, L
z	dimensionless displacement $(x/\epsilon L)$
Fr	Froude number $(U^2/g\ D_p)$
N_{TR}	Transition number $(g\ D_p^3)^{0.5}\ ((\rho_s-\rho_f)/\mu)$
Re	Reynolds number $(\rho_f\ U\ D_p/\mu)$
α	angle between slope and plane of rotation, ^{o}
β	angle of repose, ^{o}
γ	angle of the distributor with the horizontal, ^{o}
Δ	particle surface roughness, L
δ	logarithmic decrement of the amplitude
δ_r	angle of the slope at rolling, ^{o}
δ_s	angle of the slope of sliding, ^{o}
ϵ	porosity
ι	angle of internal friction, ^{o}

μ	dynamic viscosity, $ML^{-1}T^{-1}$
ν	frequency, T^{-1}
ρ_f	density of the fluid, ML^{-3}
ρ_s	density of the solids, ML^{-3}
τ_c	cohesion stress, $ML^{-1}T^{-2}$
τ_w	shear stress between particles and wall, $ML^{-1}T^{-2}$
ϕ	ωt
ω	cyclic frequency, T^{-1}

Indices

b	bubble
bp	bubble point
C	compression
c	critical value
d	damping
E	expansion
e	elastic
f	friction
j	indicator
k	kinetic
M	maximum
mf	minimum fluidization
o	original; equilibrium
p	particle (inter)
pb	packed bed
r	restoring
s	static , 'sur', sliding
sl	slug
t	tube

REFERENCES

1. Ind.Eng.Chem. 41 (1949) 1249.
2. Proc.Intern.Symp.Fluidization, ed. A.A.H. Drinkenburg, Neth.Univ.Press, Amsterdam, 1967.
3. M. Leva, Fluidization, McGraw Hill Book Co.Inc., New York, 1959.
4. A.A.H. Drinkenburg, Proc.Intern.Symp.Fluidization, 1967, p. 142.
5. J.F. Richardson and W.N. Zaki, Trans.Instn chem.Engrs. 32 (1954) 35.
6. P.L. Slis, Th.W. Willemse and H. Kramers, Appl.sci.Res. A8 (1959) 209.
7. K. Godard and J.F. Richardson, Tripartite Chem.Eng.Conf., Mcntreal, 1969.
8. P.N. Rowe, Trans.Instn chem.Engrs., 39 (1961) 175.
9. F.A. Zenz and D.F. Othmer, Fluidization and Fluid-Particle Systems, Reinhold Publ.Co., New York, 1960.
10. G. Narsimhan, A.E.Ch.E. Journal, 11 (1965) 550.
11. J.F. Frantz, Chem.Eng.Progr.Symp.Ser., 62, 62 (1966) 21.
12. C.Y. Wen and Y.H. Yu, Chem.Eng.Progr.Symp.Ser., 62, 62 (1966) 100.
13. J. Beránek, Chem.Techn., 14 (1962) 71.
14. P. Reboux, Phénomènes de Fluidisation, Association Française de fluidisation, Paris, 1954.
15. J.F. Davidson and D. Harrison, Fluidised Particles, Cambridge Univ. Press, Cambridge, 1963.
16. K. Rietema, Proc.Intern.Symp.Fluidization, 1967, p.154.
17. A.A.H. Drinkenburg, Ph.D. Thesis, Techn.Univ.Eindhoven, 1970.
18. J.A.H. de Jong, Ph.D. Thesis, Univ.Groningen, 1970.
19. F.C. Franklin and L.N. Johanson, Chem.Eng.Sci., 4 (1955) 119.
20. K. Terzaghi, Theoretical Soil Mechanics, John Wiley, New York, 1944.
21. V. Vaněček, S. Najnr and K. Holšan, Proc.Intern.Symp. Fluidization, 1967, p.617.
22. R.H. Wilhelm and M. Kwauk, Chem.Eng.Progr. 44 (1948) 201.
23. V. Vaněček, M. Markvart and R. Drbohlav, Fluidized Bed Drying, Leonard Hill, London, 1966.
24. D. Geldart and J.R. Kelsey, Tripartite Chem.Eng.Conf., Montreal, 1969.
25. P.N. Rowe and K.S. Sutherland, Trans.Instn chem.Engrs., 42 (1964) T55.
26. A.L. Jones and T.D. Wheelock, Tripartite Chem.Eng.Conf., Montreal, 1969.
27. D. Goldschmidt and P.Le Goff, Trans.Instn chem.Engrs., 45 (1967) T196.

28. K. Rietema, Proc.Intern.Symp.Fluidization, 1967, p.176.
29. R.T. Fowler and W.B. Chodziesner, Chem.Eng.Sci., 10 (1959) 157.
30. N. Pilpel, J.Pharm. Pharmacol., 16 (1964) 705.
31. R. Jackson, Chem.Eng.Progr.Symp.Ser., 66, 105 (1970) 3.
32. W.J. Beek, Proc.Intern.Symp.Fluidization, 1967 p.507.
33. P.N. Rowe and G.A. Henwood, Trans.Instn chem.Engrs., 39 (1961) 51.
34. R. Jackson, Trans.Instn chem.Engrs. 41 (1963) 13.
35. R.L. Pigford and T. Baron, Ind.Eng.Chem.Fund., 4 (1965) 81.
36. O. Molerus, Proc.Intern.Symp.Fluidization, 1967, p.134.
37. E.J. Cairns and J.M. Prausnitz, A.I.Ch.E. Journal, 6 (1960) 554.
38. N.J. Hassett, Brit.Chem.Eng., 6 (1961) 777.
39. H. Kramers, M.D. Westermann, J.H. de Groot and F.A.A. Dupont, Symp.Interaction between Fluids and Particles, Instn chem.Engrs., London, 1962, p.114.
40. N. Vaněček and R.L. Hummel, Tripartite Chem.Eng.Conf., Montreal, 1969.
41. T.B. Anderson and R. Jackson, Ind.Eng.Chem.Fund., 8 (1969) 137.
42. A.C. Trupp, Tripartite Chem.Eng.Conf., Montreal, 1969.
43. G.B. Wallis, One-dimensional Two-Phase Flow, McGraw Hill, New York, 1969.
44. J.A. Murray, J.Fluid Mech., 21 (1965) 465.
45. T.B. Anderson and R. Jackson, Ind.Eng.Chem.Fund., 7 (1968) 13.
46. E. Rückenstein and M. Tzeculescu-Filipescu, Chem.Eng.Sci., 23 (1968) 1121.
47. J.J. van Deemter, Proc.Intern.Symp.Fluidization, 1967,p.91.
48. K. Rietema, Private Communication, 1969.
49. R.D. Oltrogge, Private Communication, 1969.
50. W.J. Rice and R.H. Wilhelm, A.I.Ch.E. Journal 4 (1958) 423.
51. G. Volpicelli, Proc.Intern.Symp.Fluidization, 1967, p.189.
52. G.W. Housner and D.E. Hudson, Applied Mechanics (Dynamics) D. van Nortrand Co.Inc., Princeton, 1959.
53. A.L. Kimball, Trans.A.S.M.E., APM-51-21 (1929) 227.
54. R.A. Anderson, Fundamentals of Vibration.
55. J.W. Hiby, Proc.Intern.Symp.Fluidization, 1967, p.199.
56. J. Verloop and P.M. Heertjes, Chem.Eng.Sci., 25 (1970) 825.
57. D.J. Nicklin, Chem.Eng.Sci., 17 (1962) 693.
58. J.M. Matsen, Chem.Eng.Progr.Symp.Ser., 101, 66 (1970) 47.
59. G.B. Wallis, AEEW-R 162 report, 1962.
60. D. Harrison, J.F. Davidson and J.W. de Kock, Trans.Instn chem.Engrs., 39 (1961) 202.
61. L. Davies and J.F. Richardson, Trans.Instn chem.Engrs., 44 (1966) T293.

62. D. Geldart, Proc.Intern.Symp.Fluidization, 1967, p.170.
63. K. Godard and J.F. Richardson, Tripartite Chem.Eng.Conf., Montreal, 1969.
64. O. Molerus, Chemie-Ing.-Techn., 39 (1967) 341.
65. E. Muschelknautz, VDI-Berichte, 88 (1965) 19.
66. A. Godel, U.S.Patent 1.813.351.
67. O. Molerus, Proc.Intern.Symp.Fluidization, 1967, p.144.
68. P.J. Buysman and G.A.L. Peersman, Proc.Intern.Symp. Fluidization, 1967, p.38.
69. K. Godard and J.F. Richardson, Chem.Eng.Sci., 24 (1969) 194.
70. P.N. Rowe, Chem.Eng.Sci., 24 (1969) 415.
71. G.B. Wallis, Symp.Interaction between Fluids and Particles, Instn chem.Engrs., London, 1962, p.9.
72. E. Rückenstein and M. Tzeculescu, Proc.Intern.Symp. Fluidization, 1967, p.180.
73. H.C. Simpson and B.W. Rodger, Chem.Eng.Sci., 16 (1961) 53.
74. I.A. Vakhrushev and N.A. Basov, Intern.Chem.Eng., 9 (1969) 83.
75. O. Molerus, Chemie-Ing. Techn., 42 (1970) 488.
76. P.M. Heertjes, J. Verloop and R. Willems, Powder Technol, 4 (1970/1971) 38.
77. D. Goldschmidt and P. Le Goff, Chem.Eng.Sci., 18 (1963) 805.
78. W. Graham and E.A. Harvey, Canad.J.Chem.Eng., 13 (1965) 146.
79. W. Graham and E.A. Harvey, Canad.J.Chem.Eng., 14 (1966) 17.
80. A.K. Reed and W.M. Goldberger, Chem.Eng.Progr.Symp.Ser., 62, 67 (1966) 71.
81. B.S. Lee, E.J. Pyrcioch and F.C. Schora, Chem.Eng.Progr. Symp.Ser., 66, 101 (1970) 75.
82. A.L. Jones and T.D. Wheelock, Chem.Eng.Progr.Symp.Ser., 66, 105 (1970) 157.
83. W.R. Harper, Powders in Industry, Soc. of Chem.Ind., London, 1961, p.115.
84. M. Leva and M. Grummer, Chem.Eng.Progr., 48 (6)(1952) 307.
85. G.H. Reman, Chem. and Ind., Jan. 15 (1955) 46.
86. J. Verloop, L.H. de Nie and P.M. Heertjes, Powder Technol., 2 (1968/69) 32.
87. R.G. Kunz, Powder Technol., 4 (1971) 156.

APPENDIX A

THE ANGLE OF REPOSE

A.1 Instability mechanisms

In the absence of interparticle forces the value of β is determined by particle size, size distribution and shape and not by the density of the solids (29, 30). Further it is not probable that the friction factor is affected by the fluid flow as long as the porosity does not change. Thus, the decrease of tg β with increasing gas velocity cannot be caused by an evenly distributed vertical flow.

Two probable mechanisms are :

1. The flow is not evenly distributed.
   Due to the variation in the height of the bed the pressure drop varies. This may cause a larger flow at the down side of the slope and lead to instability.
2. The direction of the fluid leaving the surface is not vertical. An increase in the gas velocity can enlarge a 'downward' force, eventually leading to rolling or sliding of the surface particles.

A simple experiment indicates the influence of the two mechanisms. At a constant gas velocity the value of β is measured for various values of γ, the angle of the distributor with the horizontal. The larger γ the smaller the influence of an eventually uneven flow distribution.
Table A.1 gives the results for glass beads (D_p = 175-250 μ, U_{mf} = 4.10 cm/sec) at U/U_{mf} = 0.24 and U/U_{mf} = 0.83.

TABLE A.1

U = 0.97 cm/sec			U = 3.40 cm/sec		
γ	β_k	β_s	γ	β_k	β_s
0.0	19.8	22.1	0.0	4.5	5.1
2.3	19.0	20.7	0.6	4.0	4.5
4.0	19.1	21.7	1.1	4.0	5.1
6.6	19.0	21.0	2.5	4.2	5.1
8.6	18.8	20.6	3.4	4.5	5.1
10.4	18.9	21.2	4.0	4.0	5.2
12.7	18.9	20.6	5.2	4.6	
14.4	18.4	21.4			
17.4	19.0	21.2			
19.6	19.6				

As can be seen from table A.1 β_s and β_k are independant of γ. Thus mechanism 1 is not relevant and instability arises because the out-flow direction of the fluid is perpendicular to the surface. Another indication of a surface mechanism is that the maximum stable angle δ_r for rolling of a particle on a particle-roughened, inclined surface is close to the angle of repose (29).

A.2 The effect of the gas velocity

It is not sure whether rolling or sliding of the surface particles governs the stability of the slope. Both mechanisms have been analised with simple models. They lead qualitatively to the same results. In this section the effect of inter-particle forces is not taken into account.

A.2.1 Sliding

Figure A.1 shows the relevant forces in the event that the angle of sliding δ_s is different from the angle of repose.

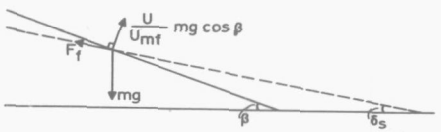

Figure A.1 The force balance for sliding

The force balance at yielding is :

$$f\{mg\cos\delta_s - \frac{U}{U_{mf}} mg \cos\beta_s \cos(\beta_s - \delta_s)\} = mg \sin\delta_s +$$

$$+ \frac{U}{U_{mf}} mg \cos\beta_s \sin(\beta_s - \delta_s) \qquad (A.1)$$

f is a constant relating the friction force F_f to the normal force. As an approximation is assumed that $\epsilon \sim \epsilon_{mf}$ so that the drag force of the fluid within the bed can be written as U/U_{mf} mg.

Eq. (A.1) can be rewritten as :

$$\operatorname{tg}\beta_s = \frac{f - \operatorname{tg}\delta_s}{1 + f \operatorname{tg}\delta_s} \left[\frac{1}{\frac{U}{U_{mf}} \cos^2\beta_s} - 1 \right] \qquad (A.2)$$

Eq. (A.2) shows that, when f is the same for all directions,

tg β_s becomes smaller as tg δ_s becomes larger. The maximum value of tg δ_s is tg β_s. As the variation of f with δ_s is not known, the simplest assumption is tg δ_s = tg β_s.

Eq. (A.2) can then be written as :

$$\text{tg } \beta_s = f \left(1 - \frac{U}{U_{mf}}\right) = \text{tg } \beta_{so} \left(1 - \frac{U}{U_{mf}}\right) \qquad \text{(A.3)}$$

Eq. (A.3) predicts a linear relation between tg β and U in agreement with the experimental results (chapter 2). The more δ_s deviates from β_s the more hyperbolic the curve will be.

A.2.2 Rolling

The conditions for the onset of rolling will be analysed for smooth, uniform spheres with the assumption that the top particle rests on particles situated in a plane making an angle β_s with the horizontal. Figure A.2 is a sketch of a two dimensional case. α is defined as the angle between the plane of the slope and the plane of rotation.

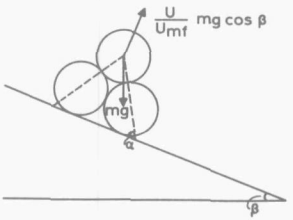

Figure A.2 The force balance for rolling

The force balance at the onset of rolling is :

$$mg \cos (\alpha + \beta_s) = \frac{U}{U_{mf}} mg \cos \beta_s \cos \alpha \qquad \text{(A.4)}$$

or

$$\text{tg } \beta_s = \frac{1}{\text{tg } \alpha} \left(1 - \frac{U}{U_{mf}}\right) \qquad \text{(A.5)}$$

Eq. (A.5) gives the same relation between tg β_s and U as eq. (A.3), with tg β_{so} = 1/tg α or simpler $\alpha + \beta_{so} = 90^o$ as can be seen immediately from figure A.2. This relation enables the prediction of the maximum value of β_{so}.

In the two-dimensional model of figure A.2, $\alpha = 60^o$ and $\beta_{so} = 30^o$ ($tg\ \beta_{so} = 0.58$).

In the three-dimensional situation a number of configurations are possible. Three probable 'ideal' positions are :

1. The top particle rests on four particles, thereby forming a regular pyramid. For this case $\alpha = 54.7^o$ and $\beta_{so} = 35.3^o$ ($tg\ \beta_{so} = 0.71$).
2. The top particle rests on three particles thereby forming a regular tetrahedron.
   a. with one support particle up-slope and two down-slope $\alpha = 70.6^o$ and $\beta_{so} = 19.4^o$ ($tg\ \beta_{so} = 0.35$)
   b. with two support particles up-slope and one down-slope $\alpha = 54.7$ and $\beta_{so} = 35.3^o$ ($tg\ \beta_{so} = 0.71$).

These values of β_{so} are in the same range as the values obtained experimentally. Table A.2 gives the results for a number of sieve fractions of glass beads.

TABLE A.2

$D_p(\mu)$	$\beta_{so}{}^o$	$tg\ \beta_{so}$	$\beta_{ko}{}^o$	$tg\ \beta_{ko}$	ε
45 - 60	34.9	0.70	27.7	0.52^5	0.445
55 - 65	31.3	0.61	24.9	0.46^5	0.493
65 - 90	30.1	0.58	24.9	0.46^5	0.428
90 - 105	29.9	0.57^5	25.4	0.48	0.431
105 - 125	30.8	0.59^5	26.4	0.49	0.438
125 - 175	26.8	0.50^5	24.4	0.45^5	0.417
175 - 250	26.7	0.50	24.0	0.44	0.413
250 - 325	25.8	0.48	23.8	0.42	0.407

The tendency of $tg\ \beta_{so}$ to increase with decreasing D_p does not have to be caused by interparticle forces. The effect of the surface roughness, which becomes more important for smaller particles is sufficient to increase $tg\ \beta_{so}$. When the average height peaks on the surface is given by Δ, the equilibrium conditions for rolling can be written as :

$$\alpha + \beta_{so} = 90^o + \text{arctg} \sqrt{\frac{2\Delta}{D_p}} \qquad (A.6)$$

Since $\sqrt{\frac{2\Delta}{D_p}}$ is small, eq. (A.6) can be written as :

$$tg\ \beta_{so} = tg\ (90^o - \alpha) + \sqrt{\frac{2\Delta}{D_p}} \qquad (A.7)$$

The values of tg β_{so} given in table A.2 are represented in figure A.3 as a function of D_p. The influence of the variation in particle size distribution and the porosity has not been accounted for. A straight line has been drawn through the experimental points, in agreement with eq. (A.7).

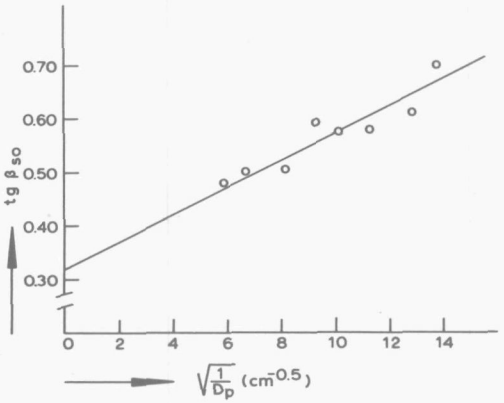

Figure A.3 β_{so} as a function of D_p

Two values can be estimated from the experimental curve.

1. Δ = 3.3 μ; a reasonable value from a physicalpoint of view.
2. tg $(90^o - \alpha)$ = 0.32; $(90^o - \alpha) = 18^o$. This is close to the value of β_{so} for smooth, uniform spheres predicted from configuration 2a. It is quite probable that this configuration is the most likely stable position of the particles.

This outcome indicates that the angle of repose probably is determined by a rolling mechanism. It confirms the assumption that interparticle forces can be neglected and it shows the remarkable effect of a small surface roughness.

A.3 The effect of interparticle forces

It is rather problematic to introduce interparticle forces into the mechanical models used in the previous section. Probably a soil mechanical approach would be more correct. However, it is not the aim to show quantitatively the effect of interparticle forces on the value of tg β_{so} and U_{mf}. It is sufficient when it can be qualitatively indicated how the relationship between tg β and U becomes affected.
Both the slide model and the roll model will be extended to

account for interparticle forces. Although it has been shown that in the absence of interparticle forces the conditions for rolling govern the value of tg β_{so}, it is not sure whether this holds when interparticle forces are present.

A.3.1 Sliding

In section A.2.1 it has been shown that the angle of sliding δ_s is close to the angle of repose β_s. This result will be used in the present analysis. The force resulting from the interparticle forces is called F_{PR}. The force balance at sliding is :

$$f\ (mg \cos \beta_s + F_{PR} - \frac{U}{U_{mf}} mg \cos \beta_s) + F_{PR} = mg \sin \beta_s \qquad (A.8)$$

$$\text{tg } \beta_s = f\ (1 - \frac{U}{U_{mf}}) + \frac{F_{PR}\ (1+f)}{mg \cos \beta} \qquad (A.9)$$

The relation between tg β_s and U is no longer linear. The presence of interparticle forces increases both the value of tg β_{so} as well as the value of U at which the angle of repose becomes zero.

A.3.2 Rolling

In a roll model the effect of interparticle forces depends upon the configuration of the particles. It will be assumed that the particles are uniform, smooth and arranged according to configuration 2a. The force F_p between two particles is directed from center to center. The critical force balance is :

$$mg \cos (\beta_s + \alpha) + F_p \cos \tfrac{1}{2} \alpha = \frac{U}{U_{mf}} mg \cos \beta_s \cos \alpha \qquad (A.10)$$

$$\text{tg } \beta_s = \frac{1}{\text{tg } \alpha} (1 - \frac{U}{U_{mf}}) + \frac{F_p}{2\ mg \sin \tfrac{1}{2} \alpha \cos \beta_s} \qquad (A.11)$$

Eq. (A.11) is similar to eq. (A.9) and the predicted effects are the same. The effect of interparticle forces on tg β_{so} and $U_{\beta=0}$ have been represented graphically in figure A-4. The graph given is rather insensitive for the value of β_{so} in the absence of interparticle forces. The relations predicted by the eqs. (A.9) and (A.11) coincide in this representation.

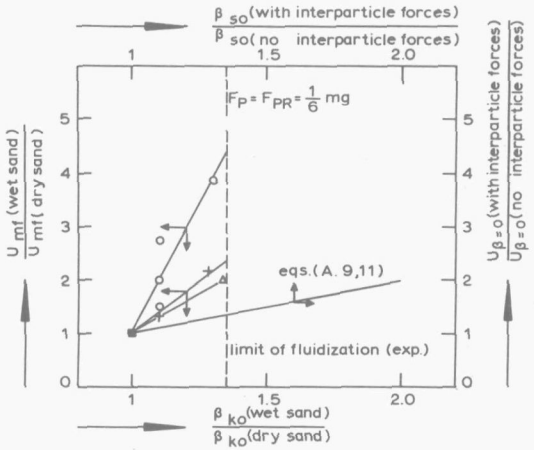

Figure A.4 The influence of interparticle forces on β and U_{mf}
Δ glass sand : D_p = 200 - 600 μ
+ river sand : D_p = 150 - 400 μ
o foundry sand : D_p = 100 - 800 μ

Also given in figure A.4 are the experimental results of Vaněček, Najmr and Holšan (31) with wet sands. They measured the value of tg β_{ko} and U_{mf} as a function of the moisture content of the sand. The value of U_{mf} was determined visually. Their results show that tg β_{ko} and U_{mf} increase with increasing interparticle forces. The visual value of U_{mf} increases much more than the value of $U_{\beta=0}$ as predicted either by eq. (A.9) or (A.11). This indicates that interparticle forces probably affect the mobility of the particles more than the stability of the slope.

A.4 Conclusions

1. Both the slide model and the roll model predict a linear relationship between tg β_s and U in the absence of interparticle forces.
2. The roll model probably gives a more realistic representation of the stability conditions. It is able to predict the value of tg β_{so} as a function of D_p.
3. The effect of interparticle forces is to increase the value of tg β_{so} and $U_{\beta=0}$.

APPENDIX B

NON LINEAR VIBRATIONS

B.1 Large amplitudes

In chapter 4 the amplitude of the oscillation was assumed to be small. In that case the restoring force is linearly proportional to the displacement and the calculation of the frequency is simple. In this section the effect of larger amplitudes will be investigated. F_r is then non-linear in x. In order to arrive at a value for the frequency the energy method will be used. This is allowed as only deviations from the harmonic frequency are considered.

For large amplitudes the restoring force per unit area can be calculated using the same method as employed in section 4.2.1; (eqs. (4.20-4.25)).

$$\Delta P_r = \frac{200\ \mu\ U_s}{D_p^2}\left[\frac{L^2\ (1-\varepsilon)^2\ (L-x)}{(\varepsilon L-x)^2} - \left(\frac{1-\varepsilon}{\varepsilon}\right)^2 L\right]$$

$$= (1-\varepsilon)(\rho_s-\rho_f)\ g\ L\left[\frac{(2-\varepsilon)\ x/\varepsilon L - (x/\varepsilon L)^2}{(1 - x/\varepsilon L)^2}\right] \qquad (B.1)$$

For convenience sake the following notation will be adopted :

$$F_z = \frac{\Delta P_r}{(1-\varepsilon)(\rho_s-\rho_f)\ g\ L} = \frac{\Delta P_r}{mg}$$

$$z = \frac{x}{\varepsilon L}$$

Eq. (B.1) can then be written as :

$$F_z = \frac{(\varepsilon-2)\ z - z^2}{(1 + z)^2} \qquad (B.2)$$

Both z and F_z are taken positively in upward direction.
Eq. (B.2) is sketched in figure B.1 for $\varepsilon = 0.5$. The force is not linear in z and asymmetric. F_z has two asymptotic values :

$F_z = -1$ for $z \to \infty$

$F_z = \infty$ for $z \to -1$

The last asymptote is physically impossible. Before z can reach the value -1 ($x = -\varepsilon L$), a packed bed will be formed.

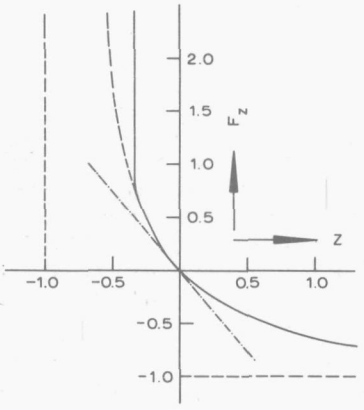

Figure B.1 The restoring force as a function of the displacement
($\varepsilon = 0.5$; $\varepsilon_{pb} = 0.4$)
——— — — — — eq. (B.2)
— · — · — · — · — · — eq. (4.26)

The maximum amplitude in the compression cycle is :

$$x = L \left(\frac{\varepsilon - \varepsilon_{pb}}{1 - \varepsilon_{pb}}\right) \qquad (B.3)$$

and F_z can be taken as infinitely large for this value of x. When e.g. $\varepsilon = 0.5$ and $\varepsilon_{pb} = 0.4$, the maximum amplitude is 1/6 L or z = - 1/3. The effect of this physical limitation will be discussed in section B.2. In order to analyse the effect of the non-linear relation between F_z and z on the frequency the following procedure has been adopted.
As the force is asymmetric the amplitudes and the periods of the compression stage and the expansion stage will differ. For each stage the frequency will be calculated. The average frequency can then be calculated from :

$$T = 1/2\ T_C + 1/2\ T_E$$

or

$$\omega = \frac{2\omega_E\ \omega_C}{\omega_E + \omega_C} \qquad (B.4)$$

Both ω_E and ω_C will be dependent upon the amplitude of their respective half cycle. The relation between A_C and A_E is given by the equality of the maximum values of the potential energy

for each stage.

$$E_{pot\ CM} = E_{pot\ EM} \tag{B.5}$$

The potential energy at displacement x per unit cross section is :

$$E_{pot} = - \int_0^x \Delta P_r dx = - mg\ \varepsilon L \int_0^z F_z\, dz$$

$$\frac{E_{pot}}{mg\ \varepsilon L} = - \int_0^z \frac{(\varepsilon-2)\ z-z^2}{(1-z)^2}\, dz$$

$$= - (\varepsilon-2) \left[\ln\ (1+z) + \frac{1}{1+z} \right]_0^z + \left[1+z- 2\ln\ (1+z) - \frac{1}{1+z} \right]_0^z$$

$$= \frac{z\ (\varepsilon+z)}{1+z} - \varepsilon\ \ln\ (1+z) \tag{B.6}$$

The right hand side of eq. (B.6) can be expanded into series for $-1 < z < +1$.

$$\frac{z(\varepsilon+z)}{1+z} = z + (1-\varepsilon) \sum_{j=1} (-z)^j$$

$$\varepsilon\ \ln\ (1+z) = - \varepsilon \sum_{j=1} \frac{(-z)^j}{j}$$

Eq. (B.6) can be written as :

$$\frac{E_{pot}}{\varepsilon L\ mg} = \sum_{j=2} \frac{\{j\ -(j-1)\varepsilon\}(-z)^j}{j}$$

Substituting $z = u/\varepsilon L$ and $m = (1-\varepsilon)(\rho_s-\rho_f)L$ gives :

$$E_{pot} = (1-\varepsilon)(\rho_s-\rho_f)\ g \sum_{j=2} \frac{\{j\ -(j-1)\varepsilon\}(-u)^j}{j\varepsilon} \tag{B.7}$$

The value of E_{pot} for the bed can then be calculated with eq. (4.16).

$$E_{pot} = (1-\varepsilon)(\rho_s-\rho_f)\, g \sum_{j=2} \frac{\{j-(j-1)\varepsilon\}(-x)^j}{j\ (j+1)\varepsilon} \qquad (B.8)$$

The maximum value of E_{pot} in the expansion stage is :

$$E_{pot\ EM} = (1-\varepsilon)(\rho_s-\rho_f) g \sum_{j=2} \frac{\{j-(j-1)\varepsilon\}(-A_E)^j}{j(j+1)\varepsilon^{j-1}\ L^{j-2}}$$

The maximum value of E_{kin} in the expansion stage is (see eq. 4.15)

$$E_{kin\ EM} = \frac{1}{6}\,(1-\varepsilon)(\rho_s-\rho_f)\ L\ A_E^{\,2}\ \omega_E^{\,2}$$

Equating the two equations above gives for the frequency :

$$\omega_E^{\,2} = \frac{g}{L} \sum_{j=2} \frac{6\{j-(j-1)\varepsilon\}(-A_E)^{j-2}}{j\ (j+1)\varepsilon^{j-1}\ L^{j-2}} \qquad (B.9)$$

The frequency of the compression stage (maximum amplitude $-A_C$) can be calculated by using the same method as employed above.

$$\omega_C^{\,2} = \frac{g}{L} \sum_{j=2} \frac{6\{j-(j-1)\varepsilon\}(A_C)^{j-2}}{j\ (j+1)\varepsilon^{j-1}\ L^{j-2}} \qquad (B.10)$$

The relation between amplitude and frequency for the two stages is :

$$A_E^{\,2}\ \omega_E^{\,2} = A_C^{\,2}\ \omega_C^{\,2} \qquad (B.11)$$

The average frequency can be calculated with eq. (B.4) and the eqs. (B.9-11). In order to compare the value of ω with the frequency found by the linear approach (ω_{LIN}) it is convenient to write the eqs. (B.9, 10) as follows :

$$\omega_E = \omega_{LIN} \sqrt{1 + \sum_{j=3} \frac{6\{j-(j-1)\varepsilon\}(-A_E)^{j-2}}{j\ (j+1)(2-\varepsilon)\varepsilon^{j-2}L^{j-2}}} \qquad (B.12)$$

$$\omega_C = \omega_{LIN} \sqrt{1 + \sum_{j=3} \frac{6\{j-(j-1)\varepsilon\}(A_C)^{j-2}}{j\ (j+1)(2-\varepsilon)\varepsilon^{j-2}L^{j-2}}} \qquad (B.13)$$

The relation between A_E and A_C is given by the maximum value of E_{pot} for each stage:

$$A_E^2 \sum_{j=2} \frac{6\{j-(j-1)\varepsilon\}(-A_E)^{j-2}}{j\ (j+1)\varepsilon^{j-1}L^{j-2}} = A_C^2 \sum_{j=2} \frac{6\{j-(j-1)\varepsilon\}(A_C)^{j-2}}{j\ (j+1)\varepsilon^{j-1}L^{j-2}} \qquad (B.14)$$

Combining the eqs. (B.4) and eq. (B.11) gives :

$$\omega = 2\ \omega_C \{\frac{A_C}{A_C + A_E}\} = 2\ \omega_E \{\frac{A_E}{A_E + A_C}\} \qquad (B.15)$$

Table B.1 shows the results of a few calculations for large amplitudes.

TABLE B.1

ε	z_{EM}	z_{CM}	A_E/L	A_C/L	ε_{max}	ε_{min}	ω_E/ω_{LIN}	ω_C/ω_{LIN}	ω/ω_{LIN}
0.50	0.40	0.32	0.20	0.16	0.58	0.40^5	0.90	1.12	1.00
0.50	0.60	0.42	0.30	0.21	0.61^5	0.37	0.85	1.19	1.00
0.70	0.57	0.43	0.40	0.30	0.78^5	0.57	0.87	1.18	1.00

The results show that for large amplitudes ω_E decreases and ω_C increases substantially, however, the average frequency remains equal to ω_{LIN}. It can be concluded that the influence of the gas velocity on the amplitude does not effect the frequency.

B.2 Restricted large amplitudes

The maximum amplitude in the compression stage is $A_{CM} = (\varepsilon-\varepsilon_{pb})L/(1-\varepsilon_{pb})$. At this value of A_C eq. (B.1) will not be correct. The correct relation between F_r and x is not known.

Therefore an approximate method will be utilized to show qualitatively the effect on the frequency. The fluidized bed will be treated as a system with one degree of freedom without damping. The relation between F_r and x in the expansion stage is assumed to be linear and given by eq. (4.26). This is acceptable as the effect is most important for gas velocities only a little above U_{mf}, where the amplitudes are small. In the compression stage the linear relation between F and x will be adapted to give the correct asymptotic value of F_r. A hyperbolic function of the form $((A_{CM})/(A_{CM}-x))^n$ seems a simple and appropriate correction factor. For convenience sake the relation between F_r and x will be taken as :

$$\Delta P_r = (1-\varepsilon)(\rho_s-\rho_f)\, g\frac{(2-\varepsilon)}{\varepsilon} \; x \; \left(\frac{A_{CM}}{A_{CM}-x}\right)^3 \qquad (B.16)$$

$$= K_r x \left(\frac{A_{CM}}{A_{CM}-x}\right)^3$$

The frequency will be calculated following the method as given in section B.1.

$$E_{pot\ C} = \int_0^x K_r x \left(\frac{A_{CM}}{A_{CM}-x}\right) dx = \tfrac{1}{2} K_r x^2 \left(\frac{A_{CM}}{A_{CM}-x}\right)^2$$

Equating the maximum values of the potential and kinetic energy :

$$\tfrac{1}{2} m \omega_C^2 A_C^2 = \tfrac{1}{2} K_r A_C^2 \left(\frac{A_{CM}}{A_{CM}-A_C}\right)^2$$

$$\omega_C = \sqrt{\frac{K_r}{m}}\, \frac{A_{CM}}{A_{CM}-A_C} = \omega_{LIN}\, \frac{A_{CM}}{A_{CM}-A_C}$$

For the expansion stage holds $\omega_E = \omega_{LIN}$.
The average frequency is given by eq. (B.4).

$$\omega = \frac{2\,\omega_C\,\omega_E}{\omega_C + \omega_E} = 2\,\omega_{LIN}\, \frac{A_{CM}}{2A_{CM} - A_C} \qquad (B.17)$$

For $A_C = A_{CM}$: $\omega = 2\,\omega_{LIN}$ (B.18)

Eq. (B.18) shows that the frequency increases by a factor 2. Although the value of the factor depends upon the relationship between F_r and x used, the above may suffice to support the intuitive opinion that the frequency increases by the restriction in amplitude caused by a minimum possible porosity.

APPENDIX C

THE CONTINUITY WAVE CRITERION

In their paper on dynamic shock waves Verloop and Heertjes (56) mention an experiment in which an artificial bubble is formed by placing an object in a fast downcoming stream of fluidized particles. The authors see this as support for the dynamic shock wave concept.
However, a continuity wave approach throws more light on the subject and will be presented here. As this hypothesis is highly tentative, first a detailed description of the phenomena will be given.

C.1 Experimental observations

The experiments with water fluidized solids have been carried out in a square column with sides of 5 cm., the gas-solids experiments in a cylindrical glass column with inside diameter of 6.5 cm. The distributors used were sintered glass plates with an average pore diameter of 40 μ. The direction of the fluid flow could be observed by tracing with ink or NO_2 respectively in water or gas fluidized beds. About 4-5 cm above the distributor objects of various size and shape could be fixed against the inside of the wall. The construction was such that the view of the object was not obstructed.
By slightly tilting the column stable circulation patterns could be obtained across the column. The velocity of the particles could be varied by the fluid flow. A photographic method has been used to measure the velocity of the particles. From the length of a particle trajectory on a photo the velocity could be calculated.To check the influence of the wall the solids velocity has also been measured inside the bed. The method used has been described elsewhere (76). Both methods, with an accuracy of about 1 cm/sec, give the same values for the velocity. The porosity in the downcoming stream is close to ε_{mf}. The objects are placed in the downcoming stream. The phenomena occurring depend upon the solids velocity. Three flow regimes are distinguished.

I. For low solids velocity the fluid flows upwards. The disturbance caused by the object looks identical to the one in a non-flowing fluidized bed. There is a cone of lower porosity above the object and a few particles, apparently restricted in their motion, below the object.

II. When the solids velocity is sufficiently high to change the direction of the fluid flow the observed phenomena are different. A packed cone of particles is pressed on top of

the object. The cone becomes smaller and flatter with increasing velocity. An exchange takes place between particles at the edge and the streaming particles. At the base of the object parvoids are formed, which rise up against the flow. They disappear when they have passed the object. An illustration is given in photo II.

III. At a certain critical solids velocity W_b, a bubble is formed under the object. The bubble is stable in time. The larger the solids velocity the larger the bubble (see photo III and IV). Once a bubble has been formed no rising parvoids can be observed. The cone on top of the object remains. When a bubble is present and the object is suddenly removed, the bubble retains its identity and will travel upwards or downwards depending on the solids velocity.

The diameter of the object D_o has been changed from D_o/D_p = 1 to D_o/D_p = 25 without a noticeable change in the phenomena or the critical velocity. Variation in the shape of the object does not alter the sequence of the phenomena, but can change the shape of the cone, the porosity of the parvoids and the critical velocity. The more streamlined the downstream part of the object is, the lower the porosity of the parvoid and the higher the critical velocity.

When the object is placed in the upward stream the phenomena are completely different. At low velocities the fluid and the particles flow in streamline around the object. At high velocities ($Re = \rho_f U_i D_o/\mu \sim 500$!!) a fluid vortex is formed behind the object. The solids flow alongside the boundary of the vortex. Gradually the vortex is filled with particles captured by the turning fluid (photo V). When the object is suddenly removed the vortex disappears. The phenomena are disturbed by the bubbles in the upward stream

C.2 Theoretical analyses

The following is an analysis of three hypothesis which attempt to explain the bubble formation in downward flow.

I The bubble is a vortex

This assumption is the most straightforward, related to similar phenomena in viscous fluids, e.g. the turbulent wake, the Karman vortex street. This concept has not been adopted for three reasons.

1. For vortex formation the Re-number can be expected to be a parameter. However, a variation of the diameter of the

object over a factor 10 did not have a measurable influence on W_b.

2. The phenomena observed in upward flow are completely different from those in downward flow. The phenomena in upward flow are easily understood as the effect of a wake, therefore the assumption of a wake or vortex for the downward flow is less likely.

3. The 'bubble' when formed does not disappear after removal of the object.

However, as long as the 'viscosity' mechanism of a fluidized bed is not known, any conclusion concerning this concept is essentially premature.

II The bubble is a dynamic shock wave

This hypothesis (56) is based on similar phenomena in compressible fluids, e.g. shock waves in wind tunnels.
In support of this concept are the shape of the void and the independency of W_b of the size of the object. On the negative side is that the shape of the object has a marked influence on W_b. Moreover, a dynamic shock wave is to be expected at the top of the object and not only at the bottom. The main problem is that the value of c_e in flowing fluidized beds is not known. When c_e is equated to the value of a non-flowing fluidized bed, the shock wave should occur at about $-W = c_e$. But bubbles are formed at solids velocities an order of magnitude lower. It is also possible to assume that the velocity of the dynamic wave becomes zero when the direction of the fluid changes. The mechanism by which the signal is transmitted may disappear, when the velocity of the particles is larger than the fluid velocity and the fluid is dragged by the particles. When this assumption is correct, the cone of packed particles on the object can be considered as a dynamic shock wave in analogy with e.g. pile-ups in traffic and bubbles in liquid fluidized beds.

III The bubble is a trapped void

This hypothesis has no close generally known analogy. When the fluid changes direction the particle streamlines will not follow the boundary of the object. The voids formed below the object can escape upwards as expansion waves (parvoids). The porosity of the wave depends upon the shape of the object. The more streamlined the downstream part of the object, the lower the porosity will be. At a certain solids velocity, W_c, the direction of the porosity wave changes. When the wave is treated as a continuity shock wave this critical velocity can

be calculated with eq. (3.12). Above W_c the void should travel downwards. This does not occur because the void is shielded by the object. The void remains below the object and forms a bubble.

C.3 Experimental results

Two sets of experiments have been carried out to check the validity of the trapped void concept.

1. W_b has been determined for various systems and cylindrical objects.
2. W_b has been determined for one system with objects of varied shape.

Table C.1 gives the experimental value of W_b and the calculated value of W_c for the systems used. W_c has been calculated from eq. (5.12b). The value of n has been estimated from the relations given by Richardson and Zaki (5). The slip velocity has been calculated with eq. (2.2). The value of ε_1 has been taken as the porosity of the undisturbed dense phase.
The value of ε_0 has been estimated from the photographs. The value of W_c is rather uncertain, since ε_0 cannot be estimated with great accuracy.

TABLE C.1

System	D_o cm	D_p μ	ρ_s g/cm³	n	ε_1	ε_0	W_b exp. cm/sec	W_c eq.(3.12b) cm/sec
silicagel/air	0.3	115	0.99	4.0	0.54	0.9	-4.0	-4.1
silicagel/air	0.3	200	0.99	3.5	0.52	0.9	-6.0	-5.5
glass/air	0.3	175	2.96	3.0	0.42	0.9	-6.0	-5.8
copper/water	0.4	360	8.56	4.0	0.42	0.8	-4.5	-3.9
steel/water	0.4	1000	5.62	2.5	0.42	0.8	-6.5	-6.0

Table C.1 shows that the experimental and theoretical values of W correspond fairly well. Although both values are uncertain a degree of agreement is evident.
Table C.2 gives W_b for objects of varied shape for a silicagel/air system (D_p = 200 μ). The objects follow the same arrangement whether streamlining or W_b is used as a sequencer. W_c follows the same sequence when ε_0 becomes lower the more streamlined the underpart of the object is. W_b and W_c are numerically the same when in case I : ε_0 = 0.95, in case V : ε = 0.9 and in case VIII : ε = 0.8. These values are in qualitative agreement with the photographical results.

TABLE C.2

number	I	II	III	IV	V	VI	VII	VIII
shape								
max.width (cm)	0.3	0.3	0.3	0.3	0.3	0.3	0.3	0.3
max.length(cm)	0.26	1.0	0.3	0.4	0.3	0.4	0.6	1.0
$-W_b$(cm/sec)	3	4	5	5	6	6.5	7	10

It can be concluded from the tables C.1 and C.2 that the theoretical predictions are consistent with the experimental results.

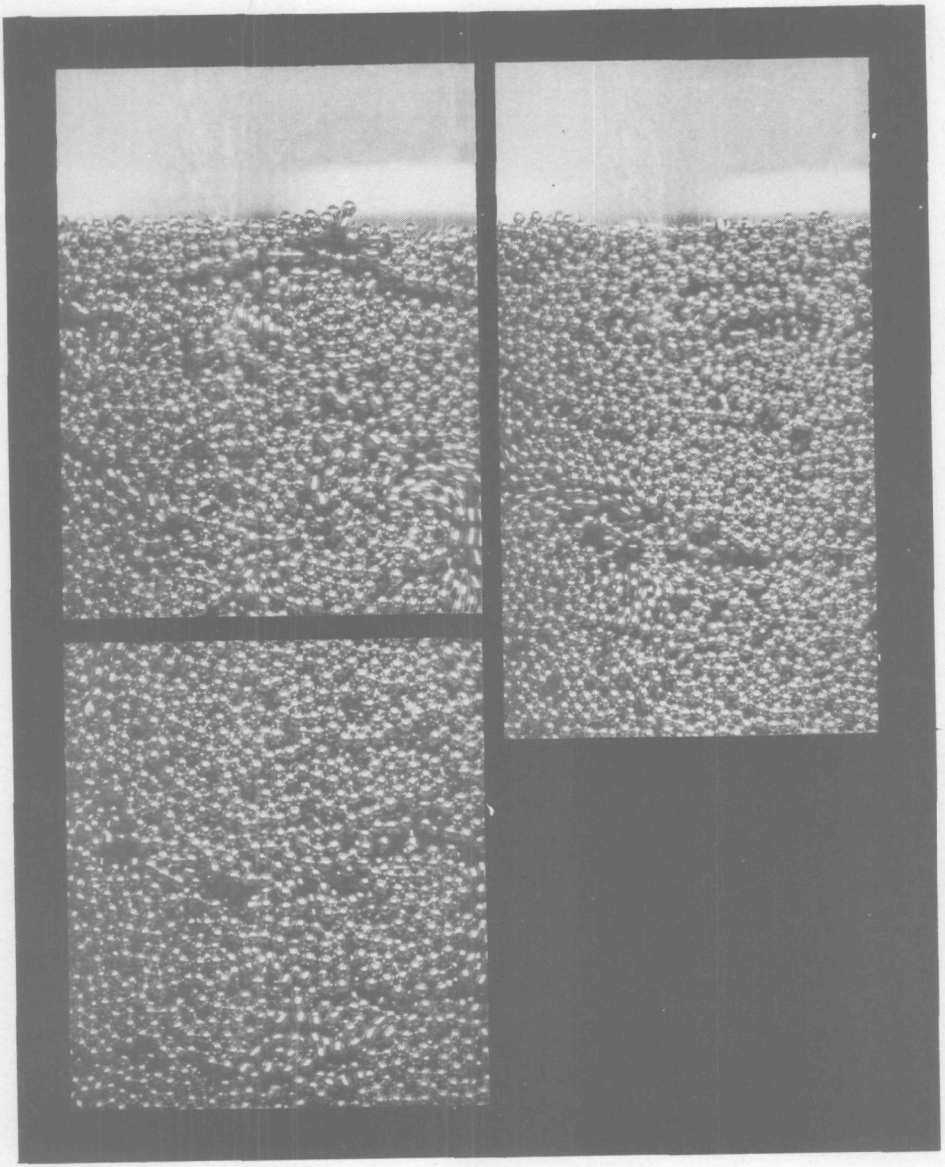

Photo I Bubbles in a liquid fluidized bed
steel/water : D_p = 1000 μ



Photo II Parvoid rising up next to the object silicagel/air : D_p = 200µ
(W ∿ 3 cm/sec)

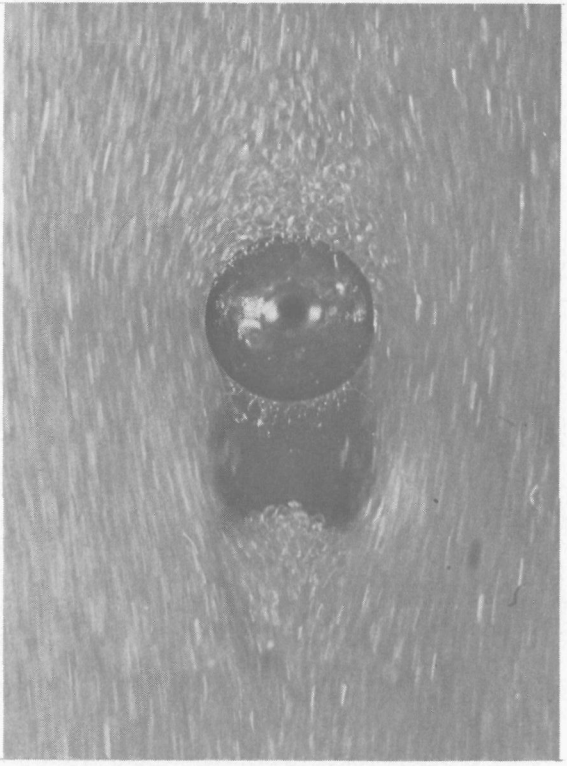

Photo III Artificial bubble below the object silicagel/air : D_p = 200µ; D_o = 3 mm
(W ∿ 10 cm/sec)

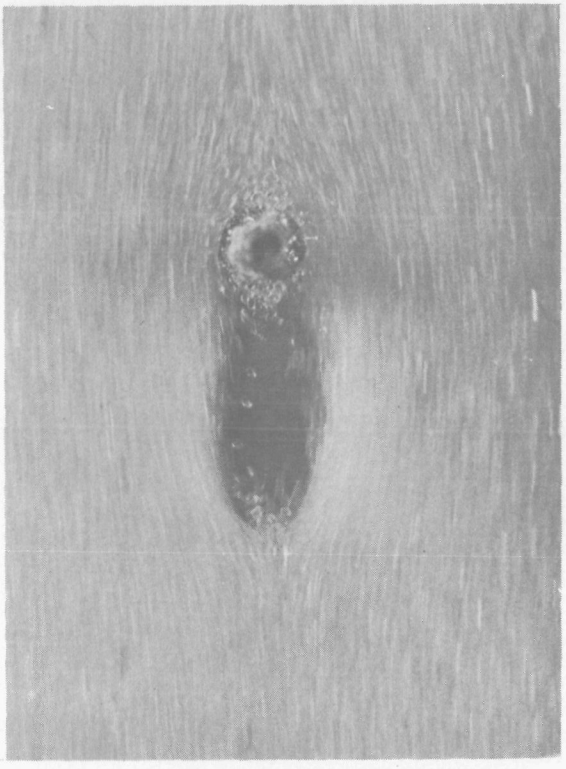

Photo IV Artificial bubble below the object
silicagel/air : D_p = 200μ; D_o = 3 mm
(W ∿ 30 cm/sec)

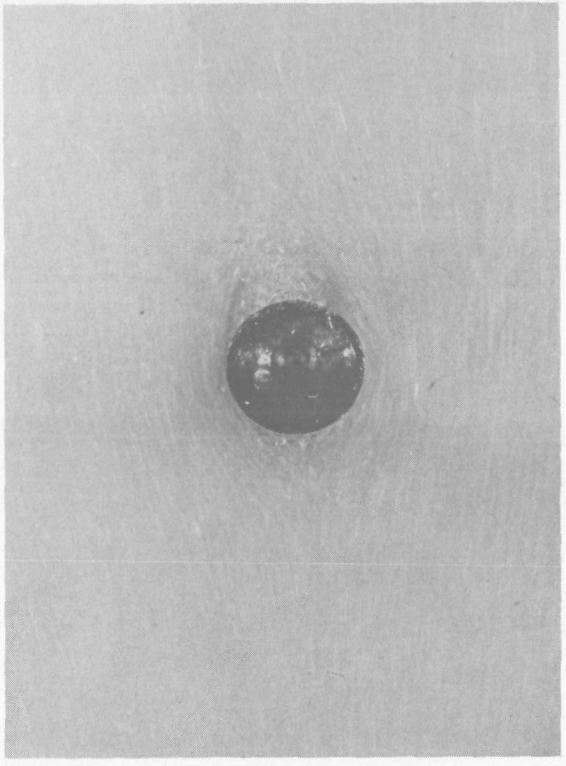

Photo V Vortex formation above the object
silicagel/air : D_p = 200μ; D_o = 3 mm
(W ∿ 20 cm/sec)